

DESIGN OF A SIX DEGREES OF FREEDOM HAPTIC DEVICE

by

ŞAKİR KABADAYI

**Submitted to the Graduate School of Engineering and Natural Sciences
in partial fulfillment of
the requirements for the degree of
Master of Science**

SABANCI UNIVERSITY

Spring 2006

DESIGN OF A SIX DEGREES OF FREEDOM HAPTIC DEVICE

APPROVED BY:

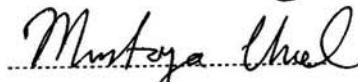
Assist. Prof. Dr. Kemalettin ERBATUR
(Thesis Advisor)



Prof. Dr. Asif ŞABANOVIÇ
(Thesis Co-Advisor)



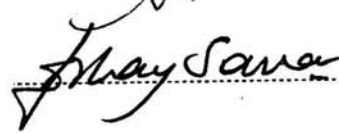
Assoc. Prof. Dr. Mustafa UNEL



Assoc. Prof. Dr. Mahmut F. AKŞİT



Assist. Prof. Dr. ErKay SAVAŞ



DATE OF APPROVAL: 14.08.2006

© Şakir Kabadayı 2006

All Rights Reserved

To my brother

ACKNOWLEDGMENTS

First of all, I wish to express my deepest gratitude and appreciation to my advisor Assist. Prof. Dr. Kemalettin Erbatur for all his guidance and assistance not only throughout this thesis but all my graduate study. It has been a pleasure to work with him.

I would like to thank Prof. Dr. Asif Şabanoviç who initiated this study and always be patient and tolerant with me.

I would also like to acknowledge the members of my defense committee: Assoc. Prof. Dr. Mustafa Unel, Assoc. Prof. Dr. Mahmut Akşit and Assist. Prof. Dr. Erkey Savaş for finding time to serve as my jurors and for their comments on this work.

I have to thank İlker Sevgen in addition to his friendship for his efforts in the completion of this thesis and Mehmet Güler for his “ultra-precise” manufacturing skills.

Among my friends who contributed to the success of this thesis in any way, I am glad to mention the following names; Burak Yılmaz who is my part-time roommate and one of the smartest and passionate people I have ever known, Nusrettin Güleç who has been nothing but a real friend for almost seven years now, Özer Ulucay whom I can always count on, Arda Burnaz who supplied foods, drinks and his unconditional friendship, Esra Nur Şahinoğlu whose friendship was precious for me, Onur Özcan who is one of the most sincere person I have known, Deniz Güçlü who was always there for me, and all others Berk Çallı, Yeşim Hümay Esin, Merve Acer, Tolga Duran, Doğucan Bayraktar, Nevzat Ataklı, Furkan Pekmez...

I would like to thank all Mechatronics graduate students for their friendship and creating a peaceful laboratory environment.

I wish to convey my special thanks to Emre Güldoğan, for her invaluable support and love that helped me a lot not only throughout this thesis but also one of the darkest periods of my life. Whenever I search for a peace of mind and some happiness to get me through the day, she is at my side, she always was, and she always will be.

I am indebted to my family for their trust, everlasting support and love that they have given me at all times. Especially I am grateful to my mother, Şükran and my sister, Makbule for their patience and faith in me, whatever I do.

Special thanks go to my brother, Faruk, to whom I cannot express my gratitude with words.

DESIGN OF A SIX DEGREES OF FREEDOM HAPTIC DEVICE

Şakir KABADAYI

MS Thesis, 2006

Thesis Advisor: Assist. Prof. Dr. Kemalettin Erbatur

Keywords: Haptic interface, Dynamics compensation, Design criteria

Abstract

From the open-loop tele-operator systems of 1950's to the modern kinesthetic training and surgery support setups, haptic systems took a long way of evolution. Application areas ranging from minimally invasive surgery to space training systems for astronauts, still there is a large room for improvements. The vast areas of emerging applications put a number of demands on haptic interfaces. Fidelity, large workspace and high force/torque capacity are among those demands.

The thesis concentrates on the design of a haptic master arm. The mechanical system with an analysis of dynamics properties, electronic hardware, algorithms for forward and inverse kinematics and software for the integration of sensors and actuators are developed to create an infrastructure for haptic interaction. Though the major design criteria applied in this design are a large workspace and high force/torque capacity, dynamics compensation techniques are also discussed as part of the developed infrastructure. The main focus of the thesis is the design of this hardware and software base for haptic applications rather than the design of haptic control algorithms.

A survey on haptic interfaces and master arm design criteria is presented firstly. A set of specifications for the master arm is determined for a general and multipurpose yet ergonomic use. Newton-Euler based simulation techniques are employed for the component selection. Sensors and controller hardware are selected according to the demands of the haptic control problem. Dynamics compensation techniques for the designed manipulator are considered and tested in simulation. Finally the designed master arm is assembled and electrically integrated.

ALTI SERBESTLİK DERECELİ HAPTİK ARABİRİMİ TASARIMI

Şakir KABADAYI

Yüksek Lisans Tezi, 2006

Tez Danışmanı: Yrd. Doç. Dr. Kemalettin Erbatur

Anahtar kelimeler: Haptik arabirim, Dinamik dengeleme, Tasarım kriterleri

Özet

Dokunma hisli (haptik) sistemlerin gelişimi, 1950'lilerdeki açık döngülü uzaktan komutalı sistemlerden bugünkü modern dokunsal öğretim ve cerrahi destek tertibatlarına kadar süren uzun bir yol katetmiştir. Uygulama alanları minimal invaziv cerrahiden astronotlar için uzay eğitim sistemlerine kadar uzanmakta olup, yine de gelişme için geniş bir alan bulunmaktadır. Çeşitli alanlarda gelişen uygulamalar dokunma hisli ara yüzler için birçok talep ortaya koymaktadır. Sadakat, geniş çalışma alanı ve yüksek kuvvet/tork kapasitesi bu talepler arasındadır.

Bu tezde dokunma hisli ana kolun tasarımı üzerine yoğunlaşmıştır. Sistemin dinamik özelliklerinin analizi ile oluşturulmuş mekanik sistem, elektronik donanım, ileri ve ters kinematik çözümleri için algoritmalar ve algılayıcı ve eyleyici uyumu için yazılım; dokunma hisli etkileşimin alt yapısını oluşturmak için geliştirilmiştir. Her ne kadar bu tasarımda ana tasarım kriterleri geniş iş alanı, yüksek kuvvet/tork kapasitesi olsa da geliştirilen altyapının bir parçası olarak sadakat kriterini geliştirmek amacıyla dinamik telafi teknikleri de tezde işlenmiştir. Tezin ana konusu dokunma hisli denetleme algoritmalarının tasarımından çok dokunma hisli uygulamalar için yazılım ve donanım tasarımıdır.

Tezde ilk olarak haptik arabirimler ve kol tasarım kriterleri üzerine yapılan literatür taraması sunulmuştur. Genel ve çok amaçlı, aynı zamanda ergonomik bir kol için tasarım belirtileri belirlenmiştir. Newton-Euler tabanlı benzeşim teknikleri kullanılarak eyleyici ve transmisyon elemanları seçilmiştir. Haptik denetleme algoritmalarının gerektirdiği algılayıcı ve denetleyici donanımı seçilmiştir. Tasarlanan manipülâtör için dinamik telafi teknikleri üzerinde durulmuş ve bu teknikler benzeşim ortamında denenmiştir. Son olarak tasarlanan kol monte edilmiş ve elektriksel bağlantıları yapılmıştır. Tez sonuçların sunulması ve tartışılması ile sonlandırılmıştır.

TABLE OF CONTENTS

ACKNOWLEDGEMENTS.....	v
ABSTRACT.....	vii
ÖZET.....	viii
LIST OF TABLES.....	xi
LIST OF FIGURES.....	xii
LIST OF SYMBOLS.....	xv
ABBREVIATIONS.....	xvi
1 INTRODUCTION.....	1
2 LITERATURE SURVEY.....	4
3 DESIGN CRITERIA.....	10
3.1 Main Design Criteria.....	10
3.2 Ergonomics.....	11
3.3 Workspace.....	12
3.4 Force/Torque Capacity.....	12
3.5 Resolution.....	13
4 DESIGN OF THE KINEMATICS ARRANGEMENT.....	14
4.1 Parallel or Serial Arrangement?.....	14
4.2 Spherical Wrist.....	15
4.3 Kinematic Arrangement of the Main Axes.....	15
4.4 Placement of the Spherical Wrist.....	16
4.5 Link Sizes.....	19
4.6 Axis Assignment and Denavit - Hartenberg parameters.....	21
4.7 Forward Kinematics.....	23
4.8 Inverse Kinematics.....	24
5 COMPONENT SELECTION.....	26
5.1 Selection of Actuators.....	26
5.2 Stress Analysis.....	28

5.3	Design Verification with Newton-Euler Based Inverse Dynamics Simulation	35
5.4	Selection of Sensors.....	52
5.4.1	Position Sensor Selection.....	52
5.4.2	Force Sensor Selection.....	54
5.5	Controller Hardware, Actuator and Sensor Integration.....	55
6	DYNAMICS COMPENSATION ALGORITHMS.....	59
7	ASSEMBLY.....	66
8	CONCLUSION.....	71
	REFERENCES.....	72
	APPENDIX A. HARMONIC DRIVE DATASHEET.....	76

LIST OF TABLES

Table 4.1 D-H parameters for the designed arm.....	23
Table 5.1 Comparison of actuator options.....	27
Table 5.2 Maximum displacement of the links.....	32
Table 5.3 Max von-Mises stresses and safety factors.....	35
Table 5.4 Comparison of position sensor options.....	53
Table 5.5 Resolution of encoders	53
Table 5.6 Comparison of F/T sensor options.....	54
Table 6.1 Dominant dynamics effects at the joints.....	59
Table 6.2 Values of ω_{nk} used for the joints.....	62

LIST OF FIGURES

Figure 2.1. The first “force feedback” system developed by Goertz.....	4
Figure 2.2 The Pantograph linkage.....	5
Figure 2.3 SHaDe	6
Figure 2.4 SPIDAR-G.....	7
Figure 2.5 Phantom desktop	7
Figure 2.6 LHIFAM.....	8
Figure 2.7 ViSHARD6	9
Figure 2.8 ViSHARD10	9
Figure 4.1 The alternative revolute z axis.....	16
Figure 4.2 Main axis arrangement.....	16
Figure 4.3 Spherical wrist mounted to the bottom of z axis	17
Figure 4.4 Spherical wrist mounted on top of the z axis.....	17
Figure 4.5 Typical spherical wrist	18
Figure 4.6 Placement options for the spherical wrist.....	19
Figure 4.7 Comparison of link lengths and workspace	20
Figure 4.8 Workspace with a hole in the middle	21
Figure 4.9 Joint axes assignment	22
Figure 4.10 Complete axes assignment	22
Figure 5.1 Displacement distribution of link 1	30
Figure 5.2 Displacement distribution of link 2	30
Figure 5.3 Displacement distribution of link 3	31
Figure 5.4 Displacement distribution of link 4	31
Figure 5.5 Displacement distribution of link 5	32
Figure 5.6 von-Mises stress distribution for link 1	33
Figure 5.7 von-Mises stress distribution for link 2.....	33
Figure 5.8 von-Mises stress distribution for link 3	34
Figure 5.9 von-Mises stress distribution for link 4.....	34
Figure 5.10 von-Mises stress distribution for link 5.....	35

Figure 5.11 The inputs and outputs of the N-E algorithm	37
Figure 5.12 Total joint torque requirement and its components for shoulder joint, high joint speed, high end effector force/torque case	39
Figure 5.13 Total joint torque requirement and its components for shoulder joint, high joint speed, low end effector force/torque case	40
Figure 5.14 Total joint torque requirement and its components for shoulder joint, low joint speed, low end effector force/torque case	40
Figure 5.15 Total joint torque requirement and its components for shoulder joint, low joint speed, high end effector force/torque case	41
Figure 5.16 Total joint torque requirement and its components for elbow joint, high joint speed, high end effector force/torque case	41
Figure 5.17 Total joint torque requirement and its components for elbow joint, high joint speed, low end effector force/torque case	42
Figure 5.18 Total joint torque requirement and its components for elbow joint, low joint speed, low end effector force/torque case.....	42
Figure 5.19 Total joint torque requirement and its components for elbow joint, low joint speed, high end effector force/torque case.....	43
Figure 5.20 Total joint torque requirement and its components for vertical axis joint, high joint speed, high end effector force/torque case	43
Figure 5.21 Total joint torque requirement and its components for vertical axis joint, high joint speed, low end effector force/torque case	44
Figure 5.22 Total joint torque requirement and its components for vertical axis joint, low joint speed, low end effector force/torque case	44
Figure 5.23 Total joint torque requirement and its components for vertical axis joint, low joint speed, high end effector force/torque case	45
Figure 5.24 Total joint torque requirement and its components for roll 1 joint, high joint speed, high end effector force/torque case.....	45
Figure 5.25 Total joint torque requirement and its components for roll 1 joint, high joint speed, low end effector force/torque case.....	46
Figure 5.26 Total joint torque requirement and its components for roll 1 joint, low joint speed, low end effector force/torque case.....	46
Figure 5.27 Total joint torque requirement and its components for roll 1 joint, low joint speed, high end effector force/torque case.....	47

Figure 5.28 Total joint torque requirement and its components for pitch joint, high joint speed, high end effector force/torque case.....	47
Figure 5.29 Total joint torque requirement and its components for pitch joint, high joint speed, low end effector force/torque case.....	48
Figure 5.30 Total joint torque requirement and its components for pitch joint, low joint speed, low end effector force/torque case.....	48
Figure 5.31 Total joint torque requirement and its components for pitch joint, low joint speed, high end effector force/torque case.....	49
Figure 5.32 Total joint torque requirement and its components for roll 2 joint, high joint speed, high end effector force/torque case.....	49
Figure 5.33 Total joint torque requirement and its components for roll 2 joint, high joint speed, low end effector force/torque case.....	50
Figure 5.34 Total joint torque requirement and its components for roll 2 joint, low joint speed, low end effector force/torque case.....	50
Figure 5.35 Total joint torque requirement and its components for roll 2 joint, low joint speed, high end effector force/torque case.....	51
Figure 5.36 Animation window	52
Figure 5.37 Maxon motor and driver connections for current control mode	56
Figure 5.38 F/T sensor GUI.....	57
Figure 5.39 F/T sensor VB program GUI.....	58
Figure 6.1 PD control performance without fine tuning.....	63
Figure 6.2 PD control performance with fine tuning.....	64
Figure 6.3 PD control with gravity compensation.....	64
Figure 6.4 PD control with gravity and Coulomb friction compensation	65
Figure 7.1 Base and planar elbow manipulator assembly	66
Figure 7.2 Vertical axis mechanism	67
Figure 7.3 Spherical wrist mechanism.....	67
Figure 7.4 Spherical wrist mechanism.....	67
Figure 7.5 Full view of the haptic device	68
Figure 7.6 Close view of the vertical axis and spherical wrist	69

LIST OF SYMBOLS

D	Manipulator inertia matrix
q	Vector of joint variables
\dot{q}	Joint velocity vector
\ddot{q}	Joint acceleration vector
J	Manipulator Jacobian
J_a	Actuator inertia
J_m	Motor side combined inertia
J_g	Reduction system inertia
g_g	Gravity constant
$g(q)$	Gravity effect vector
$C(q, \dot{q})$	Matrix for the computation of centripetal and Coriolis forces
F_e	Force and torque vector exerted by the manipulator tool tip on the environment as expressed in the world frame
α_i	Denavit Hartenberg twist parameter for link i
d_i	Denavit Hartenberg offset parameter for link i
θ_i	Denavit Hartenberg angle parameter for link i
a_i	Denavit Hartenberg length parameter for link i
B_f	Joint viscous friction constant matrix
b_c	Joint Coulomb friction vector
u	Generalized force/torque control input
τ	Vector of joint force/torque
K_{P_k}	Proportional gain for joint k
K_{D_k}	Derivative gain for joint k

ABBREVIATIONS

D-H	Denavit Hartenberg
DOF	Degree of Freedom
E-L	Euler Lagrange
F/T	Force / Torque
GUI	Graphical User Interface
LHifAM	Large Haptic Interface for Aeronautics Maintenance
M/S	Master / Slave
MIS	Minimally Invasive Surgery
MS	Microsoft
N-E	Newton Euler
SCARA	Selective Compliant Articulated Robot for Assembly
SHaDe	Spherical Haptic Device
SPIDAR-G	SPace Interface Device for Artificial Reality with Grip
TCP/IP	Transmission Control Protocol / Internet Protocol
VB	Visual Basic
VC	Visual C
ViSHARD	Virtual Scenario Haptic Rendering Device with 6 DOF
VR	Virtual Reality

1 INTRODUCTION

Haptic is a term that refers to sense of touch. Haptic manipulators or interfaces are force-reflecting devices which allow a user to touch, feel, manipulate, create and/or alter simulated objects in a virtual environment. The main purpose of using haptic devices is to enhance user experience when he/she is interaction with a simulated or remote environment. In order to realize tele-presence completely all related information should be at disposal of the user. Visual and aural feedback topics are well-covered in the literature in comparison to haptics. Haptic feedback conveys physical information about the environment such as inertia, friction, compliance, and roughness which can not be directly sensed by other sensory systems.

A haptic interface together with computer hardware and software produces the sensation of touch and interaction with the environment. The environment in which the device is used can be either real physical surrounding or a simulated environment generated by software. Virtual environments might contain objects with masses and friction, springs and dampers and virtual walls. Examples of real environments might be remote locations or relatively nearby locations where user cannot access due to hazardous conditions.

It has numerous application areas, such as robotic surgery, virtual reality (VR), tele-operation, entertainment industry etc. MIS (Minimally Invasive Surgery) is one of the application areas where haptic feedback is gravely desired. Compared to traditional surgery procedures, MIS employ small incisions through which the cameras and instruments are passed to carry out the operation. Haptic feedback is essential in such an application since the surgeon do not have direct visual or tactile feedback. It enables the surgeon to determine the rigidity of the tissue he/she is manipulating. ZEUS surgery robot from Computer Motion Inc. and DaVinci from Intuitive Surgical Inc. are two examples of widely-used surgery robots which do not have force feedback. Integration

of haptic feedback to these devices could not only improve the quality of operation but also increase the speed of the surgeon [1].

Virtual Reality applications are used in various industrial areas such as medical operation, tele-operation and entertainment. With the incorporation of haptic feedback to VR applications, user's perception of the environment becomes more realistic. Haptic devices are the successors of the historical hand controllers used in tele-operation and today find a wide usage in the VR applications. As a natural result of the improvements in the computer technology, rendering of virtual environments in real-time could be achieved. Development of virtual reality technology brought along the increasing demand for haptic devices. These robotic mechanisms form the kinesthetic counterpart of the VR environment as a complement to the visual, in some cases also aural, feedback. Desktop haptic devices are already finding usage as force "displays" for computer games, nano-manipulation applications and surgical simulators.

The main objective of this technology is to create a realistic force-position interface between the user and the VR environment. The device commands motion and force to its slave counterpart, it receives feedback signals, depending on the control algorithm, and reflects the forces felt by the slave side to the user. The quality of this interface can be evaluated in terms of "impedance accuracy" and "impedance resolution" [2]. Impedance accuracy is the criteria for matching the impedance of the haptic device to the environments. Impedance accuracy plays an important role in the high-torque applications such as driving simulators and smart exercise machines. Impedance resolution or fidelity refers to the sensitivity of the device for discrimination of different impedances. Fidelity is more crucial for dexterous applications such as surgery where the impedance of the environment is changing.

In order to achieve high impedance accuracy and resolution, dynamics of the haptic device should be optimized. Natural dynamics of the device diminish the realism of the haptic feedback since they are sensed by the user as a part of the simulated environment. Robotic researchers show great effort to reduce the natural dynamics of the manipulators by means of using more efficient drive trains and transmission mechanisms or higher strength-to-weight ratio materials.

However, reduction of the natural dynamics cannot be achieved further by physical means for high force/torque output devices. For high output purposes, usage of large actuators, drive mechanisms and linkages lead to more inertia and friction thus resulting in high natural dynamics. The demand for haptic devices with high

force/torque capability is obvious since traditional industrial manipulators are used as haptic interfaces. As illustrated in [3], [4] industrial manipulators are used as driving and flight simulators. Motorized “smart” exercise machines [5] and Astronaut extravehicular training systems [6], [7] are other examples of application areas of manipulators as high output haptic devices.

High fidelity criteria may also suggest that the dynamics of the device should be minimized relative to the impedance of task environment. Although the output of the haptic device is adequate, natural dynamics of the device might impair the impedance discrimination performance. During surgical procedures where the environmental impedance is changing, stiffness encountered during the penetration of the scalpel to a layer of tissue is a significant example of this phenomenon [8], [9].

In addition to mechanical improvement to reduce dynamics, active control can be utilized to further cancel dynamical effects. Dynamics compensation can be employed as model feedforward or force feedback from an F/T sensor mounted on the haptic device itself. Gravity and friction feedforward are also used in dynamic compensation, however to employ inertial compensation force or acceleration feedback is required. Inclusion of feedback in the control loop leads to a more robust design as well, especially when the physical properties of the haptic device are changing.

What this thesis aims at is the development of a harmonious collection of hardware and software components to form the infrastructure for general purpose haptic interaction. The primary specifications which are tried to be met are a large workspace and high force/torque capacity. Dynamic and kinematic properties, sensor and actuator specifications, strengths and weaknesses of the designed system as a haptic interface are presented in detail. What this thesis is not about is the development of haptic control algorithms. The focus is on kinematic arrangement, mechanical design and instrumentation.

The next chapter presents a survey on haptic interfaces and haptic master arms. Chapter 3 develops the design criteria employed for the master arm designed in this thesis. The design of the kinematic arrangement to fulfill the workspace specifications follows in Chapter 4. Chapter 5 discusses the selection of actuators and transmission systems based on stress analysis and dynamics simulations. Sensor selection and control hardware integration is also presented in this chapter. A set of dynamics compensation tools are presented in Chapter 6. Chapter 7 discusses the production of the device, and evaluates the built mechanism. Finally, conclusions are presented.

2 LITERATURE SURVEY

The evolution of haptic devices dates back to the first “force feedback” system developed by Goertz for remote handling of radioactive materials. This system featured a master/slave (M/S) architecture where the master and slave arms were identical and were connected to each other via rigid mechanical link (Figure 2.1). After a while, these rigid links were replaced with servomotors which enabled the usage of the system over larger distances [10].



Figure 2.1. The first “force feedback” system developed by Goertz

Before emergence of haptic devices, master/slave manipulators were used for tele-operation. In the beginning, passive replicas of the master manipulator were used at the remote site, which were commanded by the operator via the master manipulator. Later, master arms were motorized so that they could provide force feedback to the operator which was present on the slave side. Addition of force feedback to the M/S system increased task execution speed, especially in unpredictable or changing environments.

Computational requirements were minimal since M/S systems employed joint-to-joint control. With the development of computer technology, complex kinematics

computations could be carried out in real-time. This released the limitation of constructing master and slave arms identical. The JPL Force Reflecting Hand Controller was one of the first systems that employed different kinematics arrangement and it had better resolution than the devices built earlier [11].

Later on, these M/S slave systems were begun to be used for simulation of virtual environments or reproducing forces sensed in a real physical environment. Usage of haptic devices brought new research areas with it. Transparency or low dynamics issues were scrutinized.

There are various haptic devices in the literature that feature different kinematic structures, actuators, number of DOF, and have ranging workspace and force capabilities. All of these devices have their advantages and disadvantages depending on the application areas. Although it is still at an early stage, commercial haptic devices are also available.

Pantograph is also a parallel mechanism device which was designed by [12] in McGill University. Pantograph was initially designed as 2 DOF, however there are different versions of that device that employ more DOF [13], [14]. It has a planar structure which the user commands with the fingertip thus enabling the device feedback forces. This process resembles exploring a surface. (Figure 2.2)



Figure 2.2 The Pantograph linkage

SHaDe is a haptic device designed recently by members of department of mechanical engineering, Laval University [15]. This haptic device differs from other

devices in the literature with its spherical structure. It has three DOF and only gives rotational feedback around a central fixed point. The aim of the authors was to emulate the human wrist. It has some advantages compared to other devices such as pure rotation around a point located inside the user's hand, large workspace and ergonomics. All actuators are fixed to the base of the device thus yielding a rigid structure. A force sensor is also used, placed between the end-effector and the joystick, in order to measure torques at the central point.



Figure 2.3 SHaDe

SPIDAR-G [16] (Space Interface Device for Artificial Reality with Grip) is a tension-based force feedback device that has seven DOF. It allows the user to interact with the virtual objects by manipulating two hemispherical grips located at a center point. Haptic sensation is achieved by controlling the tension of eight cables which are connected to the vertices of a cube. Its characteristics are smooth force feedback, no backlash, low inertia and safety. It is ideally suitable for engineering design applications.

One of the most popular commercial haptic devices is SensAble's Phantom. Several versions of this haptic device are available. Phantom Desktop [17], which is also available in Sabanci University Mechatronics laboratory, has six degree of freedom and three degrees of force feedback. It is a portable device and it can be connected to any computer having a parallel port. It provides the position of its stylus in x, y, and z axes and the rotation of its stylus as roll, pitch, yaw forming a total of six degree freedom. Force feedback is provided for only x, y, and z axes at a maximum force of 1.75 Newton. It has a purely serial kinematic structure and do not employ force or

torque sensors. It is commonly used for many types of haptic research and the freeform modeling applications.

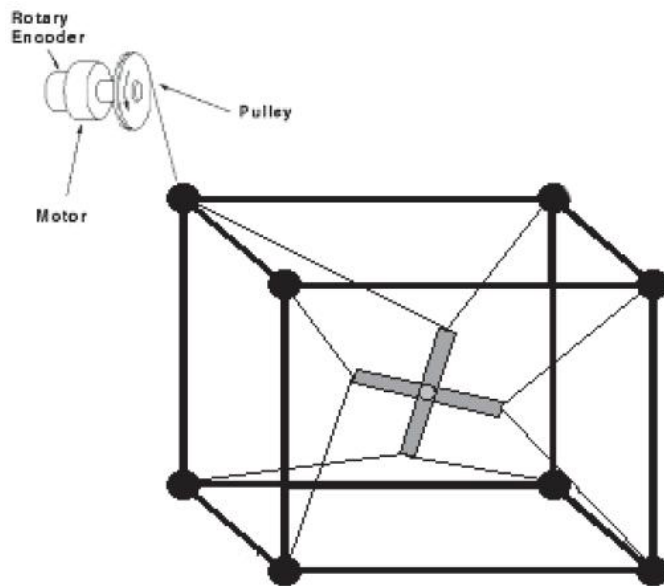


Figure 2.4 SPIDAR-G



Figure 2.5 Phantom desktop

Another interesting haptic device with its huge structure and workspace is LHifAM, (Large Haptic Interface for Aeronautic Maintainability) [18] which is specially designed for aeronautic industry. It has a serial structure and provides 6 DOF movement and 3 DOF force feedback, with a force sensor integrated in its spherical wrist. Its large workspace and possibility for the user to work in different positions are remarkable features of LHifAM (Fig 2.6).

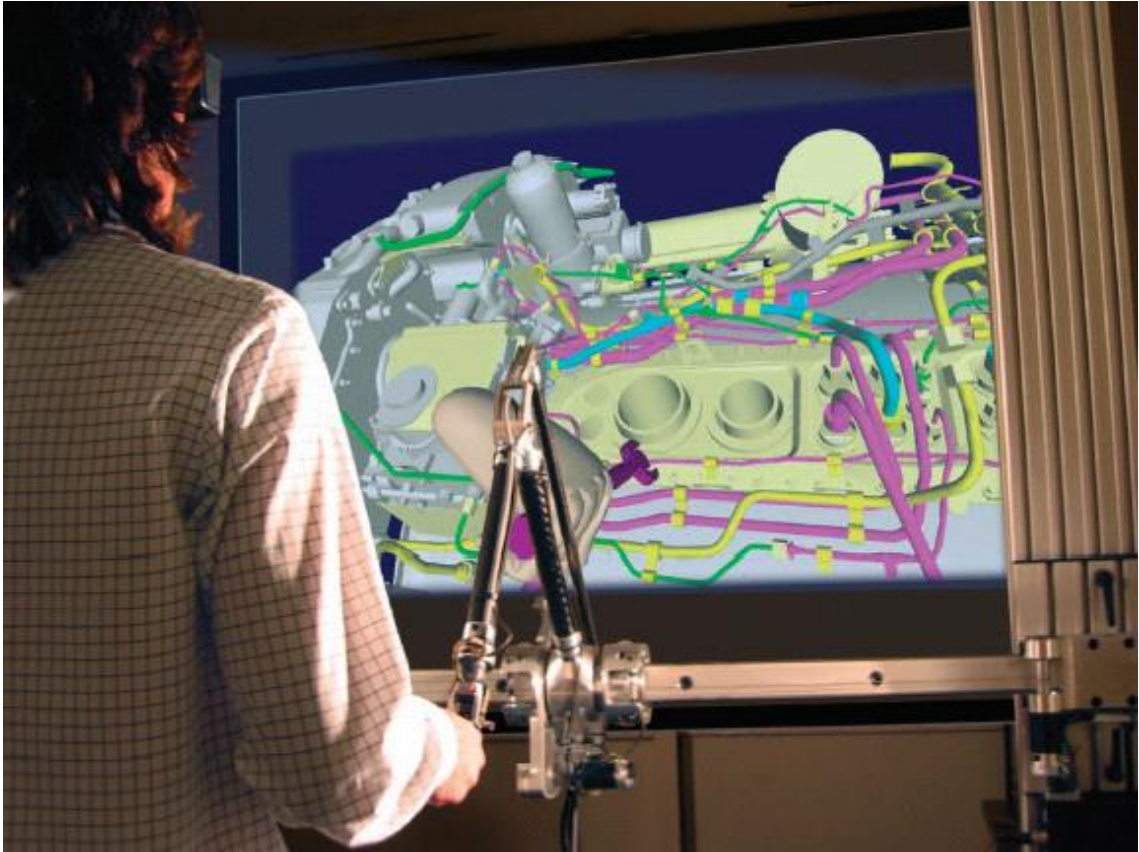


Figure 2.6 LHifAM

VISHaRD6 [19] (Virtual Scenario Haptic Rendering Device with 6 DOF) shown in Figure 2.7 is another haptic device that aims to overcome the force and workspace limitations of other devices. It has a purely serial structure and employs force sensor. Also, a kinematically redundant version (Figure 2.8) of that haptic device is also built, for more flexibility [20]. Both of these devices provide comparatively large workspace and high force capability.

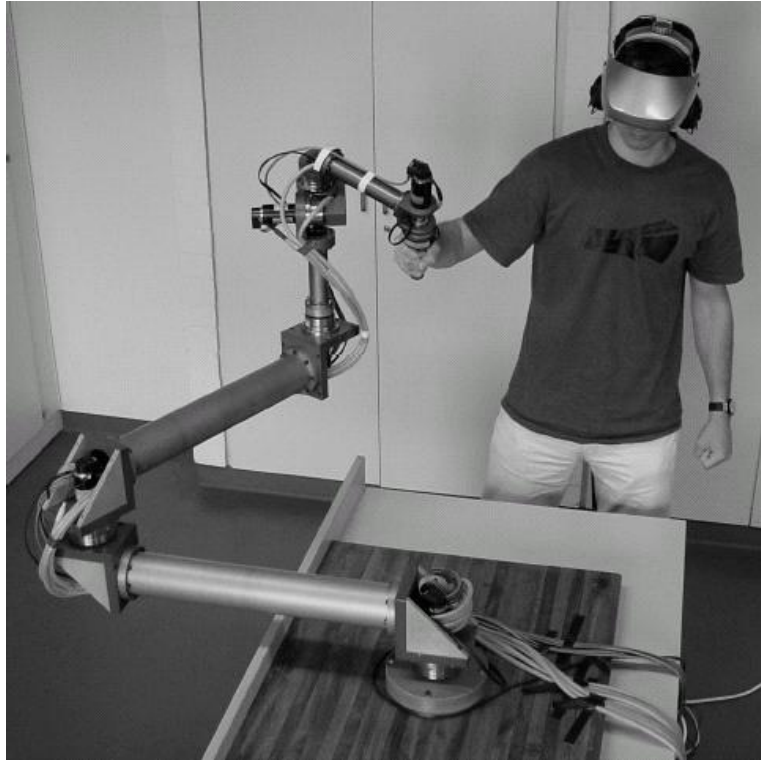


Figure 2.7 ViSHARD6

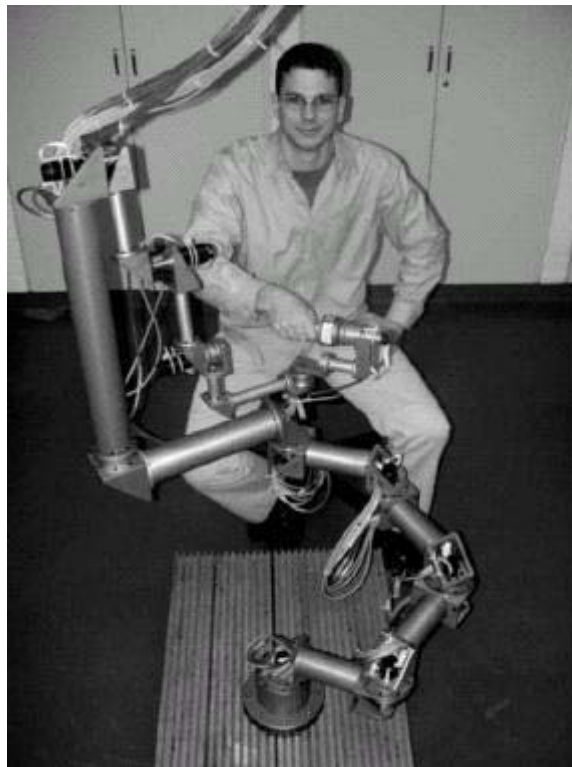


Figure 2.8 ViSHARD10

3 DESIGN CRITERIA

3.1 Main Design Criteria

Depending on the application area, haptic interfaces with different features and capabilities are designed. However, there are three major criteria that have to be satisfied regardless of the usage purpose of the device [21]. These main criteria can be summarized as below:

- Free space must feel free
- Solid objects must feel stiff
- Virtual or “real” constraints must not saturate easily

The first criterion implies that the natural dynamics of the device should not disturb the user’s perception of reality. Apparent mass and friction of the device should be reduced as much as possible. Through active control or passive design required conditions could be met.

In some cases, dynamics of the device might be reduced relative to the task environment. For example characteristics of the environment in a micro-manipulation task and an aeronautic training task are obviously different. Different applications might require different dynamics. However, generally obtaining the minimum dynamics is preferred.

The second criterion imposes that the stiffness of the device should be realistic enough to convince the user that he/she is in contact with a solid object, such as immovable wall. Either in a VR application or a tele-operation task, the device should be resistant enough to simulate a solid object. The stiffness coefficient is generally taken 20 N/cm as minimum. To satisfy this criterion mechanism should be designed as rigid as possible or a high bandwidth controller should be employed. Maximum

achievable stiffness depends on the natural frequency of the device and the resolution of the sensors and actuators. Thus these factors have to be kept in mind during the design procedure.

In order to satisfy the third criterion, force capacity of the device should be high enough to simulate virtual solid objects. Force requirement changes according to the task. For instance, fingertip contact forces rarely exceed 10 N. However, grip force of the hand is much more. To avoid saturation, high force/torque actuators have to be used because it is directly related to the peak torque of the actuation mechanism.

The following sections describe additional design criteria and the specific choices made in this thesis.

3.2 Ergonomics

Ergonomics is another important criterion that has to be taken into account during design procedure. Depending on the task, operators might have to work for long periods. Fatigue and discomfort impair the operator's performance. Haptic devices are designed as support machines for some critical tasks, degrading effects of non-ergonomic design could diminish the operation efficiency. In the case of SHaDe [15], with a structure appropriate for simulation of human wrist, users can use the device while their arms resting on the desk. This avoids the user to hold his/her arm up unnecessarily.

In the design presented in this thesis we assume that the operator follows the virtual world from a desktop computer monitor in front of him/her. The ergonomics criterion is addressed by choosing the sitting posture for the operator, and assigning the device dimensions in such a way that all points in the workspace can be reached by the operator from this posture. This implies that the device should be a desktop one or it should easily be placed next to the operator if it has to have a separate base.

Also considering that the typical working environment is occupied by a variety of other interface hardware (keyboard, mouse, buttons key switches etc. depending on the application), a narrow cross section base for the mechanical interface is desirable over a large base, which would be problematic to fit into the working area of the operator.

3.3 Workspace

Workspace consideration is an essential part of the haptic device design. Usually, obtaining the largest workspace without sacrificing the performance of the device is desired.

In this work, as stated in the discussion of ergonomics, the position workspace of the mechanical interface is defined by the reach of an arm of a sitting human operator. For the average user, the range reached by the palm of a hand can be described by a rectangular prism of 50x70 cm base dimensions and 25 cm height. These dimensions are based on the assumptions that the upper body position and orientation are kept fixed and that the hand is not raised over the shoulder height and not lowered below the standard desktop height.

Orientation workspace of the tool tip has to be considered as well as the position workspace. In contrast to the positional workspace, which can be defined with the assumptions in the paragraph above, the flexibility of human joints varies a lot from human to human. Therefore, also considering that large ranges of revolute motion can be realized by state of art actuators, largest orientation space without exceeding 360° motion at the revolute joints of the mechanical device is inferred as a design specification.

3.4 Force/Torque Capacity

As mentioned above hard surfaces in the virtual environment should feel stiff and virtual constraints should not be saturated easily. In addition to these requirements, task dependent specifications also put demands on the minimum force/torque capacity of the interface.

As stated in [22], for the average user, index finger can exert 7 N, the middle finger 6 N and ring fingers 4.5 N continuously without experiencing discomfort or fatigue. Total force applied on each finger should not exceed 30-50 N for operator

safety. Considering these facts, a force capacity of 15 N is aimed in the design presented in this thesis. The torque capacity requirement is taken as 1 Nm [23].

3.5 Resolution

Position and force resolution of the device depends on the human sensory system. Minimum resolution of the device, to satisfy haptic feedback criteria, should be better than that of human. As illustrated in [1], resolution of the encoders should be 2700 pulse per revolution for the operator to feel the smallest change in the position. Force sensing resolution of a human is 0.06 N, so the resolution of the force sensing mechanism should be smaller than that value.

The next two chapters present how a suitable kinematic arrangement and hardware components can be selected in order to satisfy the design criteria discussed above.

4 DESIGN OF THE KINEMATICS ARRANGEMENT

The criteria and assumptions presented in Chapter 3 are used in this chapter as guidelines to design the kinematic arrangement and link lengths of a master arm. The sensor and actuator mechanisms and the controller hardware are discussed in the next chapter.

4.1 Parallel or Serial Arrangement?

The following factors considered in the previous chapter favor a serial kinematic arrangement for the haptic device presented in this thesis.

- The position workspace demanded is quite large and this can be addressed much easier with serial mechanisms rather than parallel mechanisms [24].
- The orientation workspace demanded is very large, in the order of 360 about the main axes. (Large roll, pitch, yaw angles range desired.) This is not practical with parallel mechanisms [25].
- The requirement that the base cross section should be small cannot be fulfilled easily with parallel mechanisms. This also eliminates a hybrid design with parallel main axes and a spherical wrist.

With this argumentation the choice is made for a serial mechanism.

4.2 Spherical Wrist

The requirement of large orientation workspace can be fulfilled with a spherical wrist structure with minimal contribution from the main axes. The spherical wrist structure also enables a very convenient inverse kinematics solution for many manipulator kinematic arrangements [26]. Therefore in this work a design decision is made for a compact spherical wrist.

4.3 Kinematic Arrangement of the Main Axes

In the decision for the main axes, one of the primary factors is the effect of the gravity. Also important are frictional factors. The main axes (between the base and the wrist) should preferably be not affected by those factors too severely. The articulated 3 DOF elbow structure [26], which is a popular arrangement for the main axes of industrial manipulators, is hence eliminated because of its nature prone to gravitational forces. The Cartesian xyz system is also not suitable because it violates our rule of minimal cross section for the base, if supported by parallel double linear guides. On the other hand the bearings would be too heavy if supported by a single linear guide over the large positional workspace. The SCARA (Selective Compliant Articulated Robot for Assembly) like main axes structure stands out by its immunity to gravity and minimal base cross section and therefore this structure is chosen for the first two joints of the mechanical interface. This leaves the question of motion in the vertical direction. The elevator structure, also used in the industrial SCARA, is the natural choice to bridge the SCARA type main two axes and the spherical wrist. Its alternative is a revolte joint; however such a joint shown in Figure 4.1 requires large contribution of the two horizontally placed main links for the vertical motion. Therefore the linear elevation mechanism is chosen as the vertical motion mechanism in this work. The main axes arrangement reached after these design decisions is shown in Figure 4.2

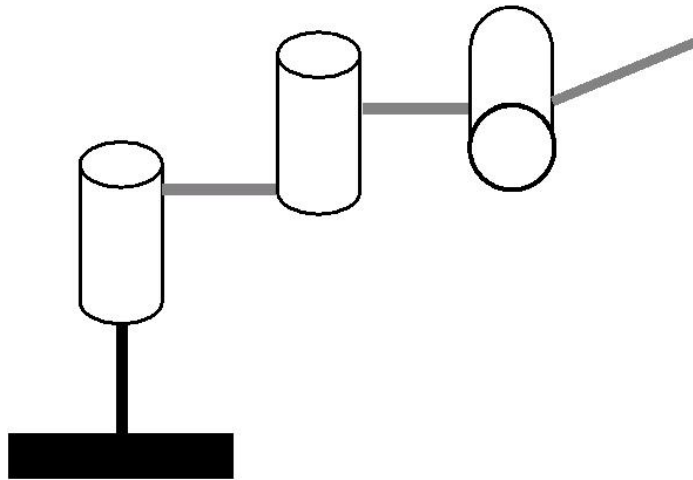


Figure 4.1 The alternative revolute z axis

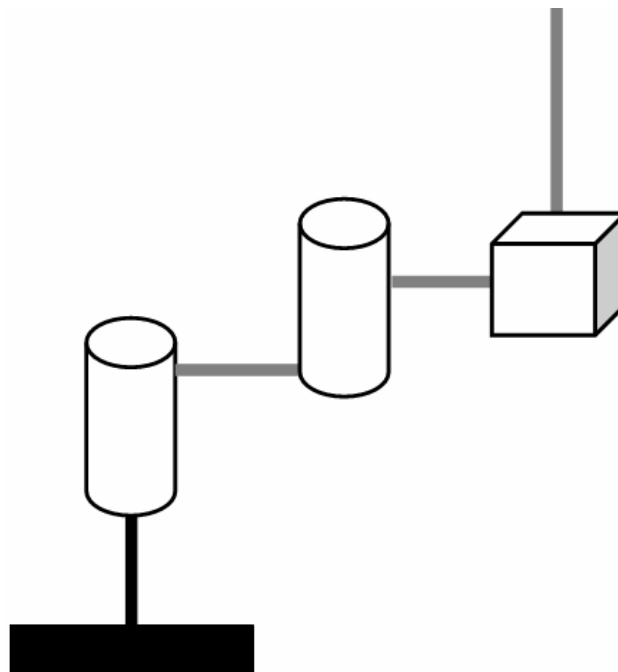


Figure 4.2 Main axis arrangement

4.4 Placement of the Spherical Wrist

For the placement of the spherical wrist, we have a number of choices. Some of those choices are investigated and the most suitable configuration for the haptic device is determined. It can be placed on top of the elevator axis or just on the bottom of it. The location at the bottom of the elevator link (vertical axis) is typical for the wrist joint of an industrial SCARA robot (Figure 4.3). However, in our case the typical use of

a haptic interface should be considered. The wrist at the bottom structure for a haptic interface implies that virtual workpiece is positioned high up in the virtual world. However, manipulating workpieces or objects on top of a desk or other workbench is more typical for human and many machines. Therefore the wrist in the presented work is positioned on top of the vertical link (Figure 4.4).

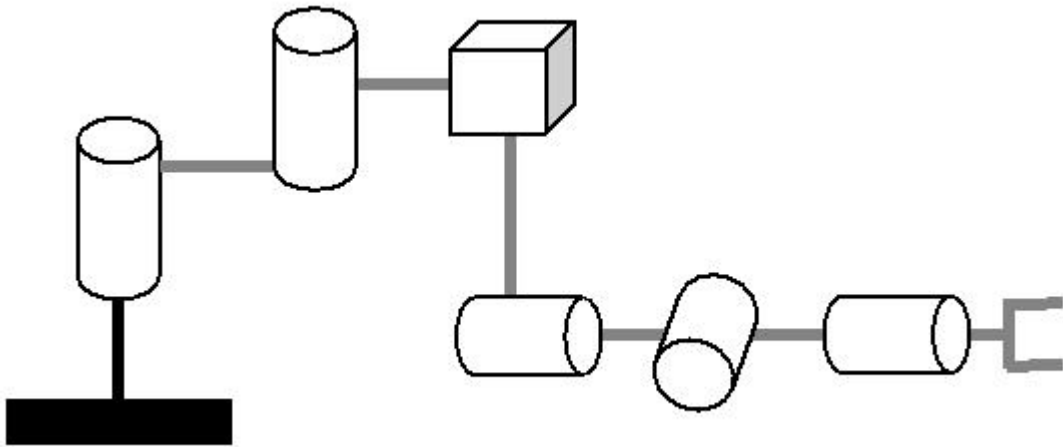


Figure 4.3 Spherical wrist mounted to the bottom of z axis

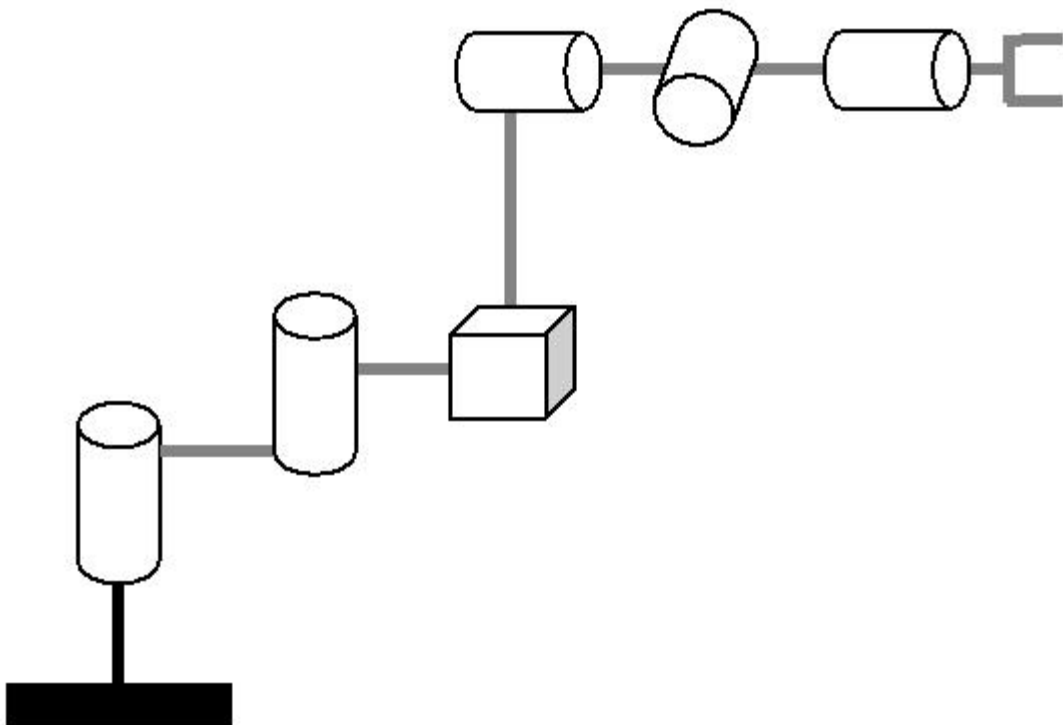


Figure 4.4 Spherical wrist mounted on top of the z axis

Typical spherical wrist shown in Figure 4.5 is composed of three revolute axes, in the roll-pitch-roll arrangement. Once the first roll is placed, the rest of the wrist location is determined. However, the placement of the roll axis relative to the uppermost point of the vertical link can be in two different ways shown in Figure 4.6. The one shown in Figure 4.6a has the largest orientation space for a user approaching and holding the tool tip from above. The one in Figure 4.6b is more suitable for a user holding the tool tip from lateral direction and it is more advantageous for the problem definition and the requirements discussed in Chapter 3. This arrangement is the one chosen for the haptic interface presented in this thesis.

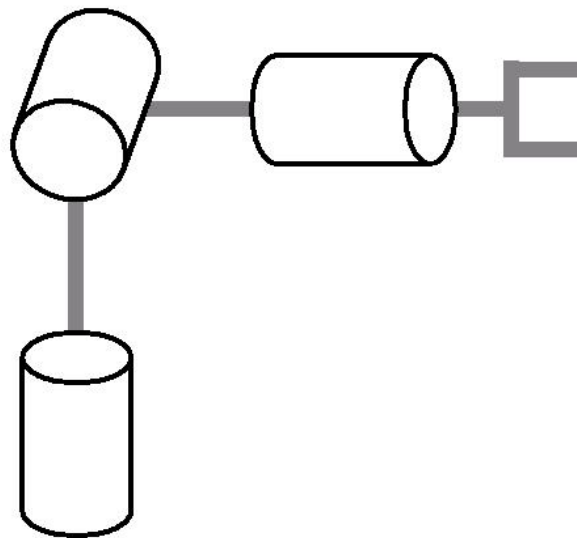


Figure 4.5 Typical spherical wrist

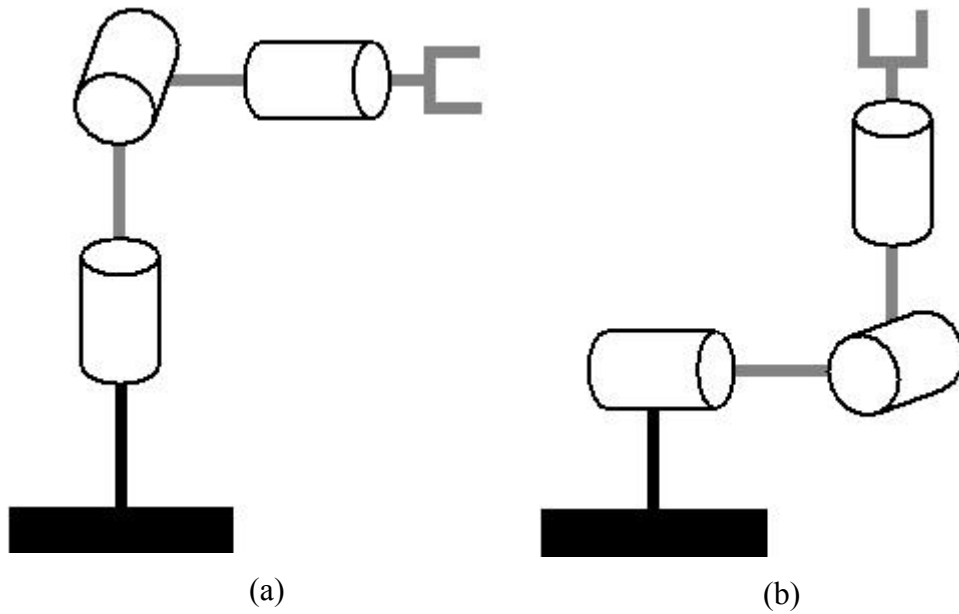


Figure 4.6 Placement options for the spherical wrist

4.5 Link Sizes

Firstly, the link sizes and the working ranges of the three main axes will be considered. The discussion for the link sizes for a compact spherical wrist to be added on top of these main links will follow.

Although the last offset (the length of the last roll link) also contributes to the x , y and z position range of the manipulator; it will be excluded from the x , y and z position range computations. This is equivalent to consider the set of points which can be reached by the center of the spherical wrist as the position range. The discussion in the previous chapter defines a prism with 50 cm x 70 cm x 25 cm as the required position workspace. Because of the orthogonal arrangement of the horizontal plane and the vertical joint axis, the x - y workspace and the z workspace problems can be considered separately. It is obvious that the vertical axis work range should be at least 25 cm to cover the required z range.

For the working area on the horizontal plane with the first two links of the SCARA structure (in other words for the planar elbow manipulator) at least the following two solutions apply as shown in Figure 4.7. The solution on the left seems to be more advantageous because smaller links can be used to cover x - y workspace. However it has a major disadvantage that reaching the points at the rear side of the arm

would cause the human operator to touch the base link. These would be a rather uncomfortable usage for the operator and therefore it is abandoned at the cost of longer links shown in Figure 4.7b on the right hand side.

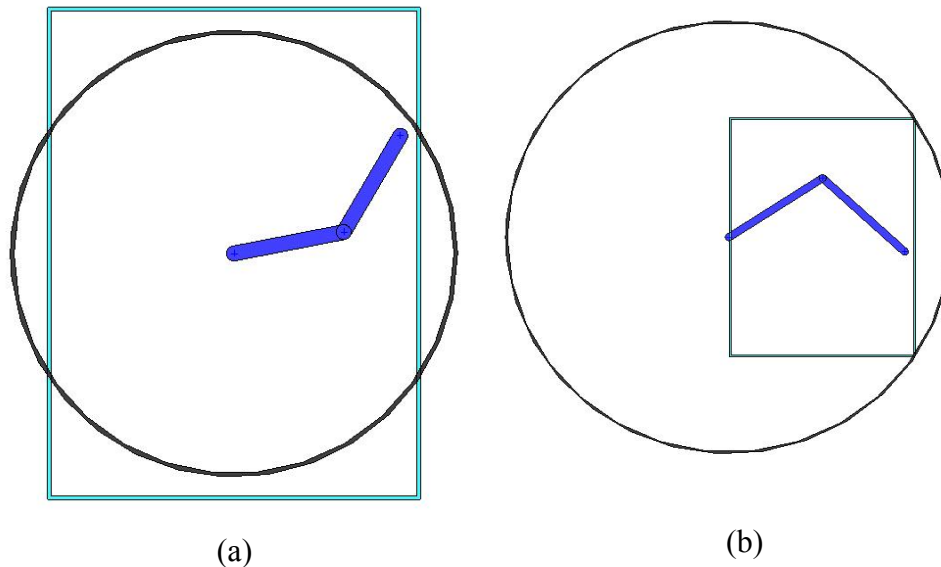


Figure 4.7 Comparison of link lengths and workspace

These figures also show that sum of the link lengths of link 1 and link 2 should be at least 60 cm to cover the x - y workspace. A natural choice for the proportion of the first and the second link lengths is 1:1. The advantage of 1:1 proportion is that the whole of the interior of a 60 cm diameter workspace can be covered by the end of the second link without leaving a “hole” at the center of the workspace (Figure 4.8). Hence the first two link lengths are 30 cm each. The last offset (from spherical wrist to handle tip) is taken as 12.5 cm which is small enough to keep the size of the whole machine as a desktop one and large enough to be kept by the human hand firmly.

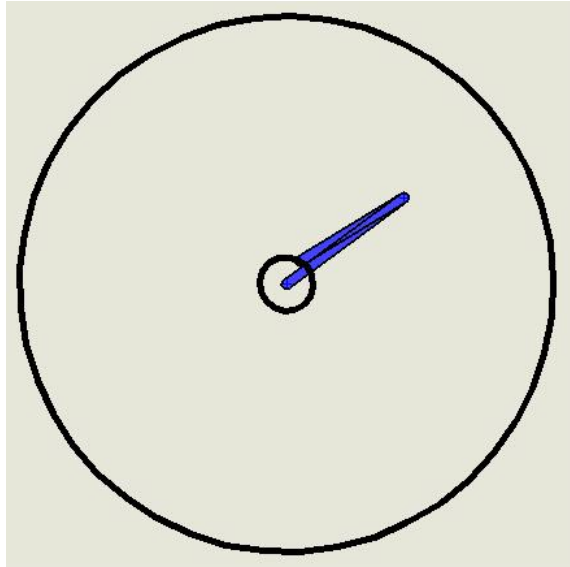


Figure 4.8 Workspace with a hole in the middle

4.6 Axis Assignment and Denavit - Hartenberg parameters

The discussion in the previous sections of this chapter enables us to assign the joint axes and to form the Denavit Hartenberg table for the master arm. Some of the values of the link lengths and offsets can be determined by the discussion above too (two main link lengths are already determined). Still, some others have to be left parametric (and unknown) in this chapter. They can only be computed after the selections of the actuation and transmission mechanisms, and hence this computation is left to the next chapter.

The joint axis assignment is shown in Figure 4.9. The origins and x axis assignments which complete the frame assignment are shown in Figure 4.10. The Denavit Hartenberg parameters derived from this figure and from the link lengths obtained before is given in Table 4.1. In this table, the angles θ_1 , θ_2 , θ_4 , θ_5 , θ_6 and the linear displacement d_3 are joint variables.

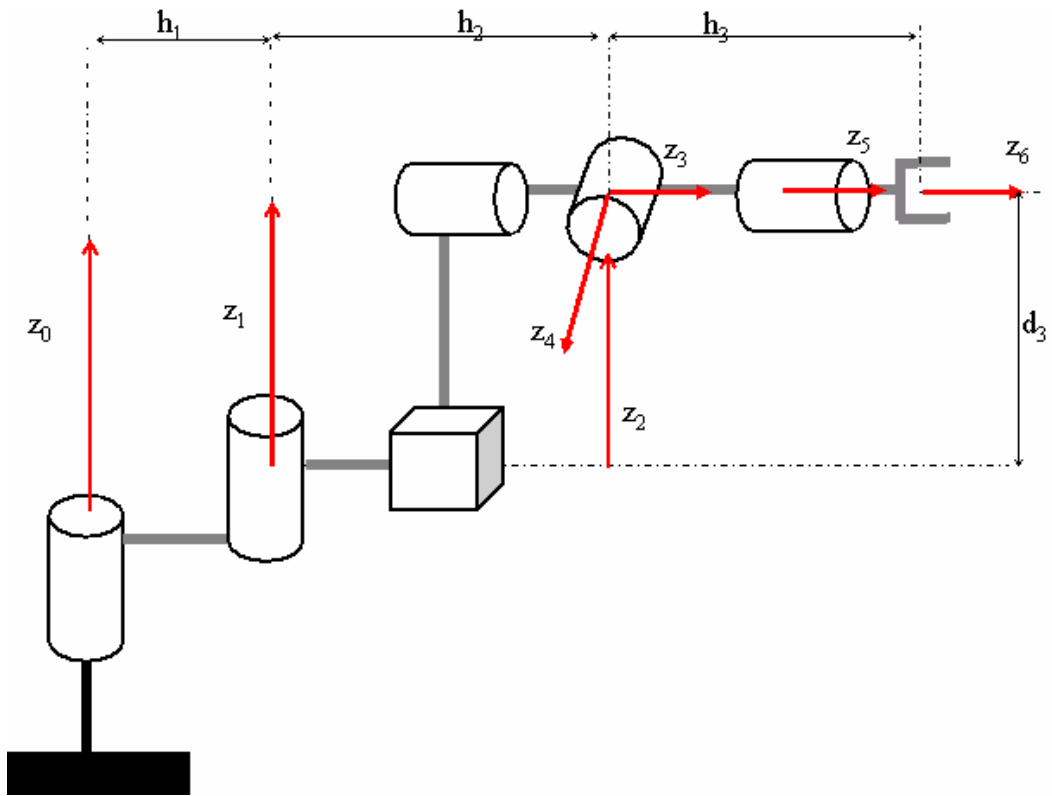


Figure 4.9 Joint axes assignment

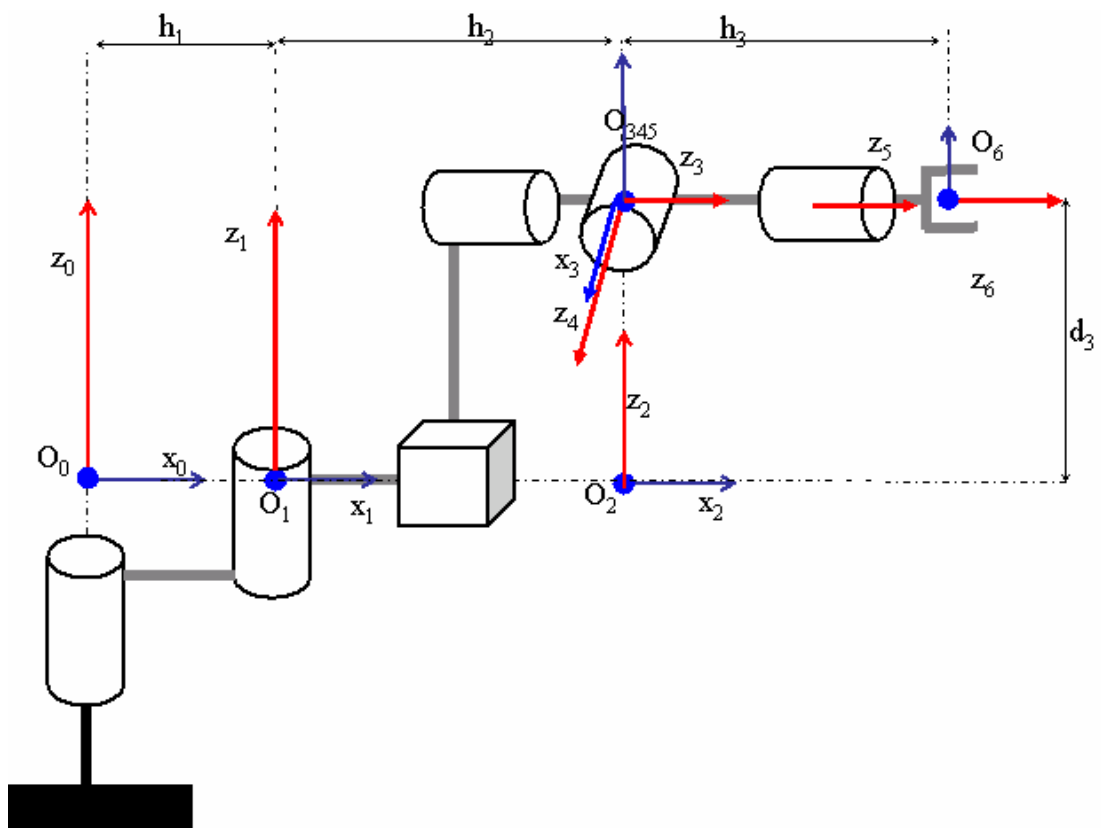


Figure 4.10 Complete axes assignment

Link #	a	α	d	θ
1	h_1	0	0	θ_1^*
2	h_2	0	0	θ_2^*
3	0	-90	d_3^*	-90
4	0	-90	0	θ_4^*
5	0	90	0	θ_5^*
6	0	0	h_3	θ_6^*

Table 4.1 D-H parameters for the designed arm

4.7 Forward Kinematics

The homogenous transformations relating adjacent link frame coordinates are given by the Denavit-Hartenberg matrix formula [26].

$$A_i = Rot_{z,\theta} Trans_{z,d} Trans_{x,a} Rot_{x,\alpha}$$

$$A_i = \begin{bmatrix} c_{\theta_i} & -s_{\theta_i}c_{\alpha_i} & s_{\theta_i}s_{\alpha_i} & c_{\theta_i} \\ s_{\theta_i} & c_{\theta_i}c_{\alpha_i} & c_{\theta_i}s_{\alpha_i} & s_{\theta_i} \\ 0 & s_{\alpha_i} & c_{\alpha_i} & d_i \\ 0 & 0 & 0 & 1 \end{bmatrix} \quad (4.1)$$

When the joint coordinates are given, the homogenous transformation matrix relating the handle frame coordinates to the base frame coordinates can be found as the product of the link-to-link homogenous transformation matrices.

$$T_0^6 = A_1 A_2 A_3 A_4 A_5 A_6 \quad (4.2)$$

4.8 Inverse Kinematics

Inverse kinematics equations of the manipulator also have to be derived, in order to be used in simulation or experiments. Solution of the inverse kinematics is relatively easier since the last three joints form a spherical wrist, thus enabling us to use kinematic decoupling. Given a 4x4 homogenous transformation matrix denoting the end effector position and orientation;

$$H = \begin{bmatrix} R & d \\ 0 & 1 \end{bmatrix} = \begin{bmatrix} r_{11} & r_{12} & r_{13} & p_x \\ r_{21} & r_{22} & r_{23} & p_y \\ r_{31} & r_{32} & r_{33} & p_z \\ 0 & 0 & 0 & 1 \end{bmatrix} \quad (4.3)$$

If $(p_{cx} \ p_{cy} \ p_{cz})$ is the position of the spherical wrist center. Inverse position problem, which is dependent of the first three joint variables $(\theta_1, \theta_2, d_3)$, is easily solved using trigonometric relations. For the first two links, elbow left configuration is selected. The following equations illustrate the relationship between joint variables and spherical wrist center point position.

$$D = \frac{(p_{cx}^2 + p_{cy}^2 - h_1^2 - h_2^2)}{2h_1h_2} \quad (4.4)$$

$$\theta_2 = a \tan 2(\sqrt{1 - D^2}, D) \quad (4.5)$$

$$\theta_1 = a \tan 2(p_{cy}, p_{cx}) - a \tan 2(h_2 \sin(\theta_2), h_1 + h_2 \cos(\theta_2)) \quad (4.6)$$

$$d_3 = p_{cz} \quad (4.7)$$

For the inverse orientation problem, firstly R_3^6 have to be computed.

$$R_3^6 = R_0^3^{-1} R = \begin{bmatrix} r_{11} & r_{12} & r_{13} \\ r_{21} & r_{22} & r_{23} \\ r_{31} & r_{32} & r_{33} \end{bmatrix} \quad (4.8)$$

From the obtained R_3^6 matrix the last three joint variables are obtained.

$$\theta_4 = a \tan 2(r_{23}, r_{13}) \quad (4.9)$$

$$\theta_6 = a \tan 2(r_{32}, -r_{31}) \quad (4.10)$$

$$\theta_5 = a \tan 2(\sqrt{1-r_{33}^2}, r_{33}) \quad (4.11)$$

This completes most of the kinematic arrangement discussions, with the exception of a few link offset parameters. The next chapter discusses the hardware component selections to go one step ahead to the complete design of the haptic device.

5 COMPONENT SELECTION

In the design procedure, motors and gears are firstly assigned for the joints by rough estimates using force/torque capacity requirements and static load considerations. The weight values of the motors, reducers and links starting from the tool tip and moving to the base of the robot are used to determine the static load on the robot links and required thickness of the materials used for the links.

All these weight and shape information is then used in a Newton-Euler based inverse dynamics simulation. The joint torque and forces recorded for demanding reference trajectories and handle forces/torques indicate whether the torque capacities of the chosen motors and reducers are appropriate or not.

The chapter further discusses a number of sensors for the haptic interface and explains how the position and force sensors are selected.

Finally, the controller hardware used is introduced and the hardware and software integration of the selected actuators and sensors is presented.

5.1 Selection of Actuators

Selection of actuators is a fundamental part of the design process. According to the design criteria described in the Chapter 3, appropriate actuator mechanisms should be selected. There are numerous actuator options which can be utilized. In this section, comparison of commonly used actuators is carried out; advantages and disadvantages of usage for haptic devices are discussed. Table 5.1 summarizes the various options [1].

<i>Actuator</i>	<i>Advantages</i>	<i>Disadvantages</i>
<i>DC Motor</i>	<i>Cheap, easy to control</i>	<i>Torque ripple, cogging, high inertia</i>
<i>DC Motor with Gearhead</i>	<i>Easy to control, high torque output, less torque ripple</i>	<i>Play in gears, backlash, high inertia, friction</i>
<i>Special DC Motor</i>	<i>Low cogging, low torque ripple</i>	<i>Expensive</i>
<i>DC Motor with Brake</i>	<i>High stiffness can be simulated</i>	<i>Bulky, difficult to control</i>
<i>Voice Coil</i>	<i>Easy to control, torque at zero velocity, smooth force signals</i>	<i>Low range of motion, suitable components commercially hardly available, Needs special treatment</i>

Table 5.1 Comparison of actuator options

The first actuator that comes to mind is DC motor. Unfortunately ordinary DC motors have some properties that make the use of DC motors as haptic actuators inappropriate. First of all, torque output of the motor depends on the shaft position. This issue causes torque ripple which will be felt by the user. To overcome this problem large number of commutators has to be used or good compensation controller has to be used. Additionally, DC motors have cogging problem and big inertia, which will also impair the user's perception of "reality".

Addition of a gearhead might improve the performance of the DC motor in terms of torque output and torque ripple. Limited torque capacity of a motor can be increased by using a gearbox. Torque ripple becomes less noticeable by the user since addition of gear increases the frequency of the torque ripple. Nevertheless geared motors have some disadvantages. It introduces backlash, friction and high inertia which are undesired in haptic applications. Friction introduced by the gears can be compensated through active control algorithms.

Combination of a motor and a brake unit might solve the problem of producing big forces at zero velocity. In that setup, motor is responsible of creating small forces, when large forces are needed brake can be used. However, addition of a brake unit also adds to the inertia and mass of the motor and complicates the control algorithm.

Specially designed DC motors are available in the market which features coreless design, special windings etc. These motors show no cogging, minimal torque ripple and small inertia depending on the selection criteria [27].

Another option is voice coil actuators. They have some characteristics which make them almost ideal for haptic interfaces: force independent of shaft position, no torque ripple, linear behavior of input current vs. force output. However rotary voice coil actuators might not be useful in cases where range of motion is large. Rotary voice coils have $\pm 60^\circ$ range of motion.

With the discussion above the use of harmonic drive reducers with output bearings and Maxon RE family DC motors stand out as candidates for the transmission and actuation mechanism. Due to their compactness Maxon planetary gears are also candidates for reduction for the joints where the place for assembly is limited. Since reducers and motors are expensive and the delivery times are quite long (in the order of 3-5 months), motor and reducers are selected from the Mechatronics Program inventory. The Maxon DC motors in the inventory range from 20 W to 150 W (20 W, 70 W, 90 W, and 150 W). Due to the starting torque specifications the suitable sizes of harmonic drives, which can be used together with 20 to 150 W Maxon motors, are 25, 20, 17 and 14. Appendix A provides various design data about those sizes.

20 W Maxon RE family DC motors and planetary gears with a reduction ratio of 86:1 are chosen for the wrist axes because of their compact size and light weight. A 90 W DC motor with a planetary gear of reduction ratio 156:1 is used for the elevator axis. For the two main revolute axes which bear the largest tilting moments due to gravity, the size 25 harmonic drives are chosen due to their large output bearing. The motors used are the highest power (150 W) ones.

5.2 Stress Analysis

Regarding the mechanical design procedure, preliminary design is completed. However link shapes and thicknesses are not decided yet. In order to satisfy the design requirements mentioned in Chapter 3, inertia and mass of the device have to be kept minimal. For proper selection of the structure of the links stress analysis has to be carried out. Since the device will be used with low speeds, static analysis of the mechanical design would be sufficient.

Lame shape is used for the links because of simplicity and ease of processing. The link shape and weights are computed for 7075 class aluminum as construction material. This material is used because of its high yield strength over weight ratio.

Since basic analysis is carried out, using COSMOSXpress plug-in of Solidworks, in which the modeling is also done, is sufficient. Analyses carried out are computation of von-Mises stresses and the static safety factor for each link. Displacement distribution is also monitored.

According to the analysis results, material or the thickness values of the links should be modified in iterations. The weight values of the motors, reducers and links starting from the tool tip and moving to the base of the robot are used to determine the static load on the robot links. Initial thicknesses of the links were assigned during preliminary design. In the case of link 6, which is the handle of the device, static loading is negligible since any force applied to that link will be transferred to the former links.

In Figure 5.1 to Figure 5.5 deformation of the manipulator under static loading is illustrated. Contour diagram and maximum and minimum deformation points are shown in the figures. Legend on the right hand side of the figure shows the distribution of contour diagram. It should be noted that displacement on these figures are scaled for better understanding.

Naturally, maximum deflection occurs at the end of the links. Table 5.2 lists the maximum deflection values obtained from the analysis. Tool tip deformation in the z direction under static loading of 15 N, which is the force capacity for the manipulator, is the sum of maximum deflections at each link which is 0.7025 mm.

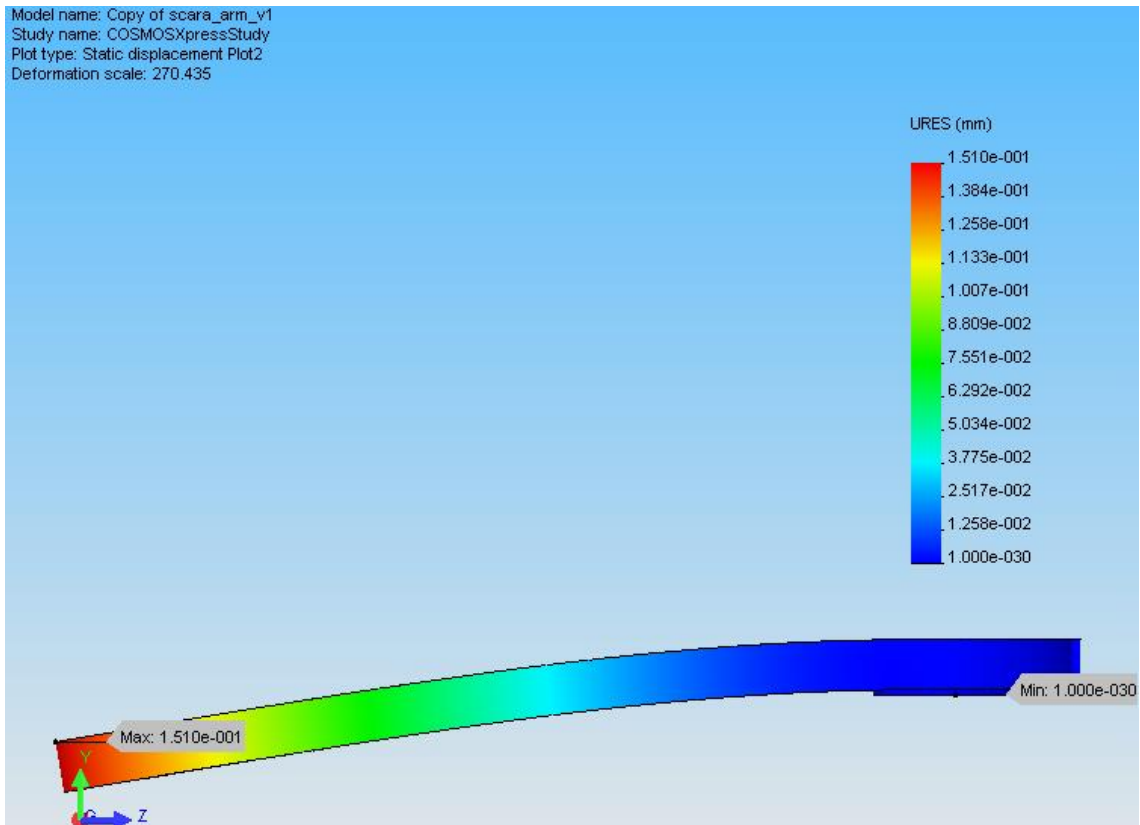


Figure 5.1 Displacement distribution of link 1

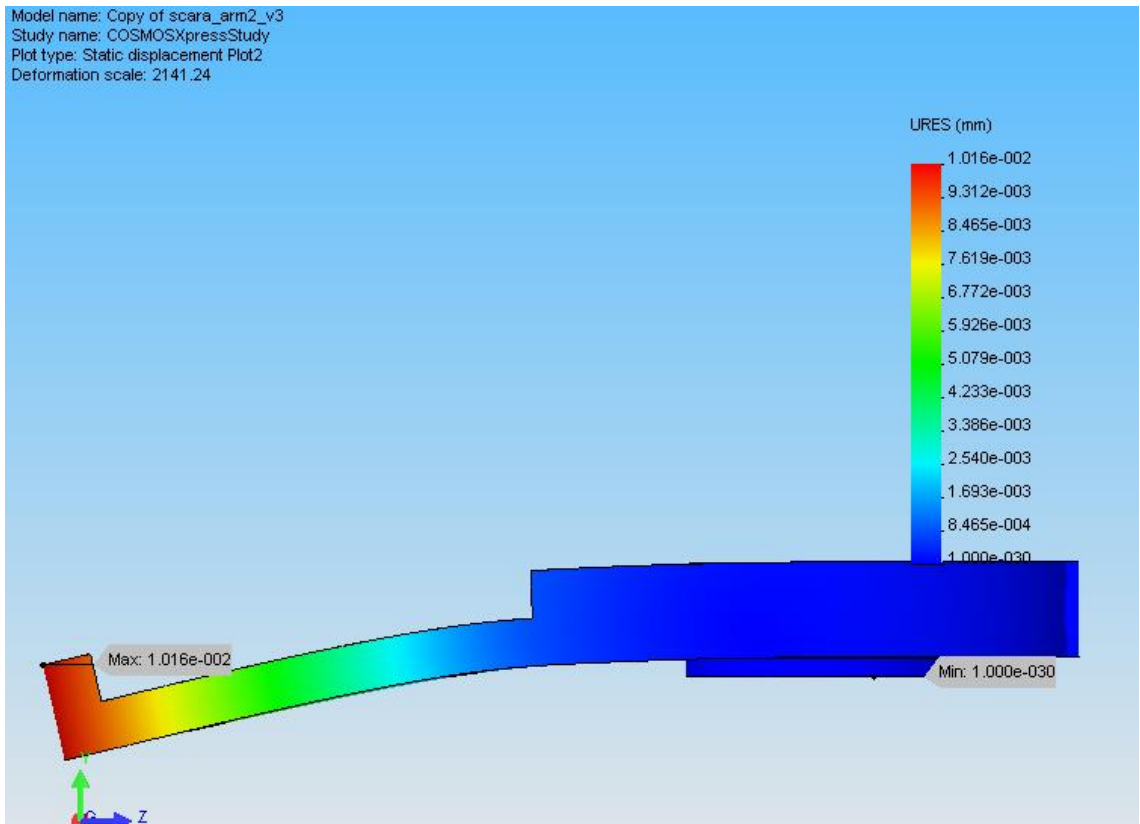


Figure 5.2 Displacement distribution of link 2

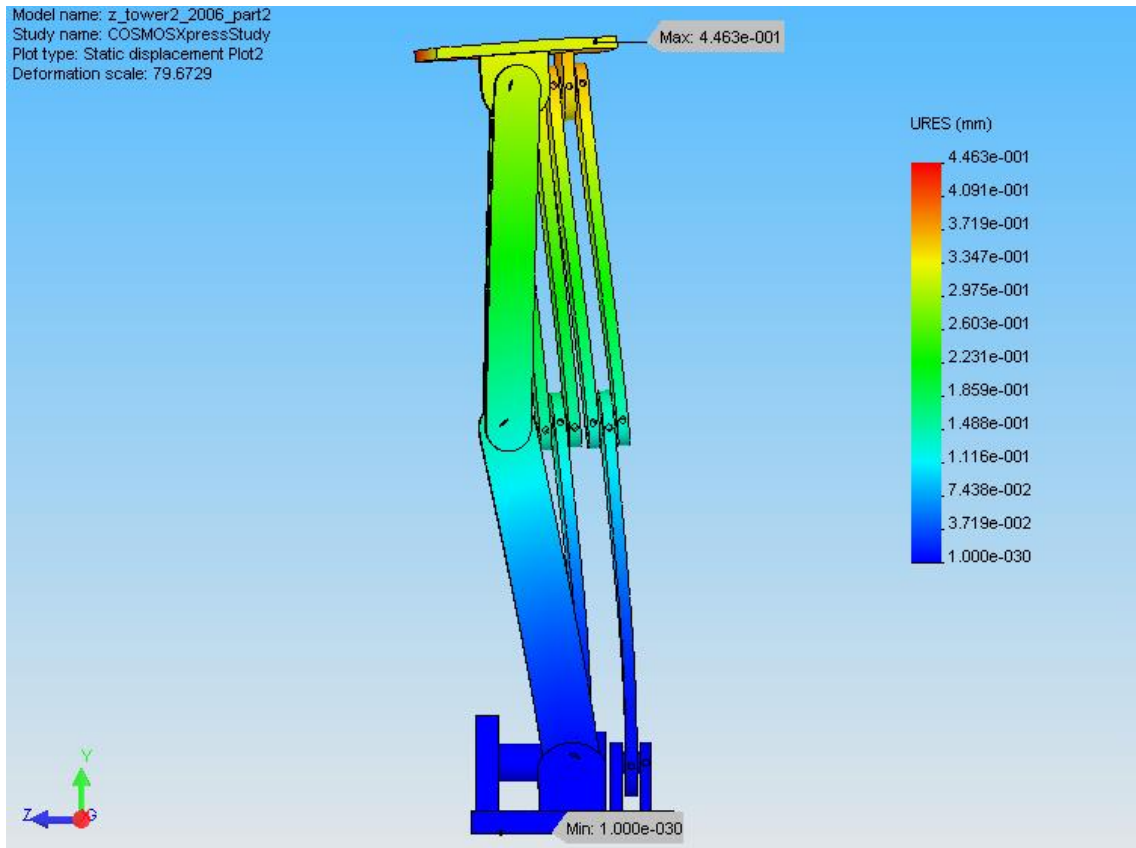


Figure 5.3 Displacement distribution of link 3

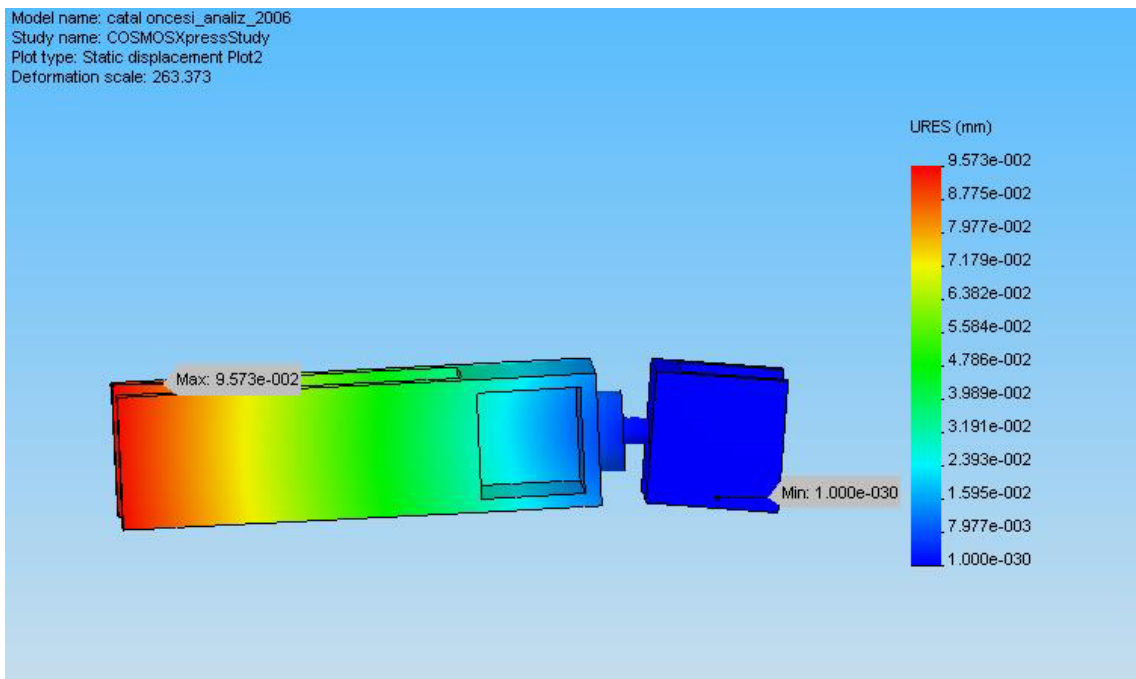


Figure 5.4 Displacement distribution of link 4

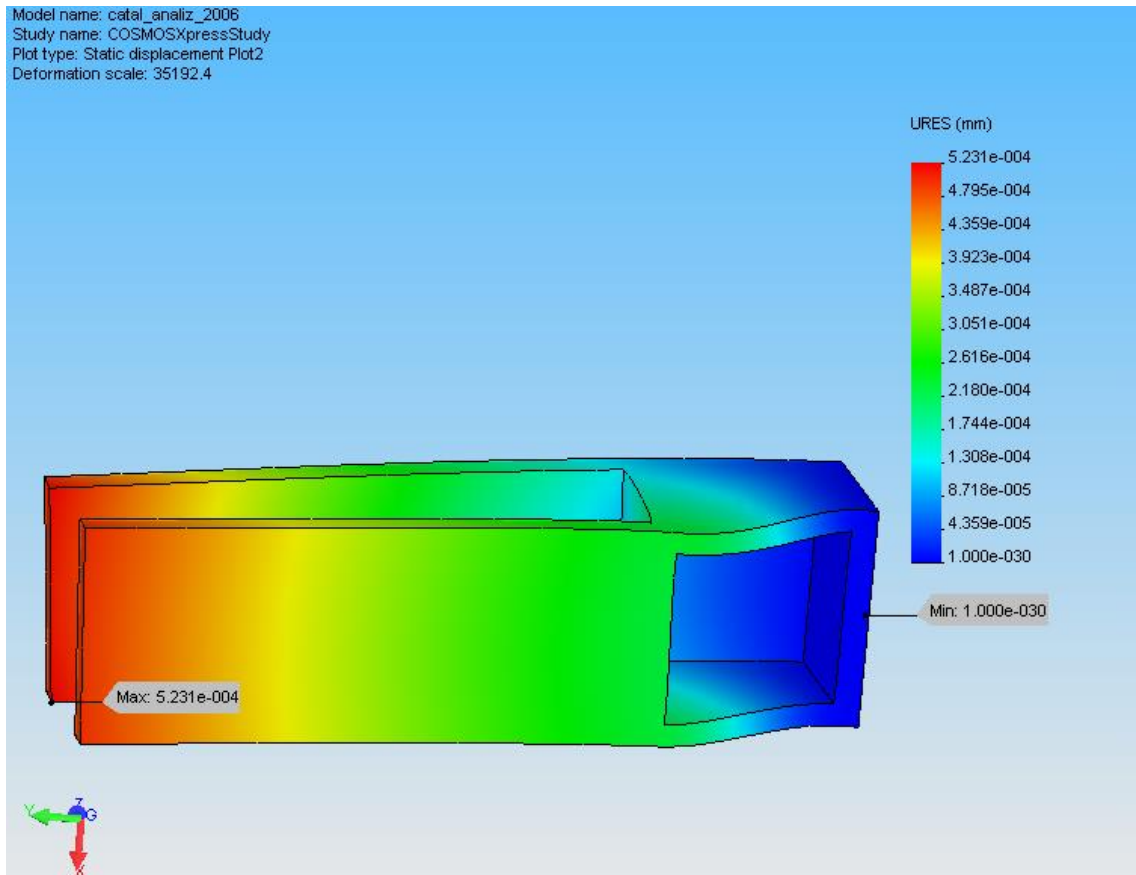


Figure 5.5 Displacement distribution of link 5

<i>Link #</i>	<i>Maximum displacement (mm)</i>
1	0.151011
2	0.0101582
3	0.44627
4	0.0957262
5	0.000523109

Table 5.2 Maximum displacement of the links

In Figure 5.6 to Figure 5.10 distribution of von-Mises stresses is illustrated. Contour diagram and maximum stress points are shown in the figures. Legend on the right side of the figure shows the distribution of contour diagram. Using the obtained maximum stress values, static safety factor is calculated for each link. Observed from the graphs, link 3 and 4 are the most critical links which are exposed to maximum stress in any condition. However the static safety factor calculated for each link is high enough. Table 5.3 shows the maximum stresses and safety factors for each link.

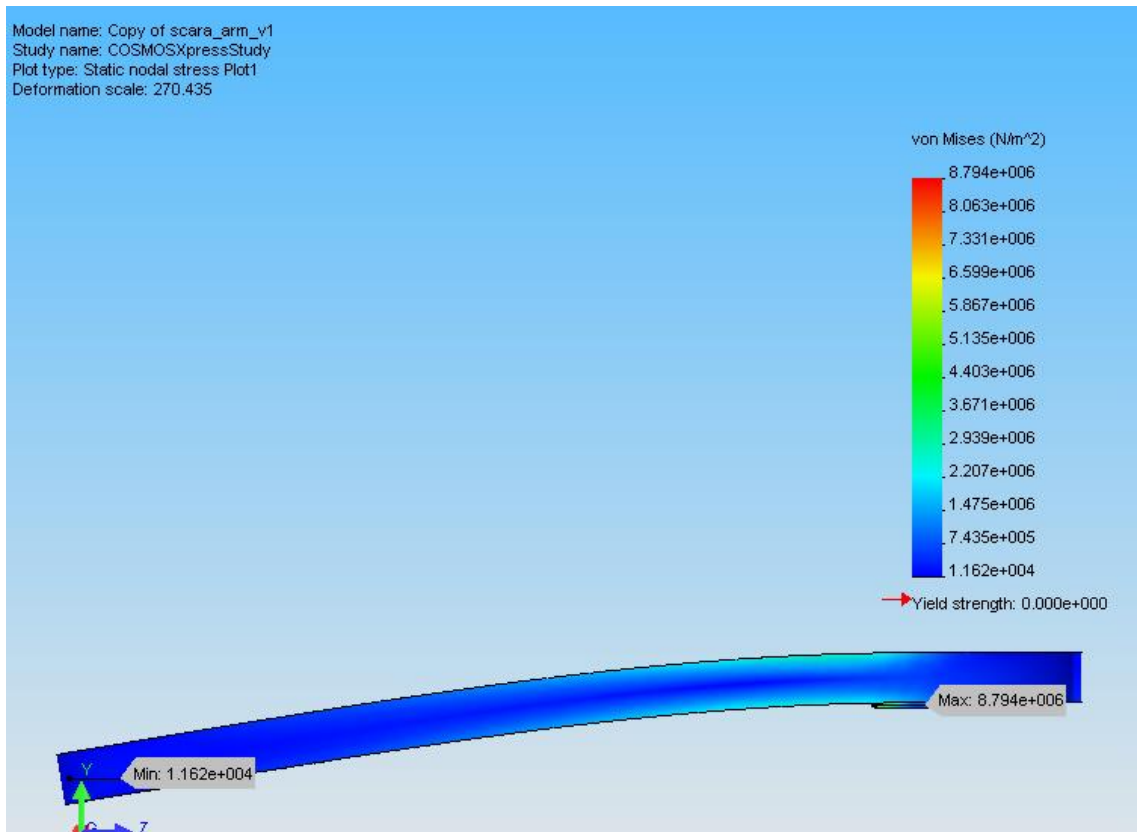


Figure 5.6 von-Mises stress distribution for link 1

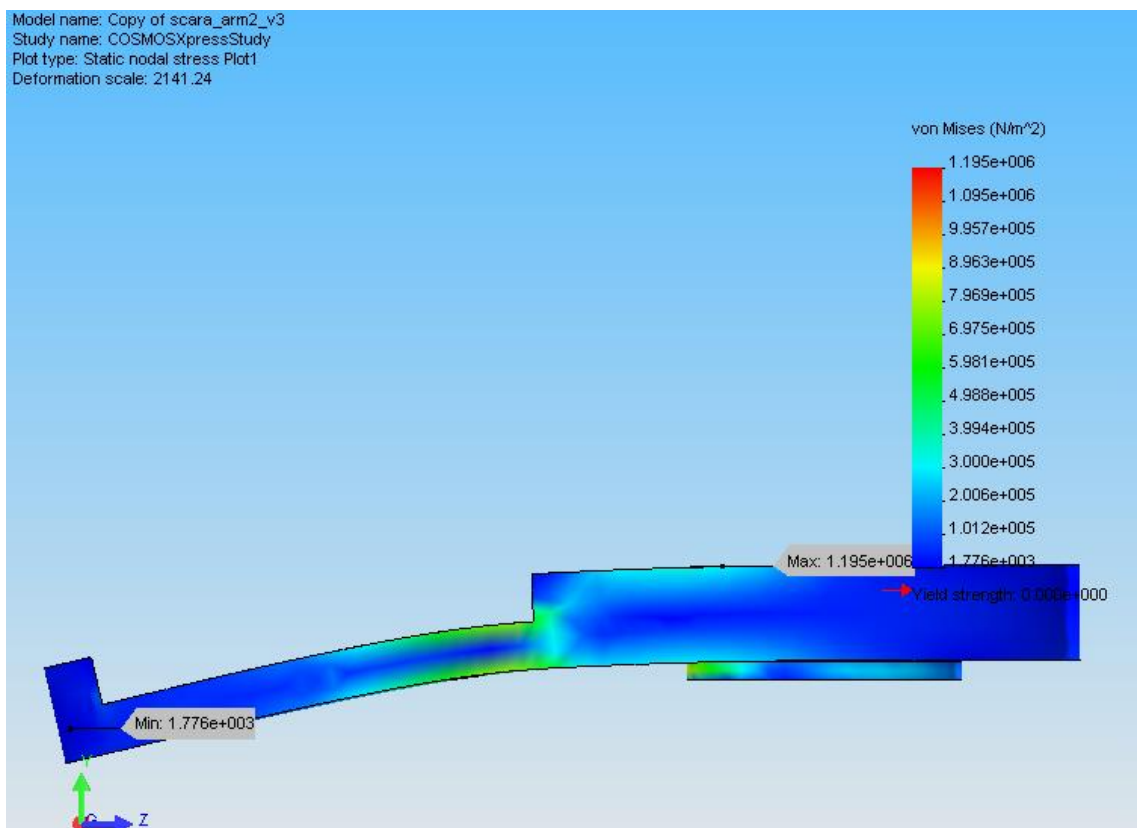


Figure 5.7 von-Mises stress distribution for link 2

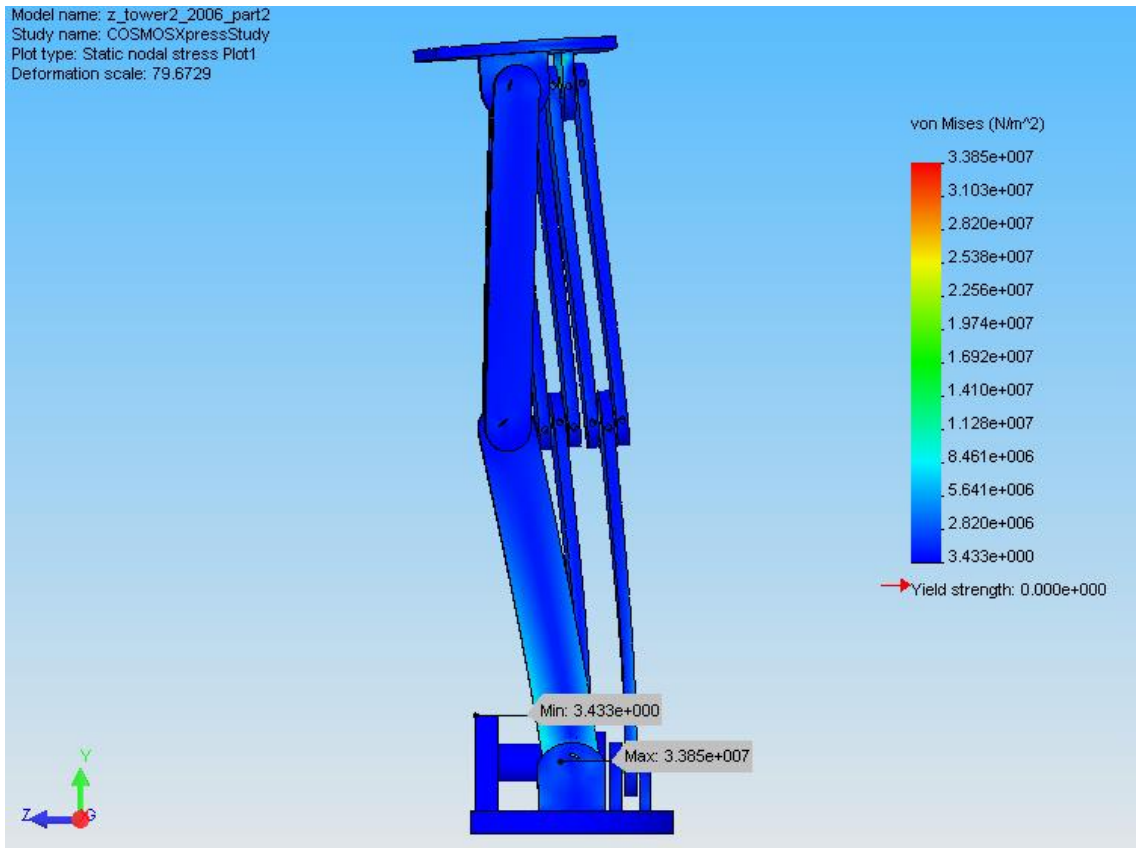


Figure 5.8 von-Mises stress distribution for link 3

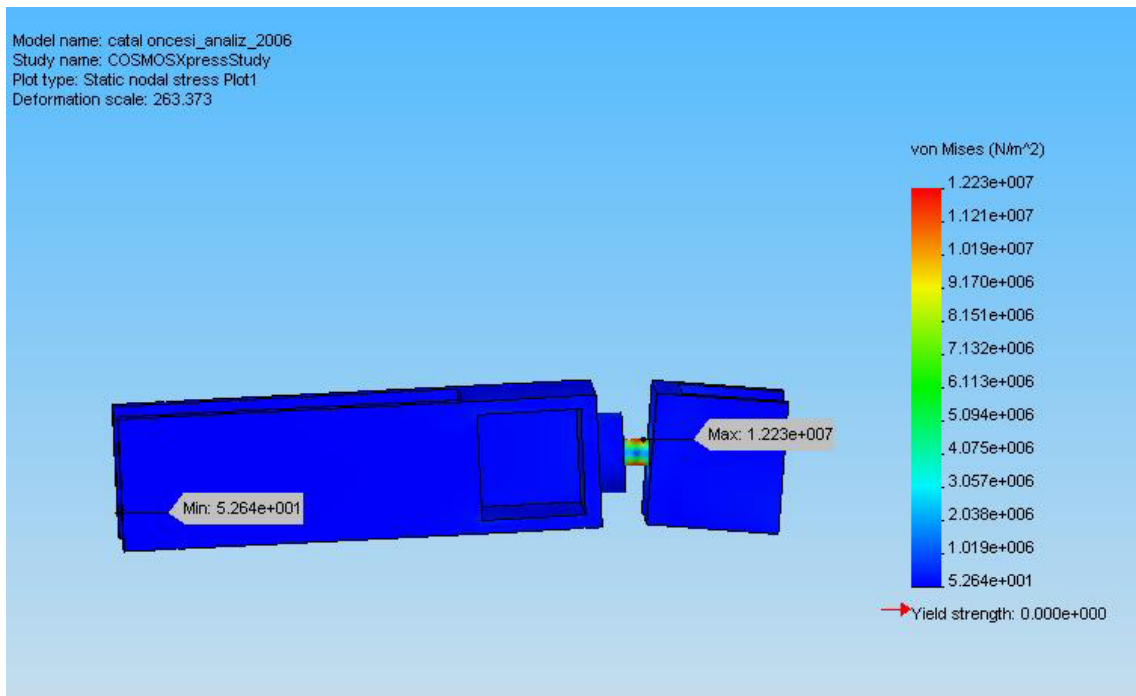


Figure 5.9 von-Mises stress distribution for link 4

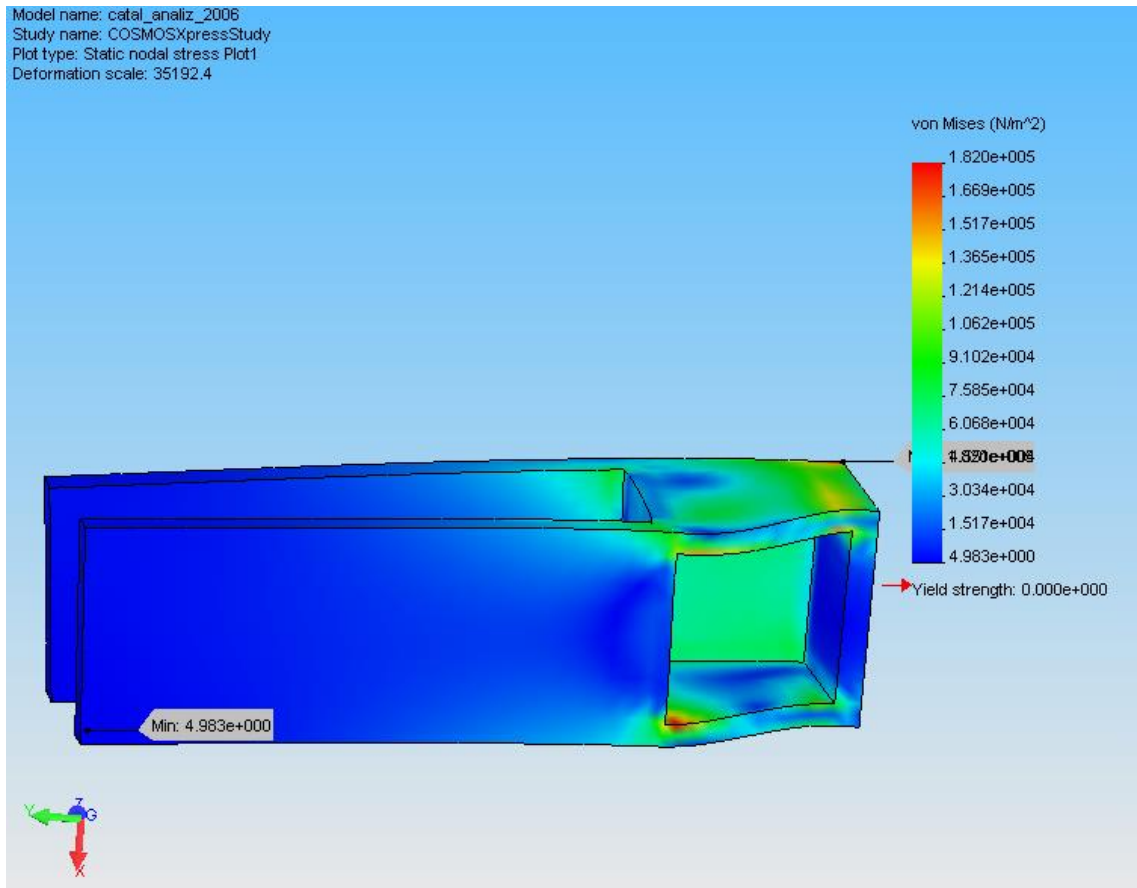


Figure 5.10 von-Mises stress distribution for link 5

<i>Link #</i>	<i>Max. von-Mises Stress (MPa)</i>	<i>Static Safety Factor</i>
1	8.79	57.45
2	1.19	424.37
3	33.85	14.91
4	12.22	41.32
5	0.18	2805.55

Table 5.3 Max von-Mises stresses and safety factors

5.3 Design Verification with Newton-Euler Based Inverse Dynamics Simulation

The weight and shape data obtained in the previous section is used in a Newton-Euler based inverse dynamics simulation. In this simulation, the master arm moves between randomly generated points in the workspace and at the same time it exerts full capacity (as defined in Chapter 3) randomly directed force and torque to the external environment at the tool tip (handle location). The joint torque and forces are recorded in

the simulation and they indicate whether the selection for motor and reducers are appropriate or not.

The dynamics of a robotic manipulator can be expressed as:

$$D(q)\ddot{q} + C(q, \dot{q})\dot{q} + g(q) + J^T F_e = u_{link} \quad (5.1)$$

when the friction and inertia effects of the actuators, the transmission and reduction elements are not considered. Therefore, the equation above can be described as the “link dynamics”. In this equation q is the vector of joint positions, \dot{q} is the joint velocity vector and \ddot{q} is the joint acceleration vector, u stands for the joint force/torque vector. D stands for the manipulator inertia matrix, C is the matrix for Coriolis and Centripetal force computation and g is the gravity effect vector. J is the manipulator Jacobian and F_e is the force / torque vector $[F_{ex} F_{ey} F_{ez} n_{ex} n_{ey} n_{ez}]$ exerted by the tool tip on the environment expressed in the world coordinates. $J^T F_e$ represents the effect of external forces and torques on the joint torques. When the actuator and transmission friction and inertia are included in the model too, the complete dynamics description can be expressed as

$$(J_m D(q))\ddot{q} + C(q, \dot{q})\dot{q} + B_V(q)\dot{q} + b_c(q, \dot{q}) + g(q) + J^T F_e = u_{link} + u_m \quad (5.2)$$

In this expression J_m is the combined actuator and transmission inertia as reflected to the joint side of the transmission:

$$J_m = \begin{bmatrix} \frac{1}{r^2_1} (J_{a1} + J_{g1}) & & \\ & \ddots & \\ & & \frac{1}{r^2_n} (J_{an} + J_{gn}) \end{bmatrix} \quad (5.3)$$

Here r is the reduction ratio (typically in the range of $[1 - 0.005]$), J_a is the actuator inertia (the rotor inertia in the case of a DC motor) and J_g is the inertia of the transmission mechanism (inertia of the gears in the case of a reductor mechanism).

B_V is usually a constant diagonal matrix with entries computed as the combined viscous friction constants of the actuator and the transmission elements as reflected to the joint side of the transmission.

$$B_L = \begin{bmatrix} \frac{1}{r_{1}^2}(B_{a1} + B_{g1}) & & & \\ & \ddots & & \\ & & & \frac{1}{r_n^2}(B_{an} + B_{gn}) \end{bmatrix} \quad (5.4)$$

In this equation, B_{ai} is the actuator viscous friction constant and B_{gi} is that of the transmission mechanism.

Similarly, b_c in (5.2) denotes the combined Coulomb friction of the actuators and transmission elements as reflected to the joint side.

$$b_e = \begin{bmatrix} \frac{1}{r_{1}^2}(b_{a1} + b_{g1}) & \cdots & \frac{1}{r_n^2}(b_{an} + b_{gn}) \end{bmatrix} \quad (5.5)$$

The inertia, friction and reduction parameters of the motors and reduction mechanisms assigned above can be found from the product specification sheets.

The generalized force/torque input u in (5.2) can be obtained by an inverse dynamics based on the Newton-Euler dynamics algorithm, when the (q, \dot{q}, \ddot{q}) trajectories are given.

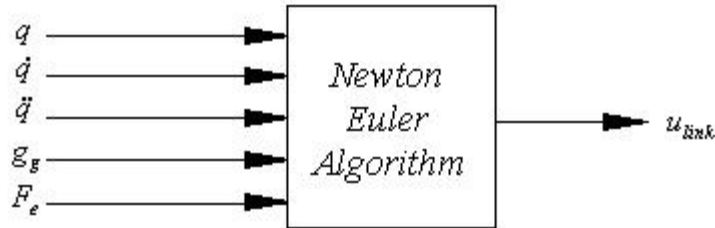


Figure 5.11 The inputs and outputs of the N-E algorithm

On the other hand, from (5.2) u_m can be computed as

$$J_m \ddot{q} + B_V \dot{q} + b_c = u_m \quad (5.6)$$

for the given joint position trajectory (q, \dot{q}, \ddot{q}) .

Therefore, the required joint forces/torques can be computed for any given g_g and F_e trajectory. Creating typical reference position trajectories (within the workspace of the robot) and demanding the highest end effector forces and torques within the specification described in Chapter 3 can reveal the order of joint torques needed for the designed master arm. Furthermore, since the NE algorithm can be used separately (with special configurations) to compute the inertial, the centripetal and Coriolis, the gravity

effects, the torque requirement can be broken down into those groups too. The same is true for a breakdown of the actuator side joint force/torque requirements too.

Hence, in the inverse dynamics simulations the total joint torque required is plotted together with the joint torque required due to end effector force/torques, joint force required due to inertial and Coriolis effect, joint force/torque required due to gravity effects and joint force/torque required due to friction effects.

In many simulations carried out, random points in the joint workspace of the arm are specified and joint space point-to-point trajectories are generated via trapezoidal velocity profiles and motion is synchronized for all joints.

Simulation results indicate that the chosen motors are appropriate in that they satisfy the speed and torque requirement as described in Chapter 3.

Below presented are four cases with different speed and external force/torque settings. In addition to demonstrating the feasibility of the motor and reductor selections, the plots in Figures 5.12 to 5.35 also serve a second purpose. Since the various components (gravity external effects inertia friction) can be monitored in the plot, we can assess the weaknesses and strengths of the joint against those factors and infer guidelines and device compensation methods for the transparency of the haptic motion.

Analyzed below, with the figures 5.12 to 5.35 are the four cases which can be shortly identified as:

- high speed – high end effector force/torque
- high speed – low end effector force/torque
- low speed – low end effector force/torque
- low speed – high end effector force/torque

These cases are chosen to observe the dominant characteristics / effects of joint actuation mechanism under different working conditions. The high-speed case is generated by choosing 0.25 rad/s velocity and 0.25 rad/s² acceleration then generating the trapezoidal velocity references. Low speed refers to 0.025 rad/s and 0.025 rad/s² velocity and acceleration, respectively. For the prismatic vertical axis 0.25 m/s and 0.025 m/s are the low and high speeds respectively and 0.25 m/s² and 0.025 m/s² are the low and high acceleration for the joint. As high handle force 15 N is chosen in random

direction. Low force is 1.5 N with random direction. For the end effector torques 1 Nm and 0.1 Nm are taken for high and low values, respectively again with random direction.

In these figures, total joint torque required is represented by solid lines, friction component represented by dash-dotted lines, inertial and Coriolis effects shown by dotted lines and torque to generate tool tip forces/torques are shown by dashed lines.

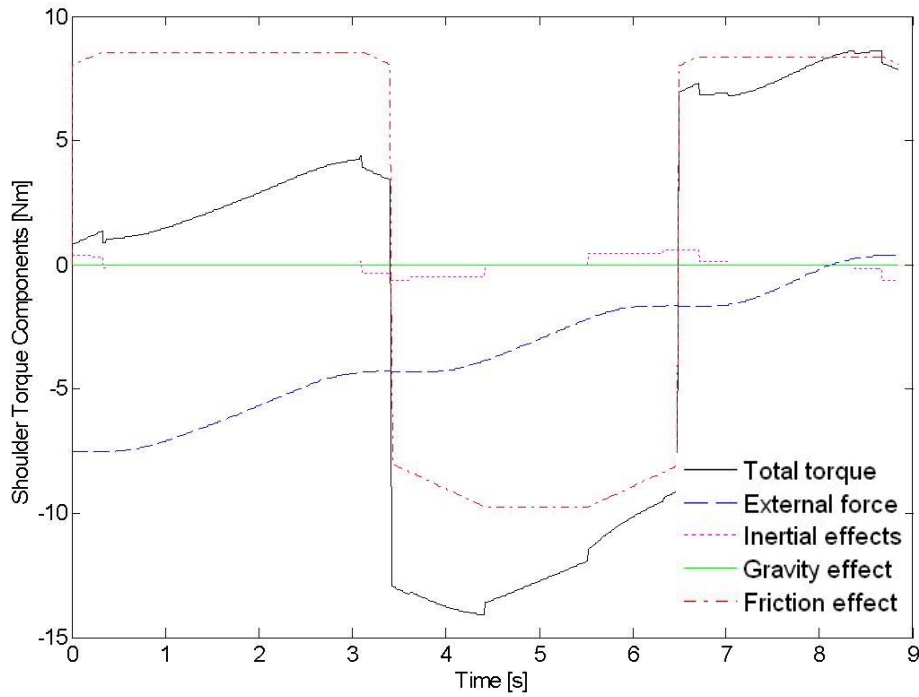


Figure 5.12 Total joint torque requirement and its components for shoulder joint, high joint speed, high end effector force/torque case

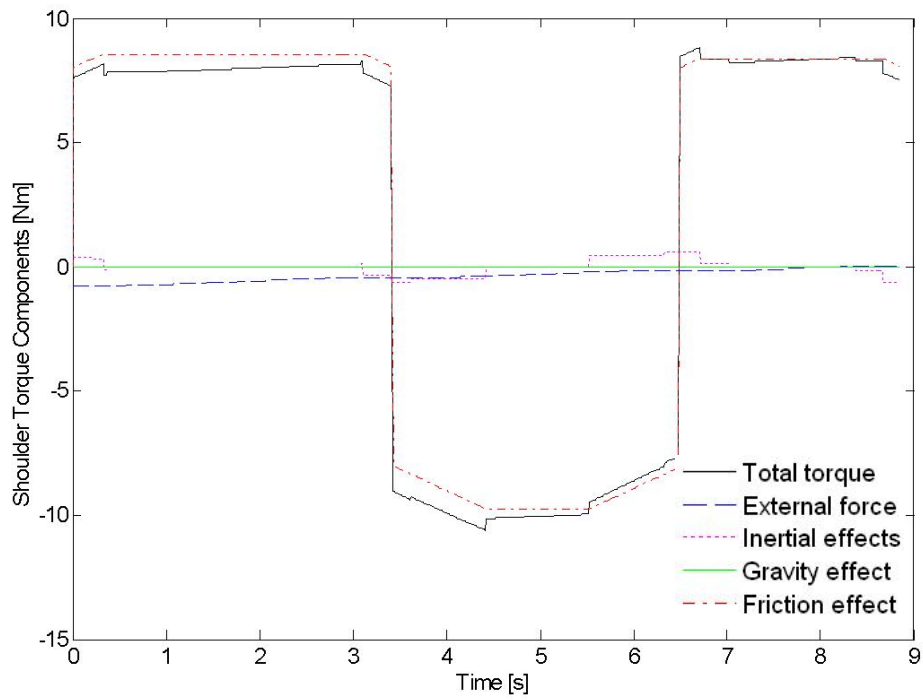


Figure 5.13 Total joint torque requirement and its components for shoulder joint, high joint speed, low end effector force/torque case

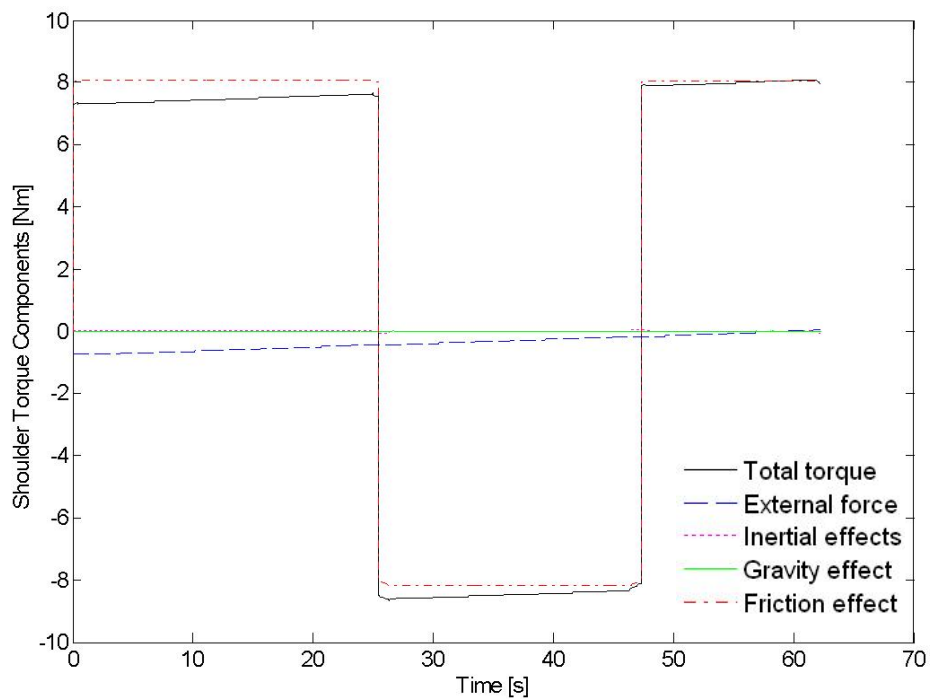


Figure 5.14 Total joint torque requirement and its components for shoulder joint, low joint speed, low end effector force/torque case

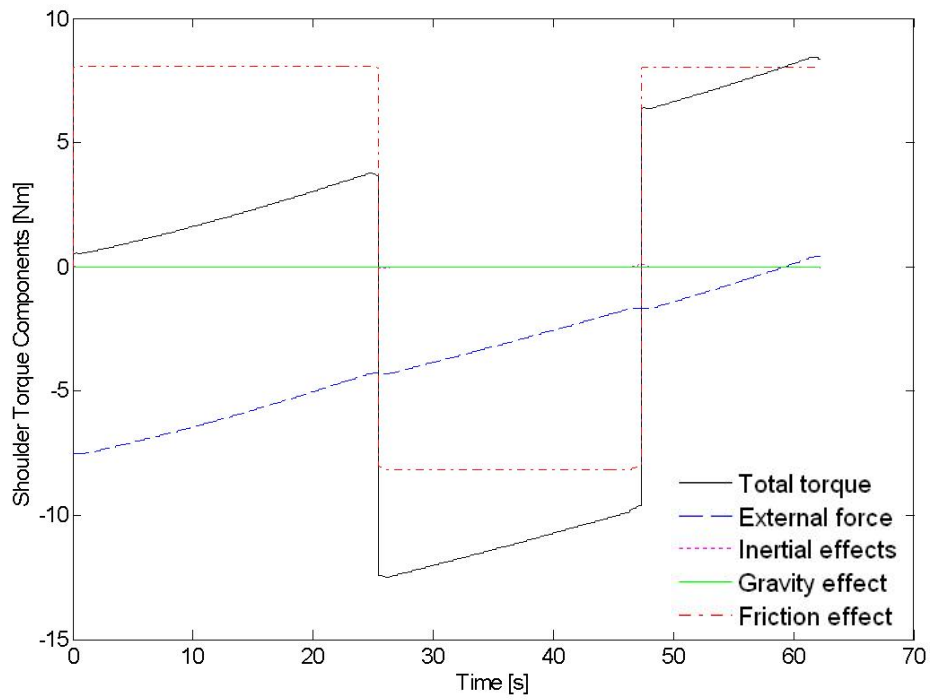


Figure 5.15 Total joint torque requirement and its components for shoulder joint, low joint speed, high end effector force/torque case

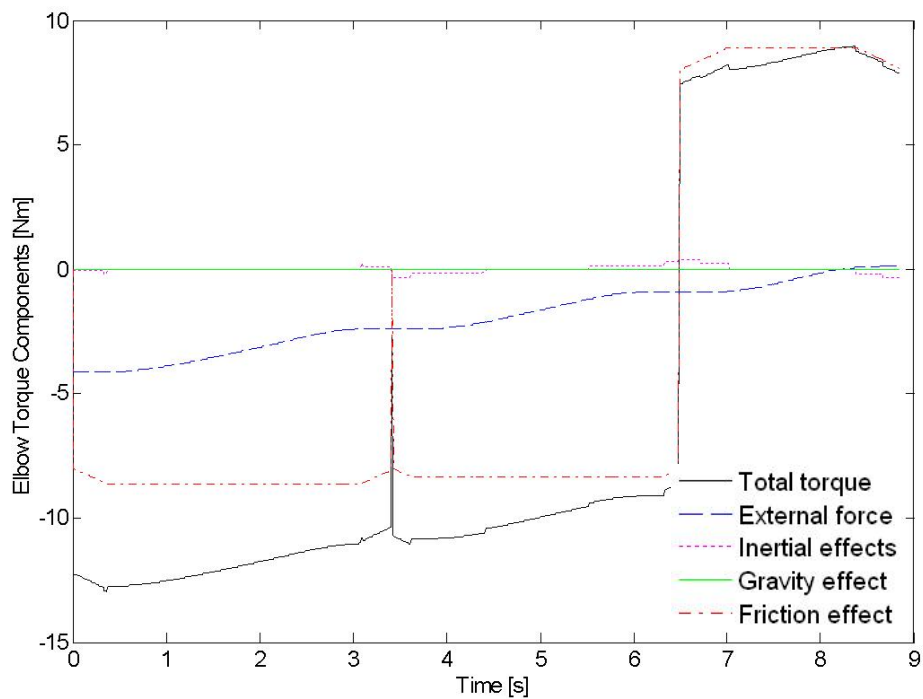


Figure 5.16 Total joint torque requirement and its components for elbow joint, high joint speed, high end effector force/torque case

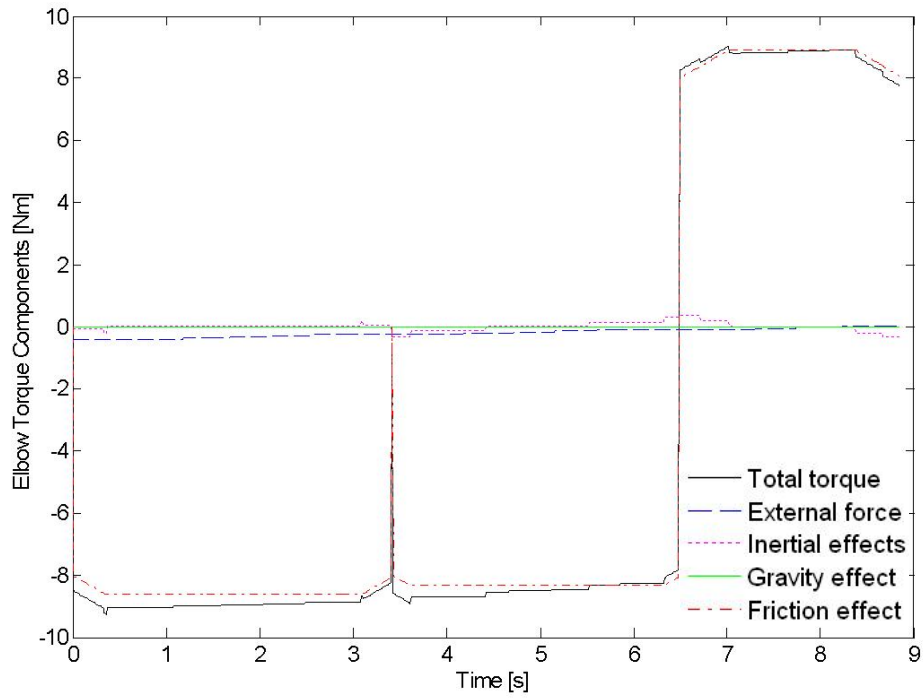


Figure 5.17 Total joint torque requirement and its components for elbow joint, high joint speed, low end effector force/torque case

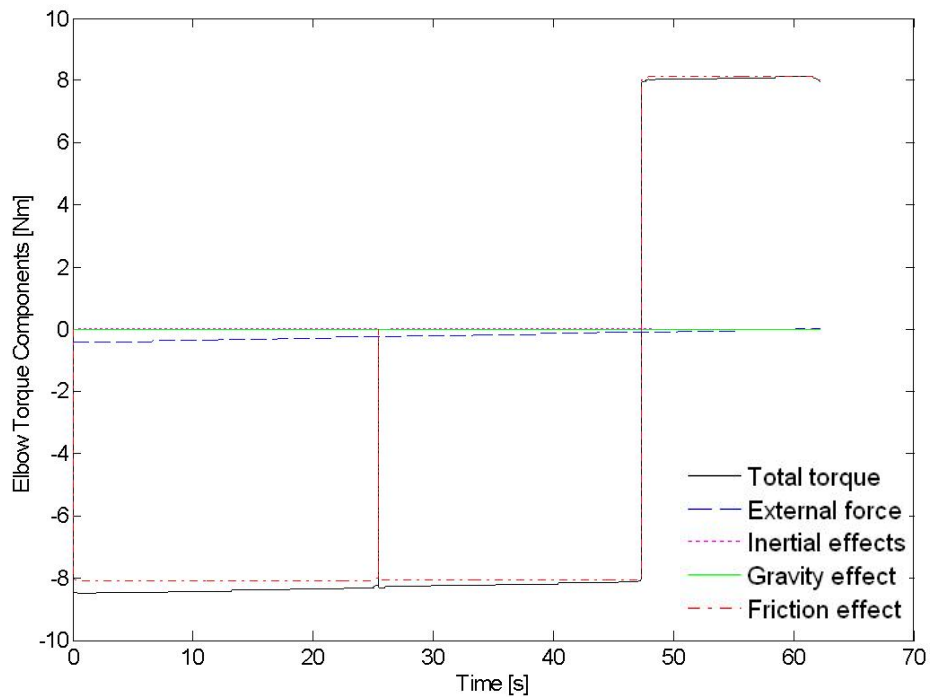


Figure 5.18 Total joint torque requirement and its components for elbow joint, low joint speed, low end effector force/torque case

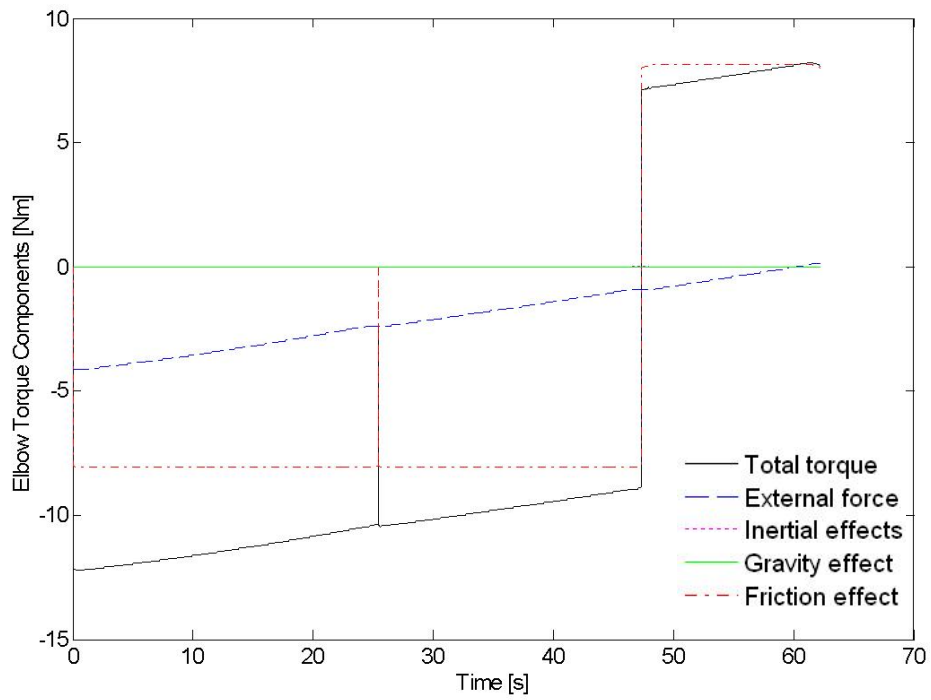


Figure 5.19 Total joint torque requirement and its components for elbow joint, low joint speed, high end effector force/torque case

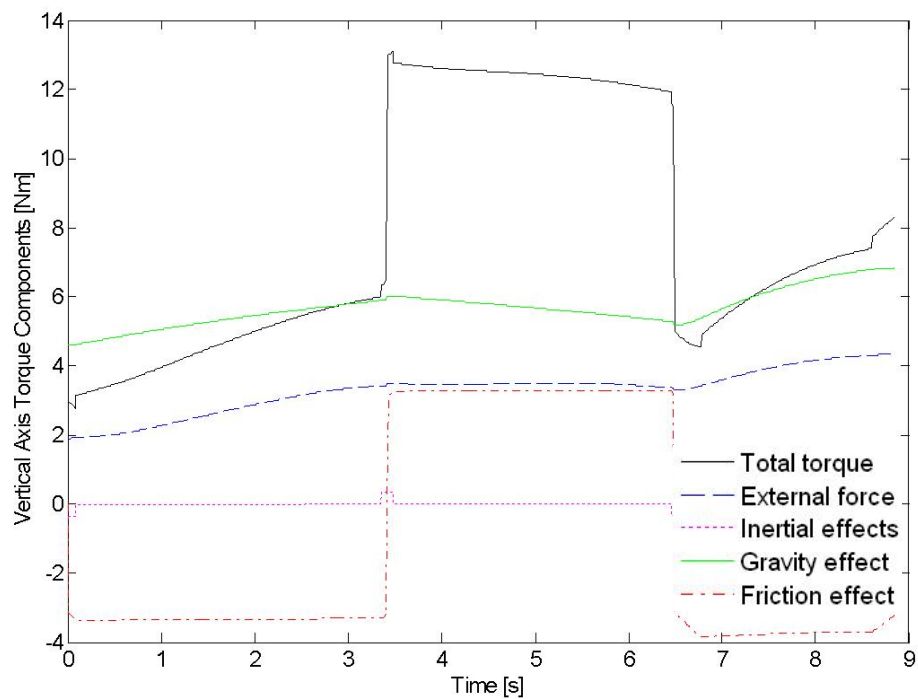


Figure 5.20 Total joint torque requirement and its components for vertical axis joint, high joint speed, high end effector force/torque case

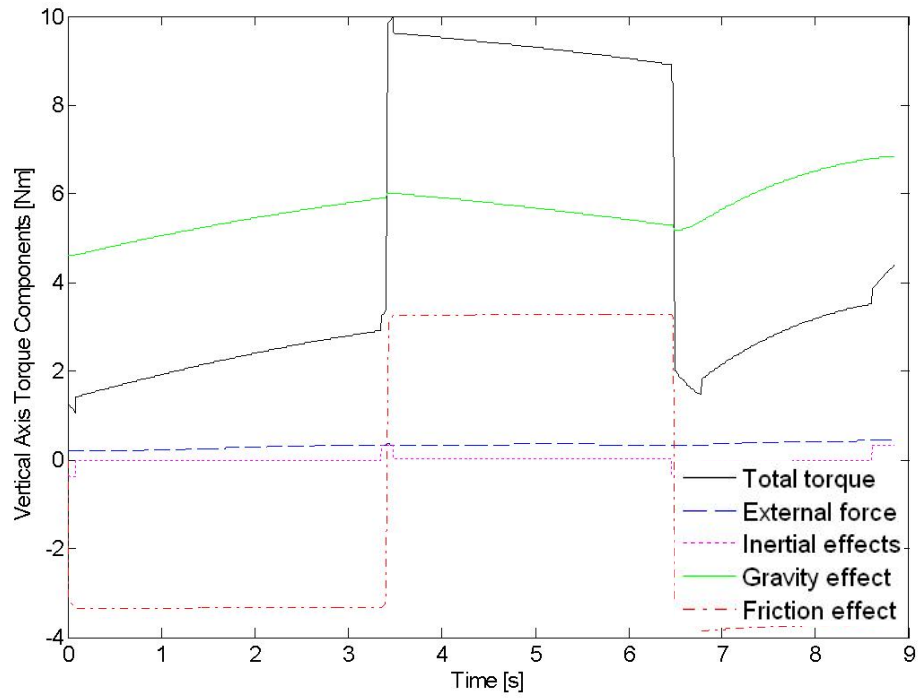


Figure 5.21 Total joint torque requirement and its components for vertical axis joint, high joint speed, low end effector force/torque case

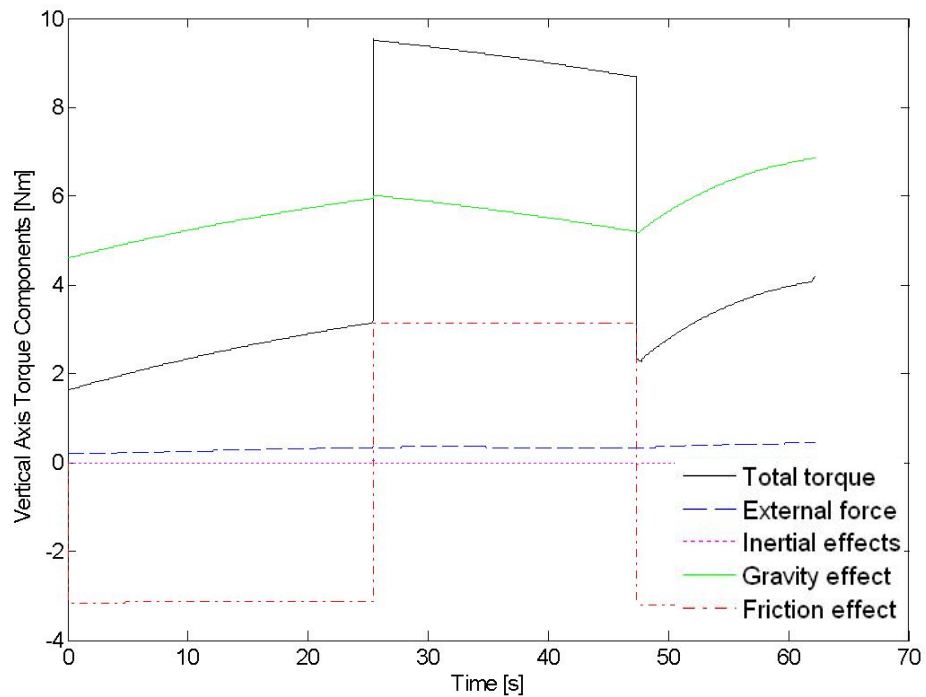


Figure 5.22 Total joint torque requirement and its components for vertical axis joint, low joint speed, low end effector force/torque case

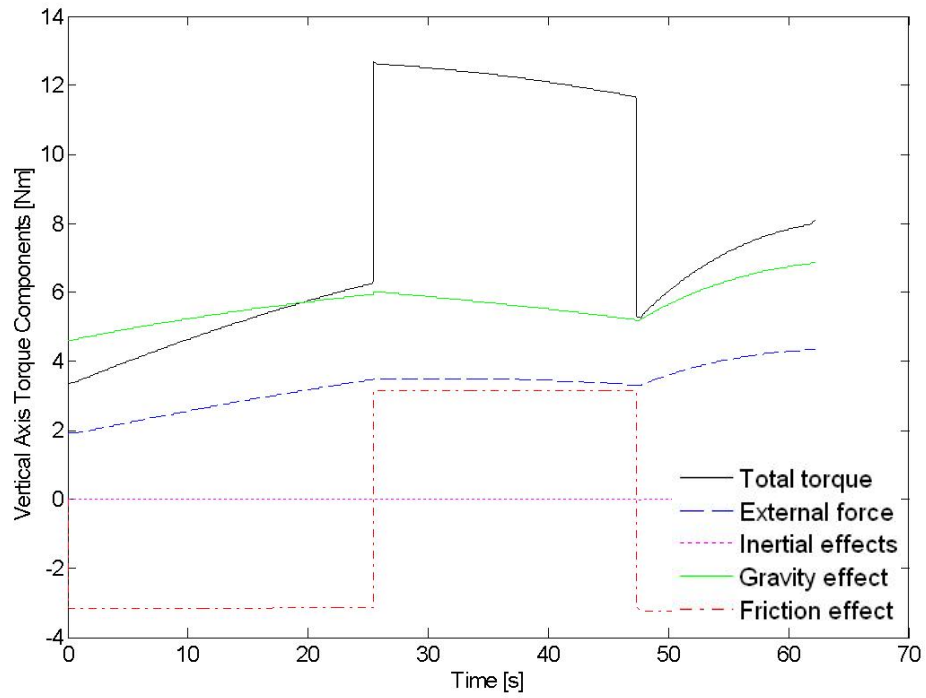


Figure 5.23 Total joint torque requirement and its components for vertical axis joint, low joint speed, high end effector force/torque case

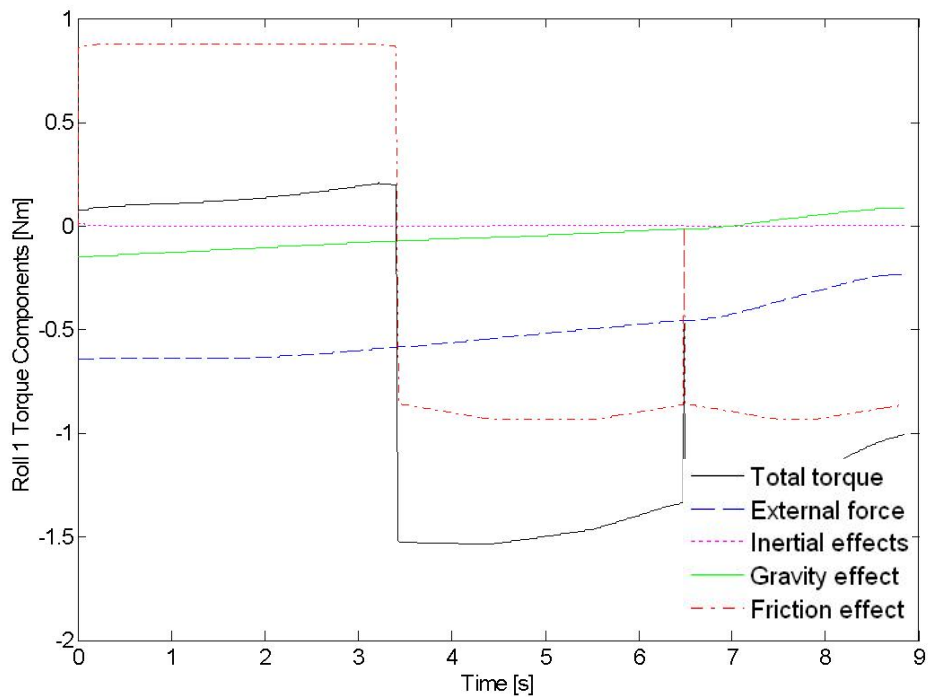


Figure 5.24 Total joint torque requirement and its components for roll 1 joint, high joint speed, high end effector force/torque case

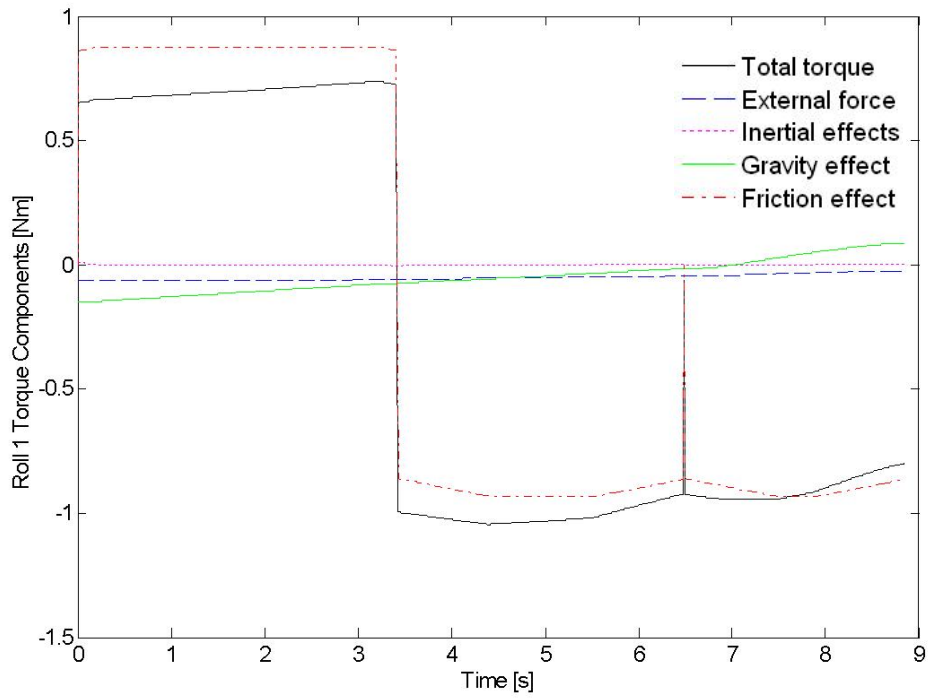


Figure 5.25 Total joint torque requirement and its components for roll 1 joint, high joint speed, low end effector force/torque case

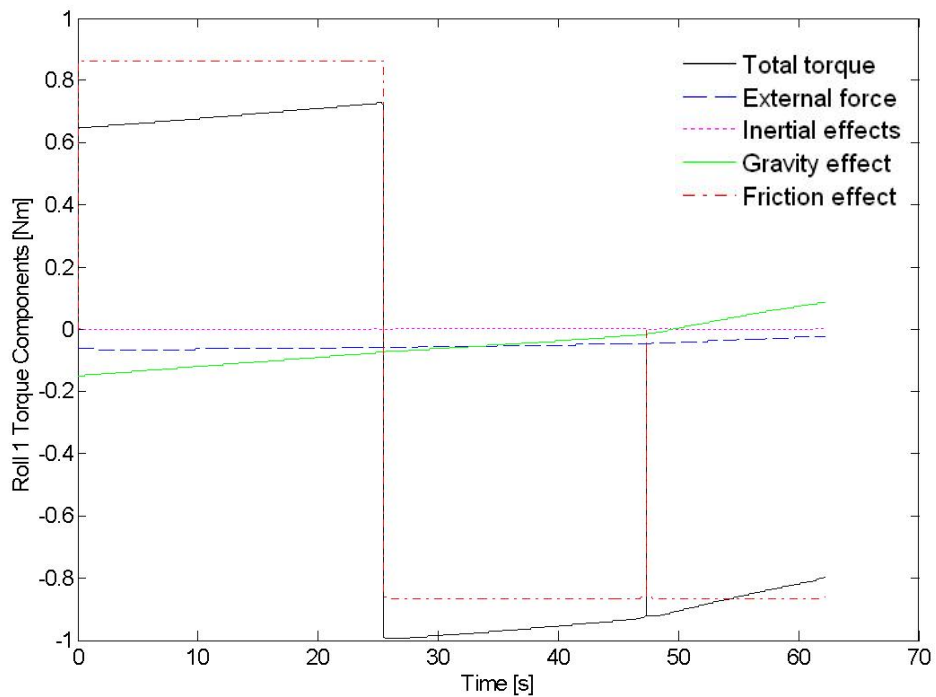


Figure 5.26 Total joint torque requirement and its components for roll 1 joint, low joint speed, low end effector force/torque case

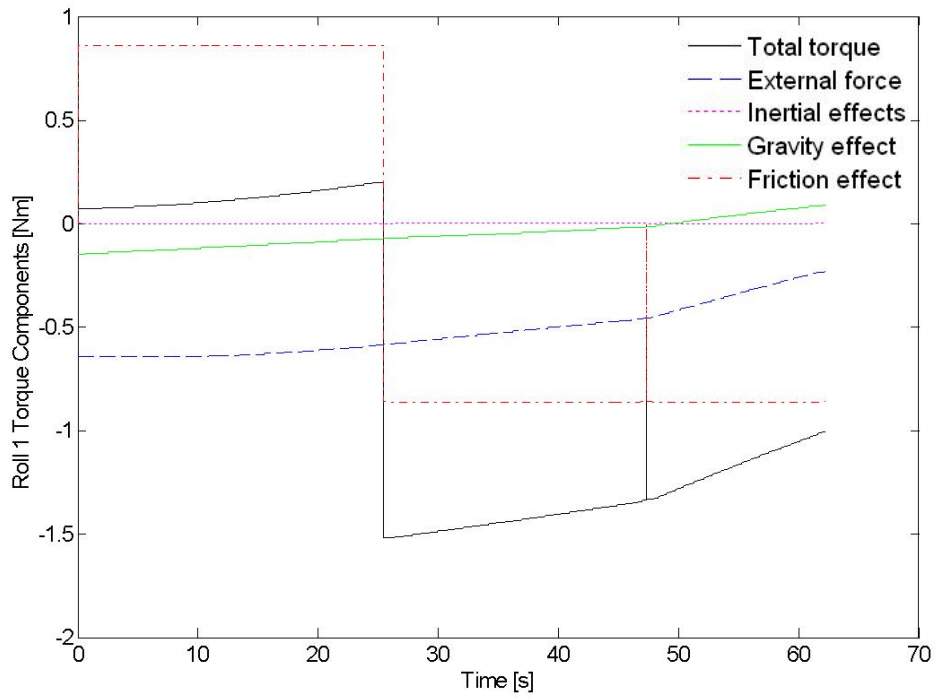


Figure 5.27 Total joint torque requirement and its components for roll 1 joint, low joint speed, high end effector force/torque case

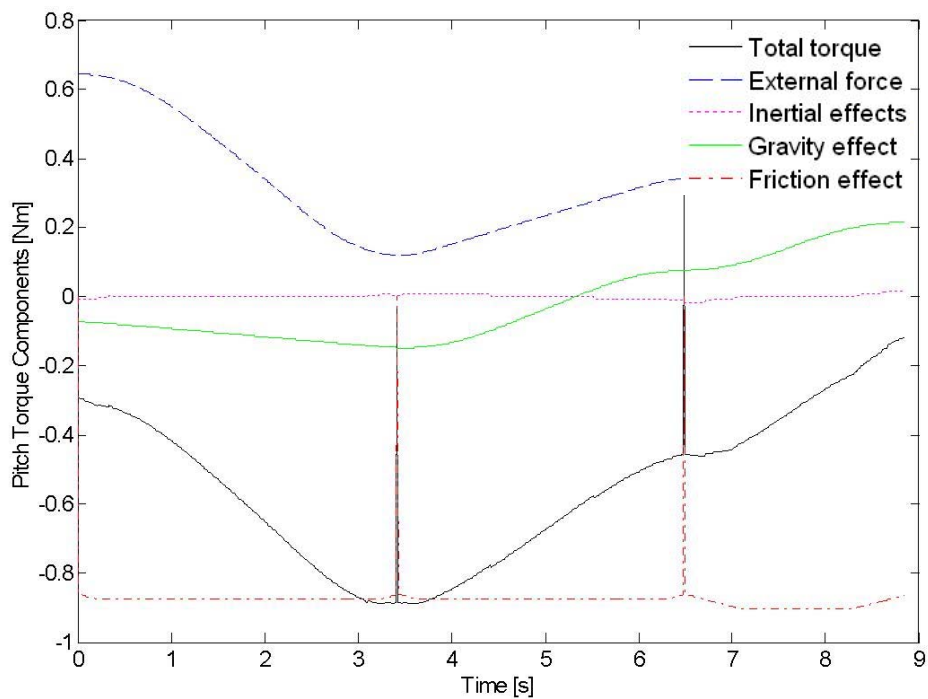


Figure 5.28 Total joint torque requirement and its components for pitch joint, high joint speed, high end effector force/torque case

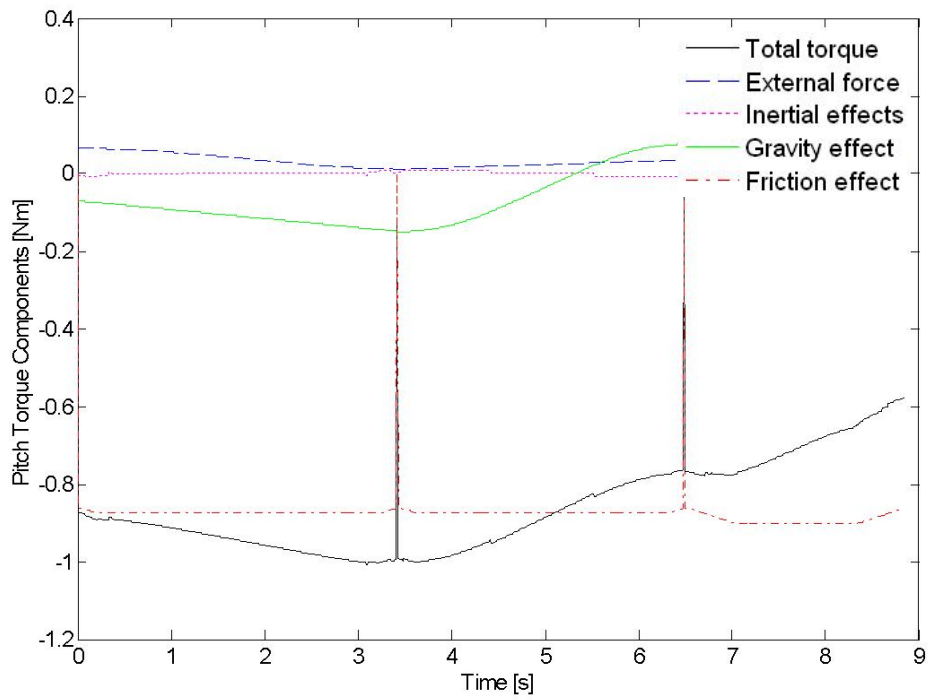


Figure 5.29 Total joint torque requirement and its components for pitch joint, high joint speed, low end effector force/torque case

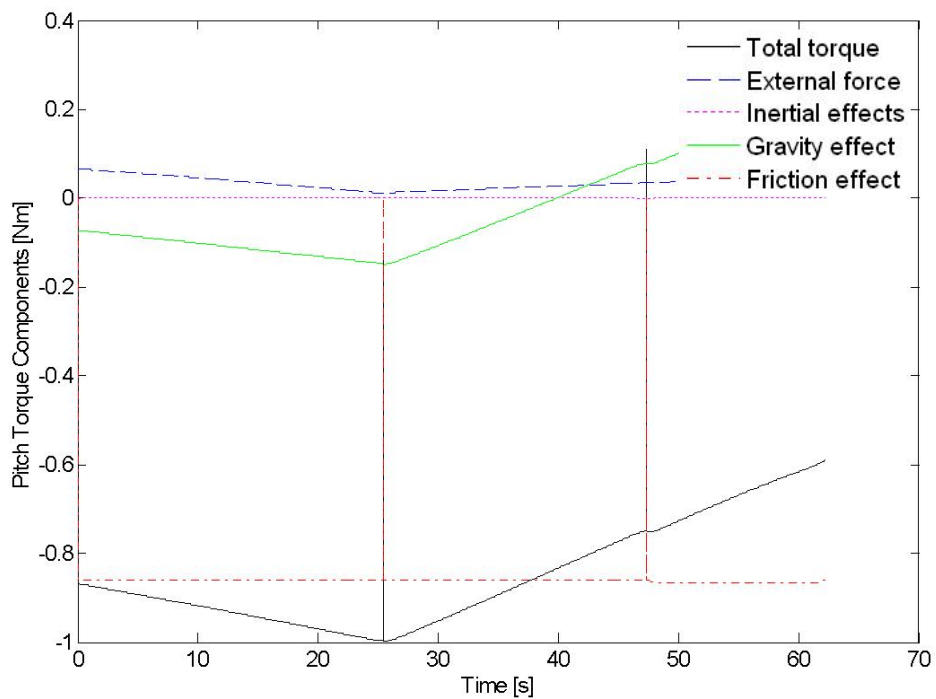


Figure 5.30 Total joint torque requirement and its components for pitch joint, low joint speed, low end effector force/torque case

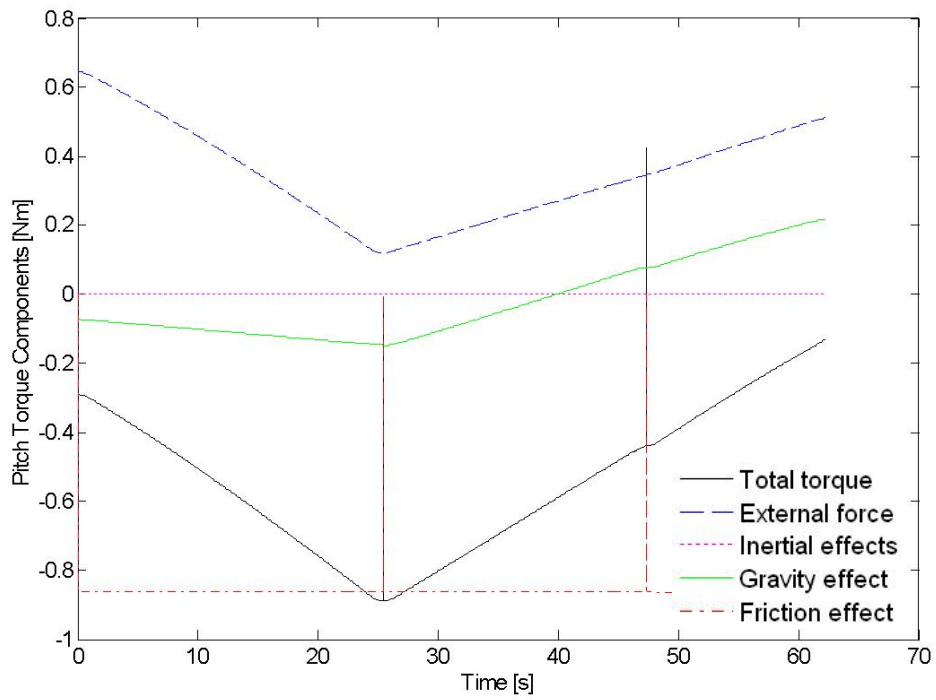


Figure 5.31 Total joint torque requirement and its components for pitch joint, low joint speed, high end effector force/torque case

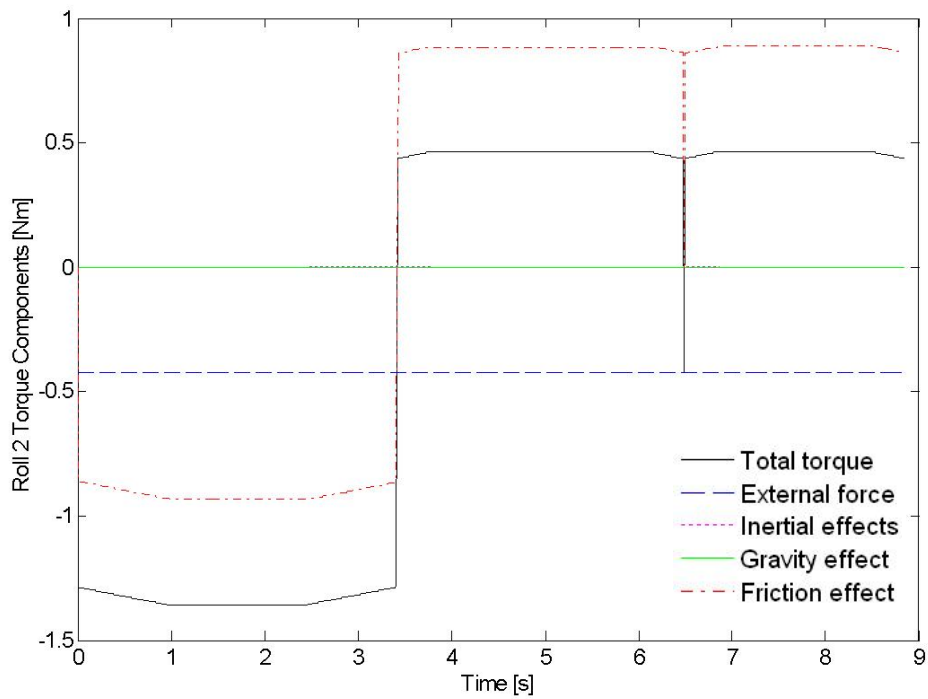


Figure 5.32 Total joint torque requirement and its components for roll 2 joint, high joint speed, high end effector force/torque case

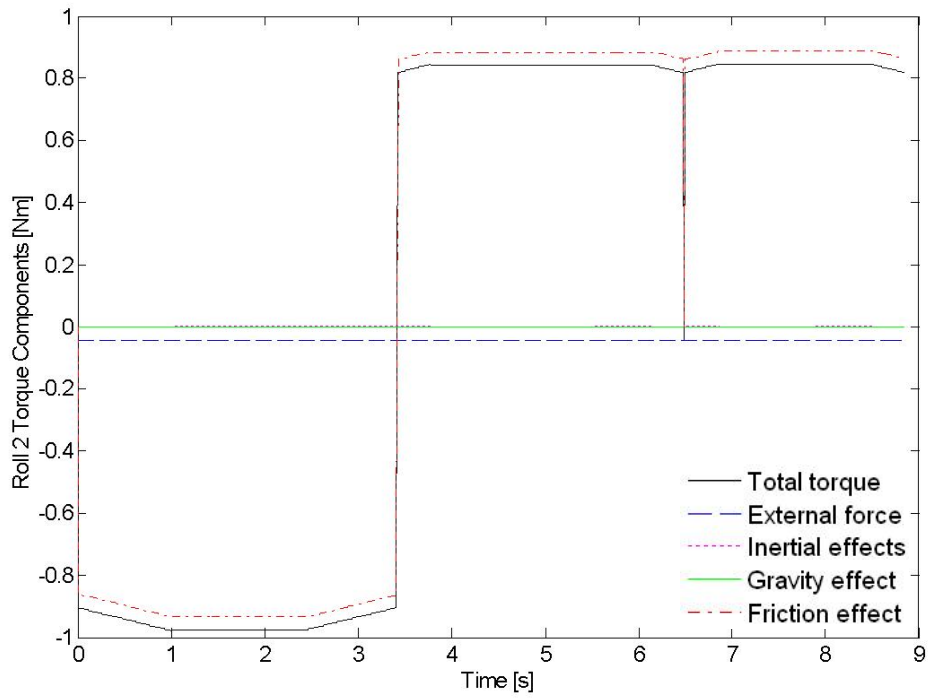


Figure 5.33 Total joint torque requirement and its components for roll 2 joint, high joint speed, low end effector force/torque case

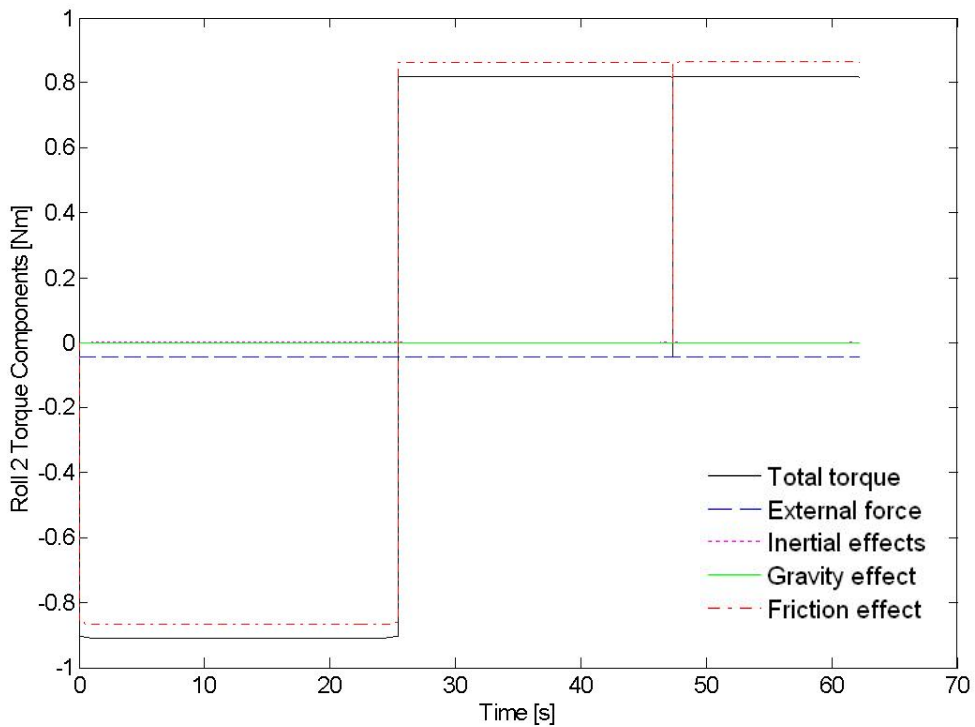


Figure 5.34 Total joint torque requirement and its components for roll 2 joint, low joint speed, low end effector force/torque case

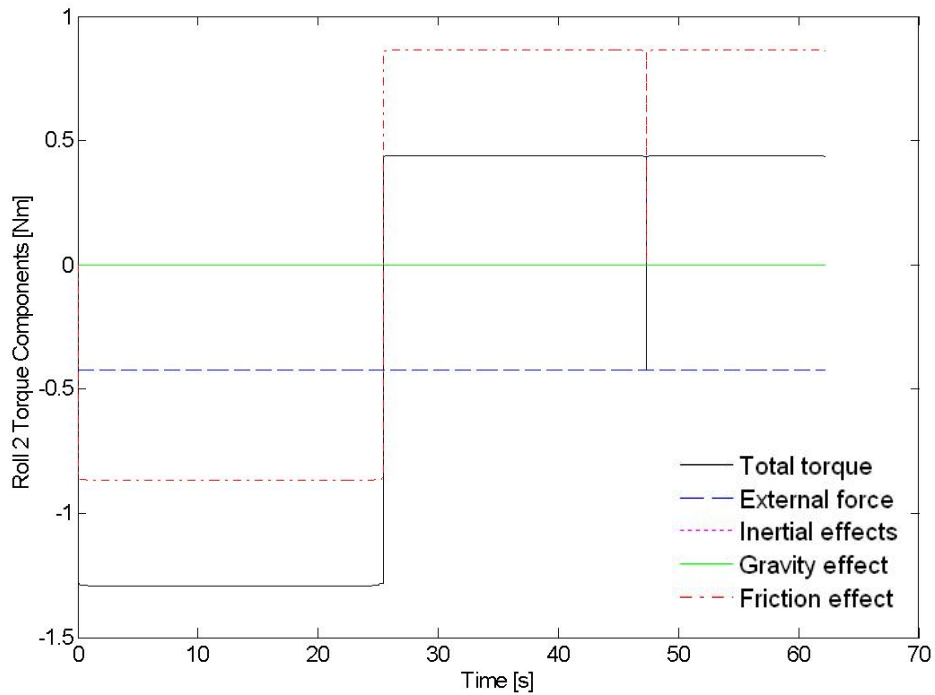


Figure 5.35 Total joint torque requirement and its components for roll 2 joint, low joint speed, high end effector force/torque case

In Figures 5.12 to 5.35, it can be observed that friction effects, and specially the coulomb friction is one of the dominant factors in the master arm dynamics. The viscous friction component within the friction curve can be identified by the trapezoidal form (due to trapezoid velocity reference profile) and the rest in friction curves belong to Coulomb friction.

The gravity term is dominating the dynamics of the third link. The speed of the motion, for the speed values used in the simulations, the inertial and Coriolis effects remain insignificant when compared to the friction terms. The requirement of end effector forces and torques reflect themselves in the joint torques requirements too. These observations are used as guidelines for compensation algorithms on Chapter 6.

The motion of the manipulator is animated in an OpenGL based animation environment shown in Figure 5.36.

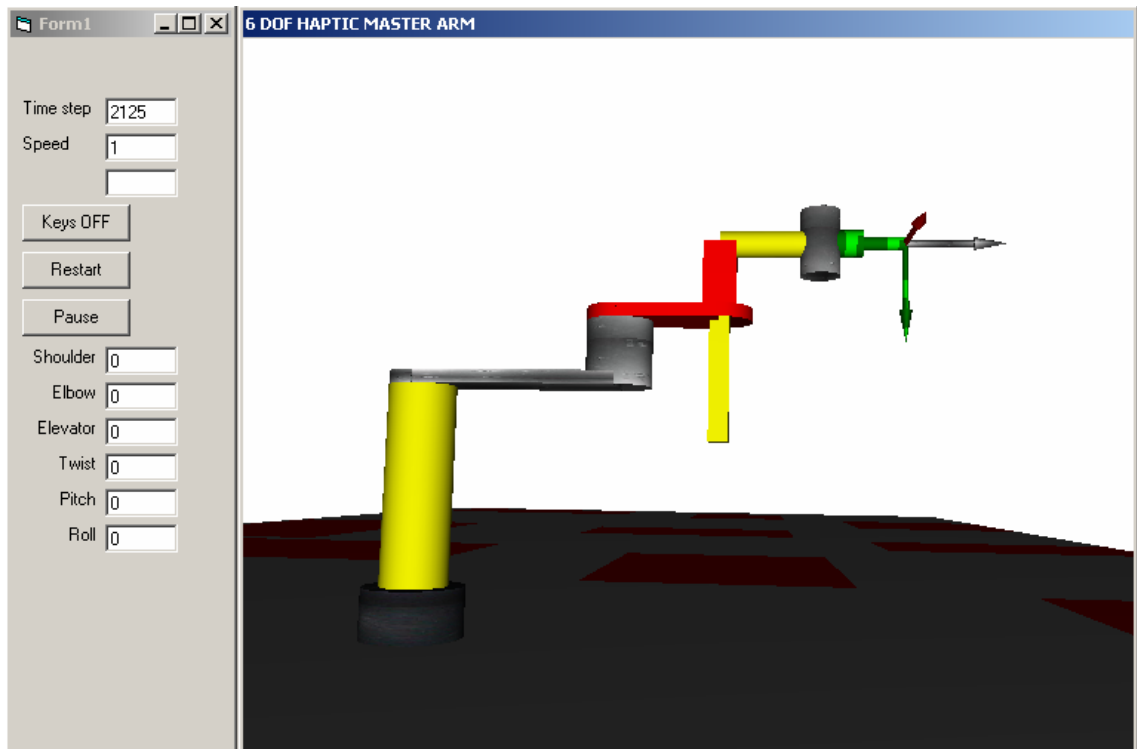


Figure 5.36 Animation window

5.4 Selection of Sensors

Sensor selection is crucial in the design procedure since the control feedback loop is closed via the information gathered from the sensors. Robustness and stability of the control loop is dependent on the quality of sensor. Since haptic device is considered as an interface between position and force, feedback of this variables are needed. Possible options are compared and evaluated according to design requirements.

5.4.1 Position Sensor Selection

Usage of position sensor is inevitable since the position of the end effector and links have to be calculated. Commonly used positions sensors are: Hall Effect sensor, resolver, and optical encoder. Advantages and disadvantages of these sensors have been summarized in Table 5.2 [28]

<i>Criteria</i>	<i>Hall Effect Sensor</i>	<i>Integral Resolver</i>	<i>Optical Encoder</i>
<i>Position Resolution</i>	<i>Good</i>	<i>Good</i>	<i>Excellent</i>
<i>Shock Resistance</i>	<i>Excellent</i>	<i>Excellent</i>	<i>Poor</i>
<i>Temp. Range</i>	<i>Fair</i>	<i>Excellent</i>	<i>Fair</i>
<i>Speed Range</i>	<i>Poor</i>	<i>Excellent</i>	<i>Good</i>
<i>Size</i>	<i>Excellent</i>	<i>Good</i>	<i>Poor</i>

Table 5.4 Comparison of position sensor options

According to Table 5.2, resolver seems to be the most appropriate position sensor for general use. However, in haptic simulation; shock resistance, temperature range and size are not as critical as resolution of the sensor. Detecting the position accurately is far more important than proper commutation of the rotor. Kinematics and dynamics equations depend on the accurately measurements of the position. The need for closing the position feedback loop is the main reason why optical encodes are preferred over Hall Effect sensors and resolvers.

While resolution of the optical encoder makes it the first preference, there is no way of sensing the initial position of the rotor, unless it is an absolute encoder. Since initial position is needed, sometimes Hall Effect sensor or resolver is used until the optical encoder hits a marker. When the marker is hit, controller automatically switches to optical encoder signal. Using combination position sensors might solve both initialization and accurate position measurement issue.

In our design, because of the aforementioned reasons optical encoders are used. Maxon motors employed in our haptic device already have incremental encoders. Encoders are mounted to the back of the motor since the deflection of the rotors is negligible in each axis. Maxon HEDL 5540 encoders with 500 pulse per revolution are used in each link. Taking the gearheads and harmonic drives into account, resolution of the encoders for each link is shown in Table 5.5 below.

<i>Joint #</i>	<i>Encoder Resolution</i>
<i>1</i>	<i>0.0072</i>
<i>2</i>	<i>0.0072</i>
<i>3</i>	<i>0.0046</i>
<i>4</i>	<i>0.0083</i>
<i>5</i>	<i>0.0083</i>
<i>6</i>	<i>0.0083</i>

Table 5.5 Resolution of encoders

5.4.2 Force Sensor Selection

Force/torque sensors are widely used in robotic applications. There are different versions available in the market, satisfying wide range of requirements. Since small-sized sensors with wide F/T measurement range are available in the market, addition of extra mass to the system is not problematic in our case.

Pressure foils are easy to implement because of their size, however their measurements are not accurate enough. Hysteresis effect in these sensors makes the software compensation for measurement error impossible.

Load cells incorporate strain gages which measures the force based on the deflection of a surface. Various sizes are available commercially. However, only axial forces can be measured and torque cannot be measured by load cells. Also, special care must be taken to ensure that the force is applied perpendicular to the surface at a predefined position.

Prediction of torques based on current flow in combination with a motor model can be used as a substitute for force sensors. Although this method gives satisfactory results, proper functioning of the software has to be ensured in order not to cause dangerous situations. This drawback of force estimation avoids the usage of it.

<i>Sensor</i>	<i>Advantages</i>	<i>Disadvantages</i>
<i>F/T sensor</i>	<i>Various versions available commercially, easy to integrate</i>	<i>Only for high angular velocities</i>
<i>Pressure foils</i>	<i>Dimension, easy to integrate, cheap</i>	<i>Not accurate, hysteresis</i>
<i>Load cell</i>	<i>Accurate measurement</i>	<i>Adds extra mass to the system, needs special construction to apply force</i>
<i>Estimation</i>	<i>Cheap, no extra mass and dynamics added to the device</i>	<i>Performance depends on software, software errors might result in dangerous situations</i>

Table 5.6 Comparison of F/T sensor options

In the literature, generally F/T sensors are employed in the high-torque applications. Mini-40 6-axis F/T sensor of ATI Automation has been selected for our design since it is already available in our laboratory and its measurement range satisfies the force requirements of our device. So as to achieve more reliable force measurement, force estimation and force sensor could be combined in the control loop of the system.

5.5 Controller Hardware, Actuator and Sensor Integration

In order to control the overall system, the DS1103 control board and the dSPACE Control Desk program were used. The DS1103 PPC board is a standalone control board which has 6 incremental encoder inputs, 8 DAC, 20 ADC units and other features (such as RS232 and CanBus channels) which makes it adequate for control purposes of the designed haptic device. With the capacity of this hardware 6 motors could be controlled at the same time.

Encoder cables of the motors could not be connected to dSPACE directly because of the different connector types. In order to overcome this problem, a small intermediate circuit which converts the flat encoder cable of the motor to D-Sub 15 connector is designed. In order to avoid noise problems with the encoder signals, special noise-immune SAB Bröckskes encoder cables were used.

Power cables of the motor were connected to the Maxon ADS_E 50/5 Servoamplifier driver card. Set-value inputs of the driver are connected to DSPACE DAC output via coaxial cables. Wiring diagram of the driver for current control mode is shown below in Figure 5.37.

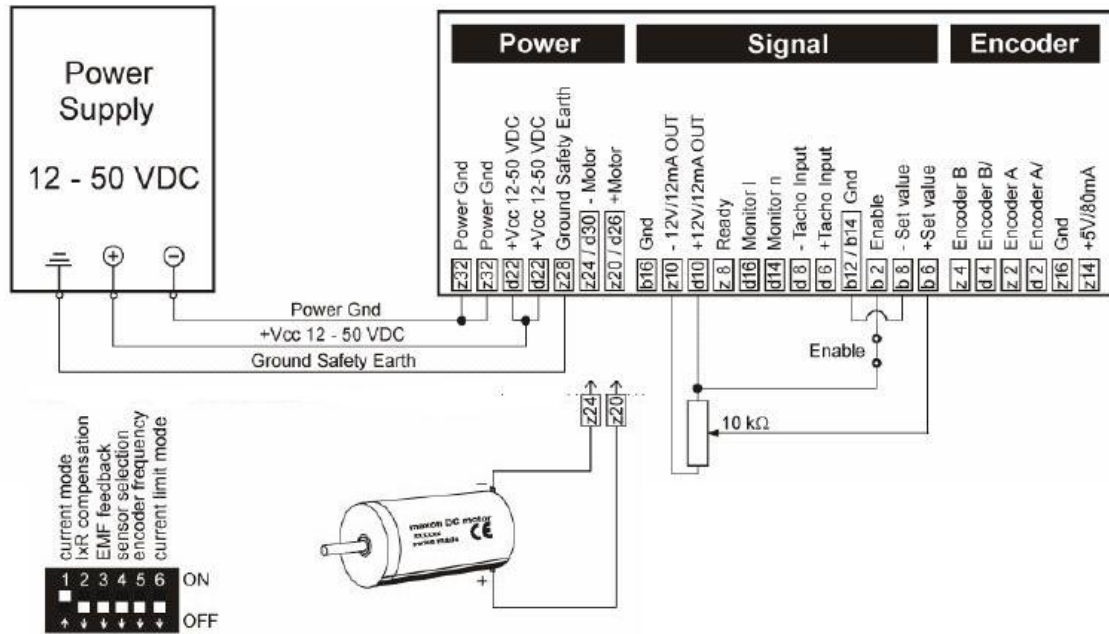


Figure 5.37 Maxon motor and driver connections for current control mode

The force sensor assembled on the end effector is ATI Mini40 6-axis force/torque sensor. The sensor comes with a driver card which is inserted to PC's PCI bus. Before starting to use the sensor, it has to be installed. A GUI is also included in the sensor software package which takes care of installation and calibration of the sensor. A snapshot of the GUI can be seen in Figure 5.38.

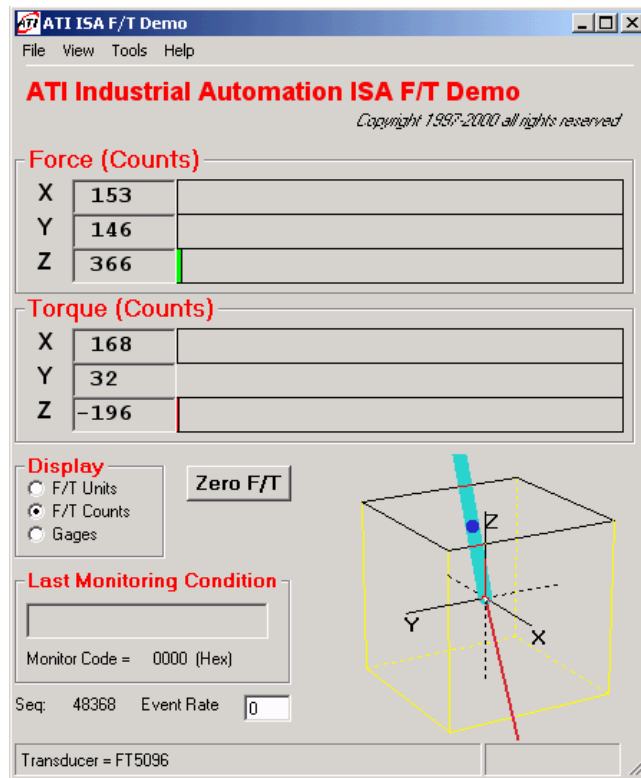


Figure 5.38 F/T sensor GUI

Gathering information from the sensor can be done via several ways:

- Via a text file
- Via C library
- Via Microsoft Excel
- Via Visual Basic

GUI of the sensor has a feature to export values read from the sensor to a text file. Transfer of the data involves the usage of the GUI program, writing the values to a text file and then reading the text file using another C program which sends the data to DSPACE. So many intermediate phases to read the sensor reduce the performance of real-time operation. This scheme also depends on the internal routines of the MS operating system which reduces the stability and reliability of the procedure.

At a first glance, the easiest way to gather data from the sensor and use in DSPACE seems using the C library of the sensor. However, the C library is not compatible with MS Windows operating system. It is implemented under Linux. Interfacing the C code with the C-Lib library of the DSPACE also ends up with failure.

Reading the force sensor via Microsoft Excel, which utilizes a Visual Basic macro, is also cumbersome since it is not intended for such real-time applications. Other innate features of the program make it slow.

Using Visual Basic seems to be the most efficient way to integrate the sensor to DSPACE. Unfortunately DSPACE do not allow Visual Basic codes to be embedded in its internal codes. Communicating VB code of the sensor with C-Lib library of DSPACE solves the problem.

A TCP/IP socket is created in both the VB and VC programs thus transferring the data between force sensor and the C-lib program. VC program also utilizes C-lib to communicate with the DSPACE's registers. VB program which has GUI as shown in Figure 5.39 reads the values from the sensor and sends them to the VC program. VC program serves as a messenger between VB program and DSPACE. It receives the data from the VB program and sends them to DSPACE registers using C-Lib.

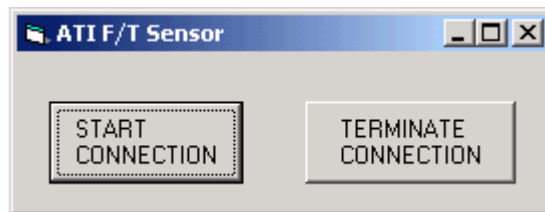


Figure 5.39 F/T sensor VB program GUI

6 DYNAMICS COMPENSATION ALGORITHMS

Transparency is one of the most important specifications for a haptic interface. Although low impedance (low friction, low inertia) mechanisms are favorable for the design of naturally low impedance interfaces, large force and torque ranges which might be demanded by the haptic interfaces and low impedance characteristics are conflicting specifications.

The N-E based inverse dynamics analysis in Chapter 5 indicates that the master arm designed is mainly affected by gravity and friction. Table 6.1 lists the dominant effects encountered at the joints of this arm.

<i>Joint #</i>	<i>Dominant effect</i>
<i>1</i>	<i>Coulomb friction</i>
<i>2</i>	<i>Coulomb friction</i>
<i>3</i>	<i>Gravity and Coulomb friction</i>
<i>4</i>	<i>Gravity and Coulomb friction</i>
<i>5</i>	<i>Gravity and Coulomb friction</i>
<i>6</i>	<i>Coulomb friction</i>

Table 6.1 Dominant dynamics effects at the joints

A number of dynamics compensation techniques like inverse dynamics, computed torque methods, gravity compensation, friction compensation can be used for removing the undesired effects of dynamic factors for the whole arm, as a multivariable approach. However, the online applicability of these approaches, which need intensive matrix multiplication, is limited. Computational power and sampling rate are of fundamental importance in the haptic control problem because master arm is in contact with the external world (the human operator). High sampling frequencies are demanded in such applications for the appropriate measurement or estimation of contact forces.

The requirement of high sampling frequencies is directly related with the computational power of the controller hardware. The execution of the code has to be fast enough to fit between two sampling instants. Since for a given controller (in our

case DSPACE 1103) the computational power available is fixed, the way to attack the computational power problem is writing efficient control code. This makes the use of full dynamics compensation algorithms in the multivariable fashion unfeasible.

Friction and gravity compensation techniques, however, can be applied to the individual joints, independently. Our observation in Chapter 5 also indicates that friction (especially Coulomb friction) and gravity are the primary source of nonlinear effects.

These arguments suggest that friction and gravity effect compensation in an independent joint scheme is favorable because of the simple nature, computational effectiveness and suitability to the specific dynamics compensation problem at hand.

In this work, the compensation techniques are tested in a joint position controller framework for simplicity. Their use in a variety of haptic controllers is straight forward. As stated in Chapter 5, this dynamics model can be described by the following equation.

$$(J_m + D)\ddot{q} + C(q, \dot{q})\dot{q} + B_V(q)\dot{q} + b_c(q, \dot{q}) + g(q) + J^T F_e = u \quad (6.1)$$

Gravity compensation is the addition of a gravity effect estimate term to the joint torque vector (control vector) as:

$$u = u_{control} + \hat{g}(q) \quad (6.2)$$

The term $u_{control}$ can be generated in many ways, for example as a proportional and derivative (PD) control scheme or any other control method.

In this thesis a PD control scheme is used as the control term $u_{control}$. The application of the independent joint friction compensation is very similar to the gravity compensation case. Here only Coulomb friction compensation is considered because it is the dominant term in the friction effect:

$$u = u_{control} + \hat{b}_c \quad (6.3)$$

It should be noted that, since the various weight and length parameters are known and joint variables are measured precisely, the computation of $\hat{g}(q)$ does not pose a significant problem. However, in the case of friction, the modeling is quite difficult.

Below presented are the results of four simulations:

- PD control with controller gains obtained from a computation based on effective inertia and friction values
- PD control based on fine tuning of the controller above
- Fine tuned PD controller with gravity compensation

- Fine tuned PD controller with gravity and Coulomb friction compensation

The first step (and the first simulation) is for obtaining rough values for the PD controller gains. The computation of the gains is based on effective joint inertia and joint viscous friction values and linear system approximations of individual joints. As discussed in Chapter 5, the motor side inertia of the joints when reflected to the joint side is computed as

$$J_{m_k} = (J_{a_k} + J_{g_k}) / r_k^2 \quad \forall k[1, \dots, 6] \quad (6.4)$$

Ignoring the coupling effects introduced by the off-diagonal terms in the manipulator inertia matrix D , the combined inertia coefficient for joint k is then $J_{m_k} D_{kk}(q) / r_k^2$ which further can be simplified to the expression $J_{m_k} \bar{D}_{kk} / r_k^2$ where \bar{D}_{kk} a constant nominal inertia value is. In this work, this term is computed from $D_{kk}(q)$ with $q = 0$ (home position of the master arm).

Similarly, (as stated in Chapter 5) the viscous friction coefficient as reflected to the joint side of the transmission and reduction is B_{f_k} / r_k^2 . These two coefficients can be used to form the simplified model.

$$J_{eff_k} \ddot{q}_k + B_{eff_k} \dot{q}_k = u_k \quad (6.5)$$

for the k^{th} joint of the arm with

$$J_{eff} = \frac{1}{r_k^2} (J_{m_k} + \bar{D}_{kk}) \quad (6.6)$$

$$B_{eff} = \frac{1}{r_k^2} (B_{f_k}) \quad (6.7)$$

Application of u in a PD control architecture with proportional and derivative gains K_{D_k} and K_{P_k} respectively results in the equality

$$J_{eff_k} \ddot{q}_k + B_{eff_k} \dot{q}_k = K_{P_k} (q_k^d - q_k) + K_{D_k} (\dot{q}_k^d - \dot{q}_k) \quad (6.8)$$

where q_k^d represents the desired joint position for joint k . Hence,

$$J_{eff_k} \ddot{q}_k + (B_{eff_k} + K_{D_k}) \dot{q}_k + K_{P_k} q_k = K_{P_k} q_k^d + K_{D_k} \dot{q}_k^d. \quad (6.9)$$

Using Laplace transform, the transfer function between desired and actual joint positions can be computed as

$$\frac{Q_k(s)}{Q_k^d(s)} = \frac{K_{D_k}s + K_{P_k}}{J_{eff_k}^2 + (B_{eff_k} + K_{D_k})s + K_{P_k}}. \quad (6.10)$$

The characteristics equation of this transfer function is

$$s^2 + \left(\frac{B_{eff_k} + K_{D_k}}{J_{eff_k}} \right) s + \frac{K_{P_k}}{J_{eff_k}} = 0. \quad (6.11)$$

Equating this expression with the typical monic second order characteristics equation $s^2 + 2\zeta_k\omega_{n_k}s + \omega_{n_k}^2 = 0$ where ζ_k is the damping coefficient and ω_{n_k} is the undamped natural frequency, we can determine the controller gains by the selection of ζ_k and ω_{n_k} .

For the fastest response without overshoot, ζ_k is chosen equal to 1 (a critically damped system). ω_{n_k} determines the speed of the response. Table 6.2 lists the values of ω_{n_k} used for the six joints of the arm.

Joint #	ω_{n_k}
1	10
2	10
3	10
4	20
5	20
6	20

Table 6.2 Values of ω_{n_k} used for the joints

Figure 6.1 shows the results obtained with this controller for reference joint positions formed as combinations of step and sinusoidal functions. It can be observed from this figure that Coulomb friction and gravity problems cause large position errors which cannot be handled by the controller. The reason of the low performance, however, is that the controller gains are obtained by a rough approximation model. Fine tuning of the gains by trial and error results in the position curves in Figure 6.2. Still the large position error in link 3 (the elevator prone to gravity) and the distortion of the joint positions due to Coulomb friction could not be solved by fine tuning.

Figure 6.3 shows the controller performance when gravity compensation is added to the PD control signal. It can be observed that the errors due to gravity are removed successfully. Also, since the amount of PD control action which can counteract the

Coulomb friction effect is larger now, position distortions due to friction are reduced too.

Finally, in Figure 6.4 the tracking performance with the PD control with gravity and Coulomb friction compensation is shown. That the estimation of the Coulomb friction is difficult is reflected in the simulation by adding an estimation error in the form of a 20 Hz sinusoidal with an amplitude equal to 10% of the Coulomb friction. The addition of Coulomb friction compensation does not actually add a lot to the controller performance after the addition of gravity compensation term. This suggests that the use of the “reliable” gravity compensation alone can be favored over using it with the hard to compute Coulomb friction compensation.

We conclude by reemphasizing that the discussion of the compensation design is equally valid for any other controllers including haptic controllers which require dynamics compensation.

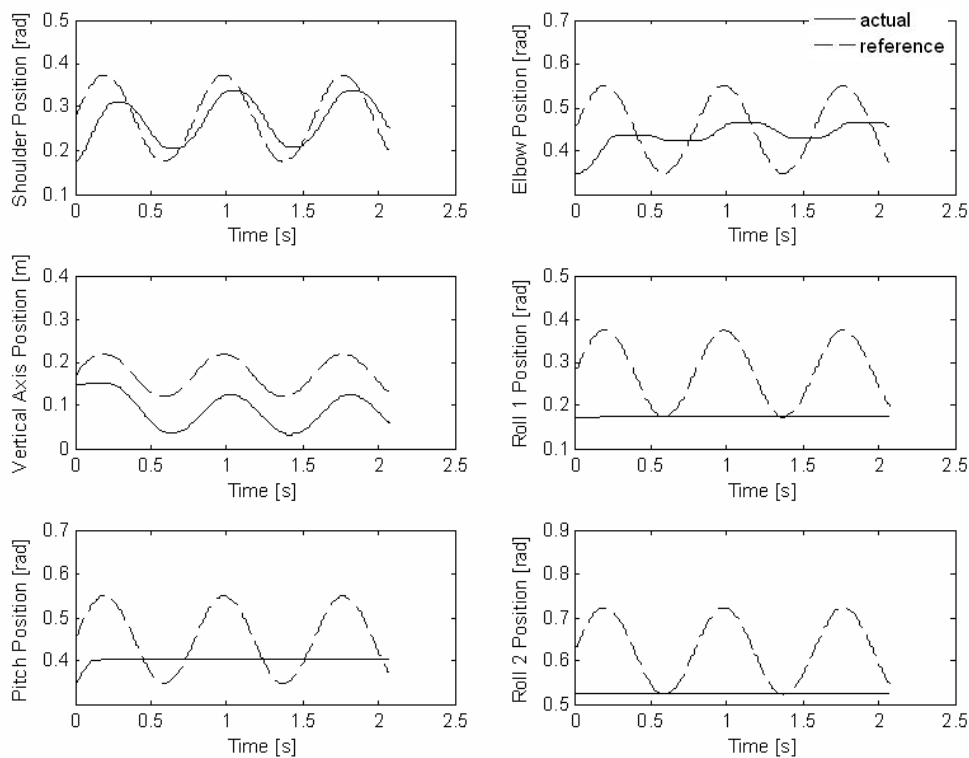


Figure 6.1 PD control performance without fine tuning

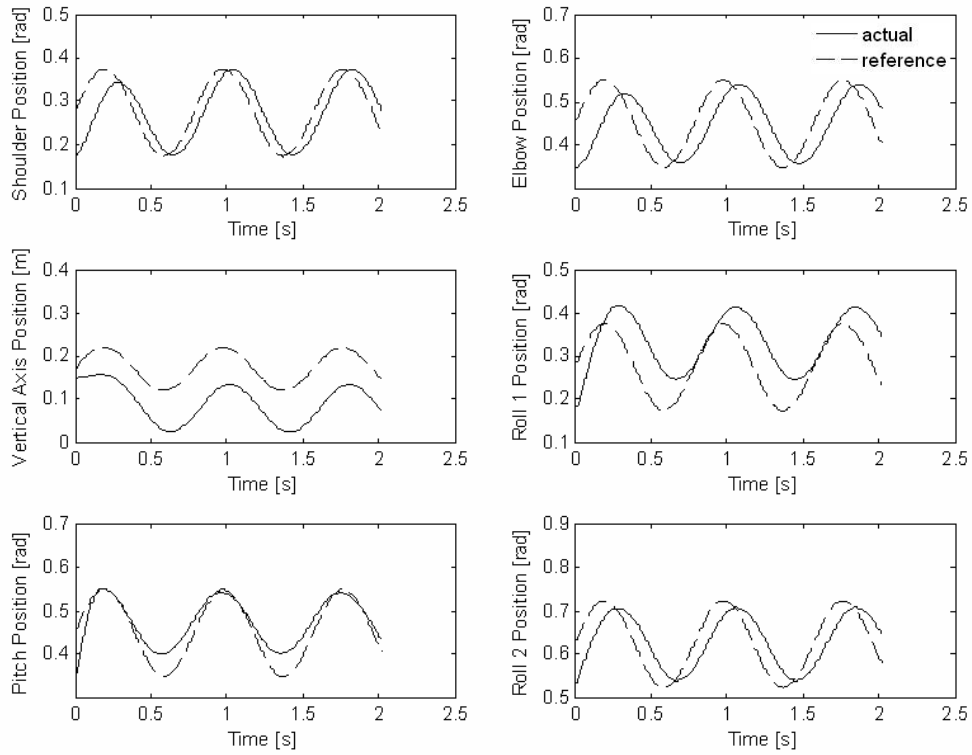


Figure 6.2 PD control performance with fine tuning

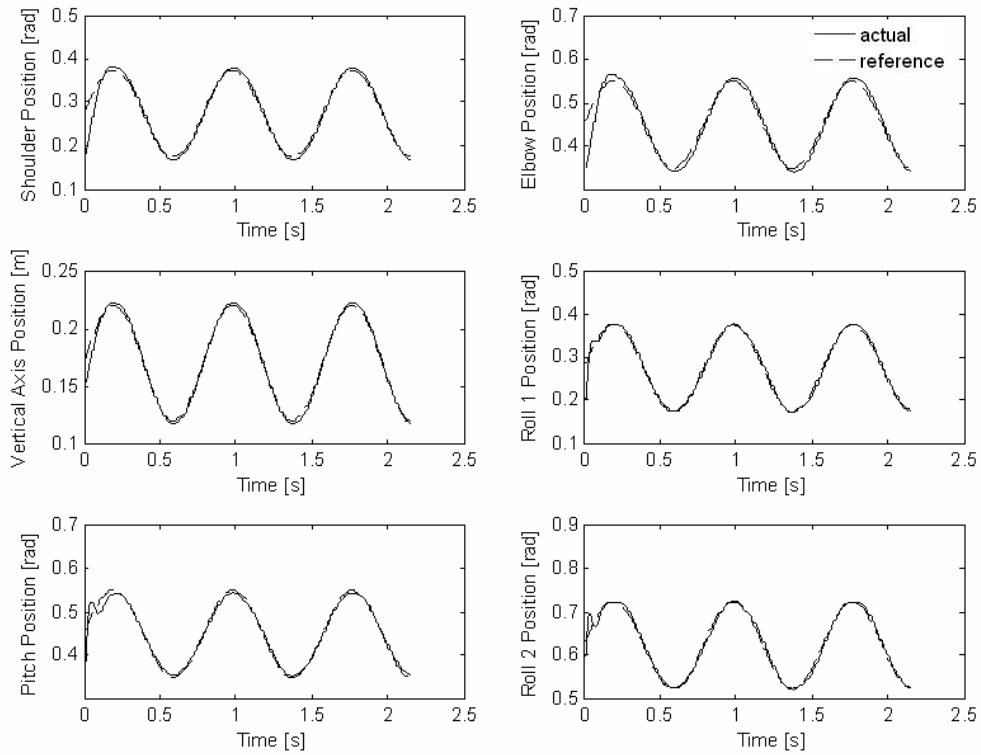


Figure 6.3 PD control with gravity compensation

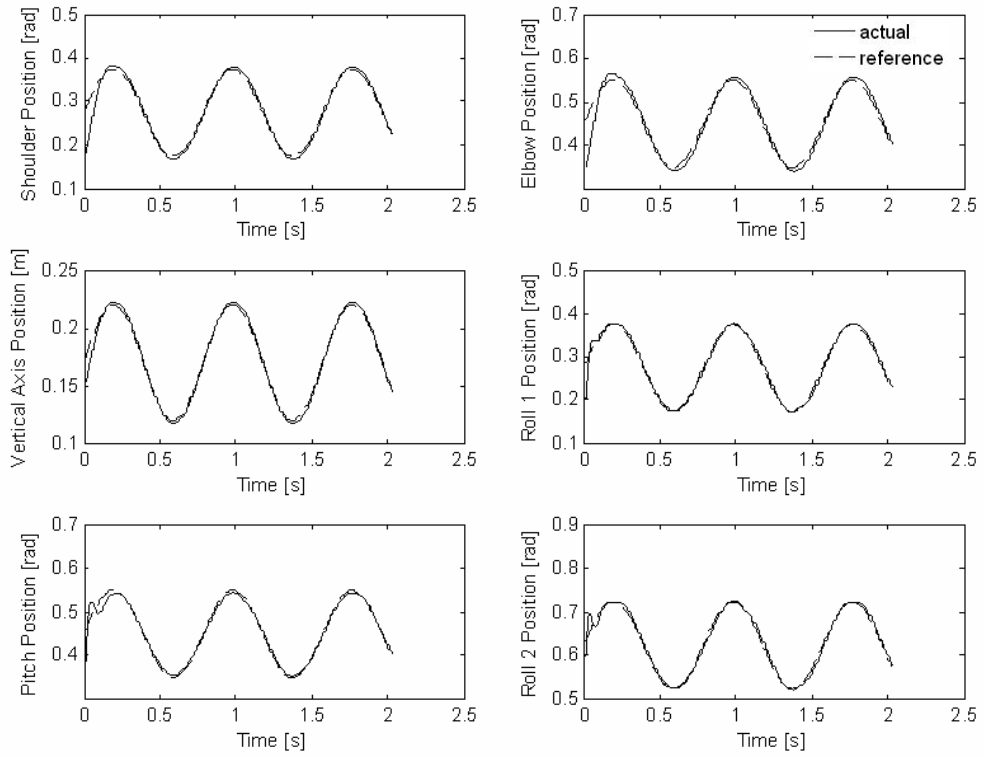


Figure 6.4 PD control with gravity and Coulomb friction compensation

7 ASSEMBLY

Mechanical design of the device is carried out in SolidWorks program. Assembly and detailed drawings have been completed prior to production. Three major sub-assemblies of the device, namely planar elbow mechanism, vertical axis assembly and spherical wrist assembly are illustrated in the following figures.

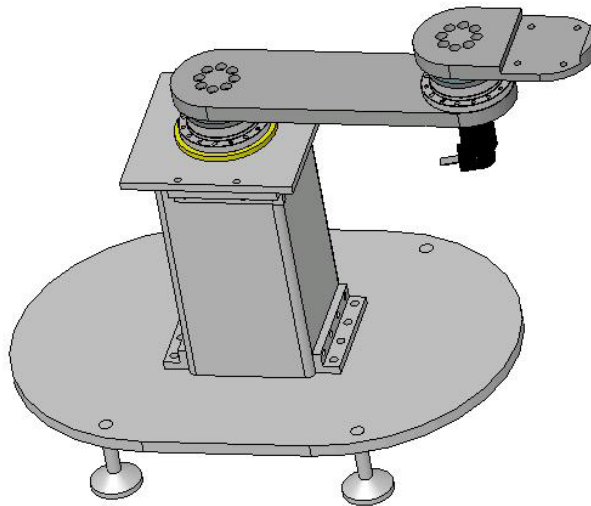


Figure 7.1 Base and planar elbow manipulator assembly

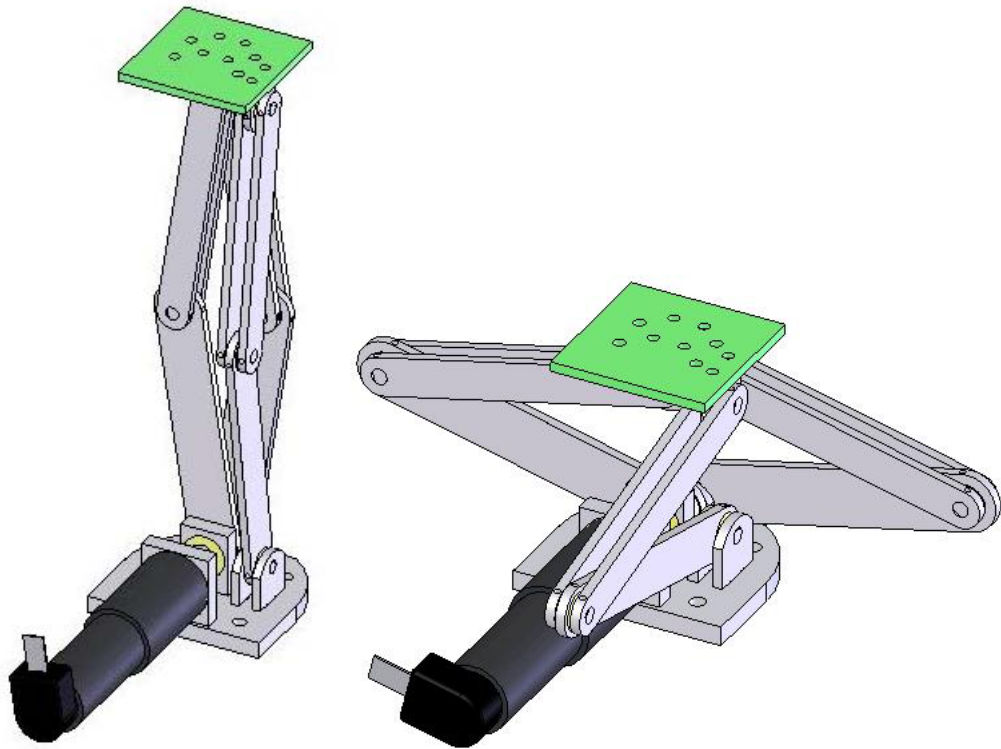


Figure 7.2 Vertical axis mechanism

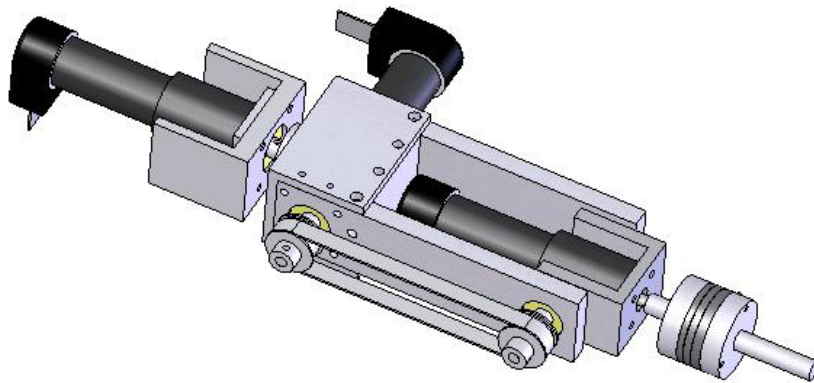


Figure 7.3 Spherical wrist mechanism

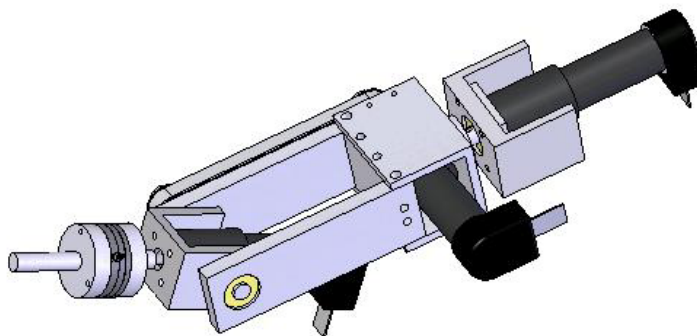


Figure 7.4 Spherical wrist mechanism

Production of the designed parts is carried out at the Sabancı University machining workshop. Some of the parts had to be reprocessed or manufactured again in order to compensate for modeling errors or inaccurate manufacturing.

Finally, the whole device containing motors, harmonic drives, bearings and force sensor is assembled. Photographs of the built device can be seen in the following figures.



Figure 7.5 Full view of the haptic device



Figure 7.6 Close view of the vertical axis and spherical wrist

After the mechanical assembly, wiring of the motors has been done and motors were tested to observe whether they operate as intended.

Harmonic drive assembly has to be done properly in order to ensure high performance. During the manufacturing process of the drive construction parts, dimensions and tolerances stated in the harmonic drive catalogue has to be satisfied in order to achieve recommended concentricity and run-out values.

Unfortunately, because of inaccuracies of our manufacturing facility, tolerances of the parts in contact with the harmonic drive are unfeasible which leads to mismatch in the axis alignment of the motor and the drive. Although harmonic drives employ Oldham couplings at the input stage, their tolerances were not sufficient to compensate for the inaccurate manufacturing. As a result of the axis misalignment and imprecise shaft tolerances, encountered friction was higher than calculated before. Thus no load running torque of the harmonic drive is increased. A large portion (almost 2/3) of torque capacity of the motor is spent to compensate the running torque of the harmonic drives.

For the vertical axis mechanism, between different options such as rack and pinion, belt drive, ball and screw mechanism etc., the linkage structure shown in Figure

7.2 was chosen. This mechanism does not have backlash or friction as with other mechanisms mentioned above. Link lengths and thicknesses were selected according to workspace requirements and stress analysis. Once the assembly of the mechanism is completed, it was realized that the friction and backlash issues of other mechanisms were indeed prevailed. During the operation of the mechanism, backlash and friction problems were not encountered, thus the motor torque was efficiently spent on gravity effect. However, the rigidity of the linkage structure was not as high as foreseen. Our observation is that this is due to the complex assembly which employed large number of parts.

Finally, spherical wrist part of the device is working properly showing expected dynamics. For the fifth link, timing belt is used which suffers play and backlash caused by elongation of the belt. In order to prevent this, a simple mechanism which provides tension to the belt is designed and built. Also the force sensor is mounted to the end effector between last roll axis motor and the handle. This procedure concludes the assembly of the device.

The machining problems observed in the last phase of the thesis made reprocessing of certain parts necessary. Since the machining process requires time in the order of a couple of weeks (sometimes months) this re-machining process is left as a future work.

8 CONCLUSION

The design and construction of a 6 DOF haptic device as an infrastructure for haptic applications is considered in this thesis. The design guidelines have been large workspace, high force-torque capacity and ergonomic use. A suitable kinematics arrangement and a set of actuation mechanisms are chosen for the specifications determined by these guidelines. Inverse dynamics simulations and stress analysis results are used to verify the performance of the selected actuators and transmission mechanisms and stiffness of the mechanical design. In order to fulfill the transparency requirements, dynamics compensation algorithms are developed for the designed haptic device. Based on the design requirements, the haptic device is built, assembled and integrated with the control hardware.

The main problem encountered in the thesis work was the misalignment in the assembly of the reduction mechanisms and transmission elements of the three main axes. Improvements in the mechanical design and re-machining is considered as a future work. After reassembly, we expect that the device can function as a versatile test bed for haptic experiments at Sabancı University Mechatronics Laboratory.

REFERENCES

- [1] Rovers, A. F. *Design of a robust master-slave controller for surgery applications with haptic feedback*. Master Thesis, Department of Mechanical Engineering, Eindhoven University of technology, 2003
- [2] Craig R. Carignan, Kevin R. Cleary. *Closed-loop force control for haptic simulation of virtual environment*. Haptics-e, The Electronic Journal of Haptics Research (www.haptics-e.org), Vol. 1, No. 2, 1999.
- [3] Lee, W.-S., Kim, J.-H., and Cho, J.-H. *A driving simulator as a virtual reality tool*. Proceedings of IEEE International Conference on Robotics and Automation, pages 71-76, 1998
- [4] Clover, C., Luecke, G., Troy, J., and McNeely, W. *Dynamic simulation of virtual mechanisms with haptic feedback using industrial robotics equipment*. Proceedings of IEEE International Conference on Robotics and Automation, pages 724-730, 1997.
- [5] Li, P. and Horowitz, R. *Control of smart exercise machines*. In *IFAC World Congress*, 1996.
- [6] Swaim, P., Thompson, C., and Campbell, P. *The Charlotte intra-vehicular robot*. Technical Report N95-23703, NASA, 1995.
- [7] Carignan, C. and Akin, D. *Actively controlled mockups for EVA training in neutral buoyancy*. Proc. IEEE Conf. on Systems, Man, and Cybernetics, pages 2369-2374, 1997.
- [8] Baumann, R. and Clavel, R. *Haptic interface for virtual reality based minimally invasive surgery simulation*. In Proc. IEEE Int. Conf. on Robotics and Automation, pages 381-386, 1998.
- [9] Popa, D. O. and Singh, S. K. *Creating realistic force sensations in a virtual environment: Experimental system, fundamental issues and results*. In Proc. IEEE Int. Conf. on Robotics and Automation, pages 59-64, 1998.

- [10] Goertz, R.C. and Thompson, R.C. *Electronically controlled manipulator*. Nucleonics, vol. 12, no. 11, pages 46-47, 1954.
- [11] Bejczy, A. and Salisbury, J. K. *Controlling remote manipulators through kinesthetic coupling*. Computers in Mechanical Engineering, vol. 2, no. 1, pages 281-290, 1983.
- [12] Ramstein, C. and Hayward. *The Pantograph: A Large Workspace Haptic Device For A Multi-Modal Human-Computer Interaction*. Conference on Human Factors in Computing Systems, pages: 57-58, 1994.
- [13] DiMaio, S.P., Salcudean, S.E. and Sirosupour, M.R. *Haptic Interaction with a Planar Environment*. 9th Symp. Haptic Interfaces for Virtual Env. & Teleop. Sys, Intl. Mech. Eng. Congr. Exp., (ASME Winter Annual Meeting), Vol. 69, No.2, pages: 1223 – 1230, 2000.
- [14] Stocco, L.J., Salcudean, S.E. and Sassani, F. *Optimal Kinematic Design of a Haptic Pen*. IEEE/ASME Transactions on Mechatronics, Vol. 6, No. 3, pages: 210 – 220, 2001.
- [15] Birglen, L., Gosselin, C., Pouliot, N., Monsarrat, B. and Laliberté, T. *SHaDe, A New 3-DOF Haptic Device*. IEEE Transactions On Robotics and Automation, Vol. 18, No. 2, 2002.
- [16] Kim, S., Berkley, J. J., Sato, M. *A Novel Seven Degree of Freedom Haptic Device for Engineering Design*. Virtual Reality, Vol. 6, No. 4, pages: 217-228, 2003.
- [17] http://www.sensable.com/products/phantom_ghost/phantom-desktop.asp
- [18] Borro, D., Savall, J., Amundarain, A., Gil, J.J., Garcia-Alonso, A., Matey, L. *A large haptic device for aircraft engine maintainability*. IEEE Computer Graphics and Applications, Volume. 24, No. 6, Pages:70 - 74, 2004
- [19] Ueberle, M., Buss, M. *Design, Control, and Evaluation of a New 6 DOF Haptic Device*. IEEE/RSJ International Conference on Intelligent Robots and System, Vol. 3, Pages: 2949 - 2954, 2002.
- [20] Ueberle, M., Mock, N., Buss, M. *VISHARD10, a novel hyper-redundant haptic interface*. Proceedings of the 12th International Symposium on Haptic Interfaces for Virtual Environment and Teleoperator Systems (HAPTICS'04) Pages :58 - 65, 2004.
- [21] Massie, T.H. and Salisbury, K. *The Phantom Haptic Interface: A Device for Probing Virtual Objects*. In Proceedings of the ASME Winter Annual Meeting,

- Symposium on Haptic Interface for Virtual Environments and Teleoperator Systems, Pages: 295-301, 1994
- [22] Smith C. M. *Human factors in haptic interfaces*. Crossroads, Vol. 3, No. 3, Pages: 14-16, 1997.
- [23] Burns, D. T. Design of a Six Degree of Freedom Haptic Interface. Master Thesis, Department of Mechanical Engineering, Northwestern University, 1996.
- [24] Soo, S.L., Jang, M.L. *Design of a general purpose 6-DOF haptic interface*. Mechatronics, Elsevier Science, Vol. 13, No.7, Pages 697-722, 2003
- [25] Savall, J., Borro, D., Gil, J.J., Matey, L. *Description of a Haptic System for Virtual Maintainability in Aeronautics*. Proceedings of 2002 International Conference on Intelligent Robots and Systems, pages: 2887-2892, 2002.
- [26] Spong M. W., Vidyasagar M. *Robot Dynamics and Control*. John Wiley & Sons, 1989.
- [27] Salcudean, S.E., Stocco, L. *Isotropy and actuator optimization in haptic interface design*. IEEE International Conference on Robotics and Automation, vol. 1, Pages: 763 - 769, 2000.
- [28] Kapuscinski, C. L. *Motor Selection And Damper Design For A Six Degree Of Freedom Haptic Display*. Master Thesis, Department of Mechanical Engineering, Northwestern University, 1997.
- [29] Jones, L.A. *Kinesthetic Sensing*. Human and Machine Haptics, MIT Press, 2000.
- [30] Griffin, W. B. *Shared Control For Dexterous Telemanipulation With Haptic Feedback*. Phd Thesis, Department Of Mechanical Engineering, Stanford University, 2003.
- [31] Chandrabalan, C. J., *Design and Construction of 1 D.O.F Haptic Interface*. Master Thesis, Department of Mechanical Engineering, Florida State University, 2004
- [32] Kapuscinski, C. L., *Motor Selection And Damper Design For A Six Degree Of Freedom Haptic Display*. Master Thesis, Department of Mechanical Engineering, Northwestern University, 1997.
- [33] Lawrence, D. A., *Stability and Transparency in Bilateral Teleoperation*. IEEE Transactions On Robotics And Automation, Vol. 9, No. 5, 1993.

- [34] Martin, J. and Savall, J., *Mechanisms for Haptic Torque Feedback*. Proceedings of the First Joint Eurohaptics Conference and Symposium on Haptic Interfaces for Virtual Environment and Teleoperator Systems, 2005.
- [35] Tsumaki, Y., Naruse, H., Nenchev, D. N. and Uchiyama M. *Design of a Compact 6-DOF Haptic Interface*. Proceedings of the 1998 IEEE International Conference on Robotics & Automation, pages: 2580 - 2585, 1998.
- [36] Faulring, E. L., Colgate, J. E. and Peshkin M. A., *A High Performance 6-DOF Haptic Cobot*. Proceedings of the 2004 IEEE International Conference on Robotics & Automation, pages: 1980 - 1985, 2004.
- [37] Yoon, j. and Ryu, J., *Design, Fabrication, and Evaluation of a New Haptic Device Using a Parallel Mechanism*. IEEE/ASME Transactions on Mechatronics, Vol. 6, No. 3, pages: 221-233, 2001.
- [38] Woo, K.Y., Jin, B.D., Kwon, D. *A 6 DOF Force-Reflecting Hand Controller Using the Fivebar Parallel Mechanism*. Proceedings of the 1998 IEEE International Conference on Robotics & Automation, pages: 1597 - 1602, 1998.

APPENDIX A. HARMONIC DRIVE DATASHEET

Leistungsdaten

Rating Table

Tabelle / Table 164.1

HFUC-2UH Baugröße	Untersetzung ⁵⁾	Grenze für wiederholbares Spitzendrehmoment	Grenze für Durchschnittsdrehmoment	Nenn-drehmoment bei 2000 min ⁻¹	Grenze für Kollisionsdrehmoment	Max. Antriebsdrehzahl min ⁻¹	Grenze für mittlere Antriebsdrehzahl min ⁻¹	Massenträgheitsmoment ³⁾	Gewicht		
HFUC-2UH Size	Ratio ⁵⁾	Limit for Repeated Peak Torque	Limit for Average Torque	Rated Torque at 2000 rpm	Limit for Momentary Peak Torque	Max. Input Speed rpm	Limit for Average Input Speed rpm	Moment of Inertia ³⁾	Weight		
		T _R Nm	T _A Nm	T _N Nm	T _M Nm	Öl ¹⁾ Oil Lub. ¹⁾	Fett ²⁾ Grease Lub. ²⁾	Öl ¹⁾ Oil Lub. ¹⁾	Fett ²⁾ Grease Lub. ²⁾	kgm ²	kg
14	30	9,0	6,8	4,0	17	14000	8500	6500	3500	0,033 x 10 ⁻⁴	0,49
	50	18	6,9	5,4	35						
	80	23	11	7,8	47						
	100	28	11	7,8	54						
17	30	16	12	8,8	30	10000	7300	6500	3500	0,079 x 10 ⁻⁴	0,64
	50	34	26	16	70						
	80	43	27	22	87						
	100	54	39	24	110						
20	30	27	20	15	50	10000	6500	6500	3500	0,193 x 10 ⁻⁴	0,98
	50	56	34	25	98						
	80	74	47	34	127						
	100	82	49	40	147						
25	30	50	38	27	95	7500	5600	5600	3500	0,413 x 10 ⁻⁴	1,5
	50	98	55	39	186						
	80	137	87	63	255						
	100	157	108	67	284						
	120	167	108	67	304						
	160	176	108	67	314						

Lastfreies Anlaufdrehmoment

No-Load Starting Torque

Tabelle / Table 168.3

[Ncm]

HFUC-2UH Untersetzung / Ratio	HFUC-2UH Baugröße / Size											
	14	17	20	25	32	40	45	50	58	65	80	90
30	6,4	9,3	15	25	54	-	-	-	-	-	-	-
50	4,1	6,1	7,8	15	31	55	77	110	160	220	360	500
80	2,8	4,0	4,9	9,2	19	35	49	66	98	140	230	320
100	2,5	3,4	4,3	8,0	18	31	43	58	88	120	200	280
120	-	3,1	3,8	7,3	15	28	39	52	80	110	190	250
160	-	-	3,3	6,3	14	24	33	45	68	93	155	220

Lastfreies Rückdrehmoment

No-Load Back Driving Torque

Tabelle / Table 168.4

[Nm]

HFUC-2UH Untersetzung / Ratio	HFUC-2UH Baugröße / Size											
	14	17	20	25	32	40	45	50	58	65	80	90
30	2,4	3,8	6,2	11	23	-	-	-	-	-	-	-
50	1,6	3	4,7	9	18	33	47	62	95	130	220	300
80	1,6	3	4,8	9,1	19	33	48	63	96	140	220	300
100	1,8	3,3	5,1	9,8	20	36	51	68	110	150	230	330
120	-	3,5	5,5	11	22	39	55	73	110	160	250	350
160	-	-	6,4	13	26	46	64	85	130	180	300	410

Tabelle / Table 173.1

HFUC-2UH Baugröße	Lager- typ 6)	Teilkreis $\sigma^4)$	Abstand ⁵⁾	Dynamische Tragzahl	Statische Tragzahl	Zulässiges dynamisches Kippmoment ¹⁾	Zulässiges statisches Kippmoment ²⁾	Kippsteifigkeit	Zulässige Axiallast ³⁾	Zulässige Radiallast ³⁾
HFUC-2UH Size	Bearing type 6)	Circle $\sigma^4)$	Offset ⁵⁾	Dynamic load rating	Static load rating	Permissible dynamic Tilting Moment ¹⁾	Permissible static Tilting Moment ²⁾	Moment Stiffness	Permissible Axial Load ²⁾	Permissible Radial Load ³⁾
		d_p [m]	R [mm]	C [N]	C_0 [N]	M [Nm]	M_0 [Nm]	K_B [Nm/arcmin]	F_a [N]	F_r [N]
14	C	0,035	9,5	4740	6070	41	53	13	3374	2256
17	C	0,043	9,5	5290	7550	64	80	22,5	3207	2148
20	C	0,050	9,5	5780	9000	91	113	37	3511	2354
25	C	0,062	11,5	9600	15100	156	234	70	5827	3904
32	C	0,080	13,0	15000	25000	313	500	157	7926	6101
40	C	0,096	14,5	21300	36500	450	876	265	11242	8652
45	C	0,111	15,5	23000	42600	686	1182	410	12174	9368
50	C	0,119	18,0	34800	60200	759	1791	497	18393	14155
58	C	0,141	20,5	51800	90400	1180	3187	823	27409	21091
65	C	0,160	22,5	55600	103000	1860	4120	1175	29371	22602
80	C	0,185	26,0	76400	143000	2740	6614	1900	37611	25200
90	C	0,214	28,5	83200	168000	4210	8988	2943	40895	27400